PNNL-13178

In Situ Redox Manipulation of Subsurface Sediments from Fort Lewis, Washington: Iron Reduction and TCE Dechlorination Mechanisms

J. E. Szecsody
J. S. Fruchter
D. S. Sklarew
J. C. Evans

March 2000

Pacific Northwest National Laboratory
Richland, Washington 99352

DISCLAIMER

DISCLAIMER

Portions of this document may be illegible in electronic image products. Images are produced from the best available original document.

Summary

The feasibility of chemically treating sediments from the Ft. Lewis, Washington, Logistics Center to develop a permeable barrier for dechlorination of trichloroethylene (TCE) was investigated in a series of laboratory experiments. The proposed remediation technology uses a chemical treatment to reduce existing iron in sediments, then relies on the ability of the ferrous iron to act as an electron donor to dechlorinate organic contaminants. The effects of temperature, partial iron reduction, and flow on these redox reactions were also studied to ascertain how to achieve viable TCE dechlorination rates at the field scale. The fraction of reducible iron in Ft. Lewis sediments would create a reduced zone that would remain anoxic for ~300 pore volumes. Because the kinetics of the reduction reaction are third-order, significant amounts of iron are reduced early in the reduction period. The reduction is slower at later times. Because the slower disproportionation reaction destroys the remaining dithionite, specific sediment/solution contact times (32 h at 25°C, 100 h at 12°C) are needed to efficiently reduce 80% of the iron in the sediment.

When the pH buffer concentration was less than four times the dithionite concentration, there was a significant loss in reduction efficiency along with a significant pH decrease and increased iron mobility. The long contact times needed for reduction at ambient aquifer temperature coupled with density effects of the solution at the field scale indicate that heated injections (with high concentration of pH buffer) can efficiently reduce the sediment zones of interest.

Dithionite-reduced Ft. Lewis sediments were shown to degrade TCE in Ft. Lewis groundwater at sufficiently fast rates (1.2 h to 19 h) during static and transport experiments to create a permeable barrier at the field scale. The TCE degradation rate can be calculated for all sediments from the product of the intrinsic degradation rate (0.0034/h μmol) and the mass of reduced iron (range of 12 μmol/g to 126 μmol/g; averaged = 63 μmol/g). Products of TCE dechlorination clearly show that 99.5% to 100% is occurring via reductive elimination, producing acetylene, ethylene, and chloro-acetylene. The TCE degradation rate decreased up to 3 orders of magnitude in partially reduced sediment. This departure on fraction of reduced iron has significant implications, because uniform full sediment reduction is not possible at the field scale. Although minimally reduced sediment had nearly no TCE reactivity, >40% reduced sediment resulted in TCE reduction rates that were viable at the field scale (<65 h). The second-order dependence of the TCE dechlorination rate on the fraction of reduced iron demonstrates the significant role of the iron oxide surface (as a catalyst or for surface coordination) in addition to Fe^{II} as the electron donor for TCE dechlorination to proceed. Reduced sediment barrier longevity was demonstrated in a column in which TCE was degraded for over 230 pore volumes. The design of a field-scale reduced iron barrier should to be wide enough to allow the TCE to be degraded to below the maximum concentration level (MCL) during the ground-water transport time through the barrier (10 half-lives). Because few sites are homogeneous, barriers are typically designed wider than needed to account for the spatial variability in the iron content and the velocity variability resulting from hydraulic conductivity variability and temporal changes.

Contents

Figures

Tables

1.0 Introduction

Pacific Northwest National Laboratory (PNNL) conducted a bench-scale study to determine how effective chemically treated Ft. Lewis sediments can degrade trichloroethylene (TCE). The objectives of this experimental study were to quantify: 1) sediment reduction and oxidation reactions, 2) TCE degradation reactions, and 3) other significant geochemical changes that occurred. Sediment reduction and oxidation were investigated to determine the mass of reducible iron in the Ft. Lewis sediments and the rate of this reduction and subsequent oxidation at different temperatures. The temperature dependence was needed to be able to predict field-scale reduction in the relatively cold (~11°C) Ft. Lewis aquifer. Results of these experiments were used in conjunction with other geochemical and hydraulic characterization to design the field-scale injection experiment and predict barrier longevity. For example, the sediment reduction rate influences the injection rate and lag time before extraction in the field experiment because the reduction rate controls the amount of time required for the dithionite solution to fully react with sediments. Sediment oxidation experiments were additionally conducted to determine the oxidation rate and provide a separate measure of the mass of reduced iron. Laboratory experiments that were used to meet these objectives included: 1) sediment reduction in batch (static) systems, 2) sediment reduction in 1-D columns, and 3) sediment oxidation in 1-D columns. Multiple reaction modeling was conducted to quantify the reactant masses and reaction rates.

The second objective of this study was to determine the pathway and rate(s) of TCE degradation by reduced Ft. Lewis sediment. Given the degradation rate, the thickness of the proposed reactive barrier can be designed. The degradation rate and pathway information was quantified in both batch and column experiments at different temperatures. Batch experiments provide the most complete pathway information, because data are not influenced by flow. However, complex geochemical rates have been shown to occur at somewhat different rates in columns relative to batch systems, due in part to a significantly higher sediment-to-water ratio and slower access to surface sites by mobile constituents (Szecsody et al. 1998a and 1998b). Therefore, degradation rate information from column experiments is generally considered more applicable to reactive transport at the field scale.

The creation of a reduced zone in the aquifer can affect the mobility of other metals, so the final objective of this study was to quantify iron and other heavy metal geochemical changes that occur. The changes in the mobility of heavy metals was addressed with column experiments and analysis of the effluent for the metals during sediment reduction and oxidation. Changes in surface iron geochemistry during reduction and oxidation were quantified because previous studies have shown that different Fe^{II} phases produced by the dithionite treatment appear to have different reduction and oxidation rates.

2.0 Geochemical Reactions for Remediation of TCE

2.1 Iron Reduction Mechanism

The remediation technology proposed for Ft. Lewis is based on the proven ability of reduced (ferrous) iron to abiotically degrade TCE and other organic contaminants (Roberts et al. 1996). The proposed technology utilizes existing iron in aquifer sediment that is chemically treated with a reductant (sodium dithionite buffered at high pH) for a short time (typically 24 h to 60 h) to reduce Fe^{III}-oxides present in the sediment to adsorbed or structural Fe^{II} phases. This reduction process of aquifer sediments results in the groundwater redox conditions becoming reducing and the disappearance of dissolved oxygen in water, as conceptually shown in Figure 1 (0 to 0.1 years).

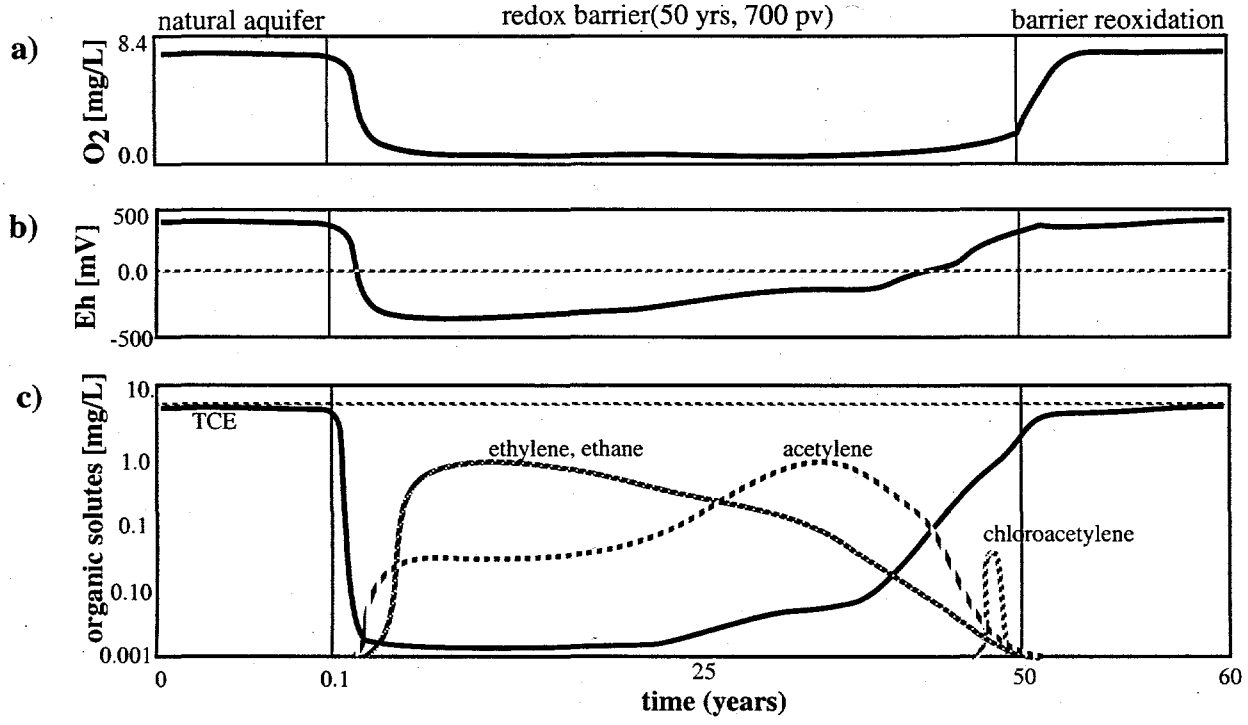

Figure 1. Conceptual diagram showing the influence of the redox barrier as a function of time on: a) dissolved oxygen in water which is the main barrier oxidant, b) the redox conditions of groundwater, and c) TCE and degradation products resulting from dechlorination by the reduced iron in the redox barrier.

The TCE dechlorination mechanism with reduced iron of this chemical treatment is generally the same as zero-valent permeable iron walls (conceptually shown in Figure 1c). Zero valent iron/mixed metal barriers also rely on the oxidation of ferrous (adsorbed or Fe^{II} minerals such as green rust; Genin et al. 1998) to ferric iron as the electron donor for remediation of chlorinated aliphatic contaminants (Balko and Tratnyek 1998; Johnson et al. 1998) or reduction of metals such as chromate (Blowes et al. 1997; Buerge and Hug 1997), and not the oxidation of Fe^0. Although aqueous Fe^{II} can

reduce chromate (Eary and Rai 1988), adsorbed or structural Fe^{II} on an Fe^{III}-oxide, clay surface, or zero-valent iron surface is necessary for dechlorination reactions. The role of the surface is not clearly understood.

The dithionite chemical treatment dissolves and reduces amorphous and some crystalline Fe^{III} oxides. The reduced Fe^{II} created by the dithionite chemical treatment appears to be present in at least two different Fe^{II} phases: adsorbed Fe^{II} and Fe^{II}-carbonate (siderite). Adsorbed Fe^{II} appears to be the dominant Fe^{II} phase. There may be other, unidentified Fe^{II} mineral phases produced. Although more than one Fe^{III} phase is likely reduced in a natural sediment, it can be useful to determine how simple a chemical model is needed to generally describe the observations. The reaction that describes a single phase of iron that is reduced by sodium dithionite:

$$S_2O_4^{-2} + 2 \equiv Fe^{3+} + 2H_2O \text{ <==> } 2 \equiv Fe^{2+} + 2(SO_3^{-2}) + 4H^+ \quad (1)$$

shows that the forward rate is a function of the dithionite concentration and the square of the reducible iron concentration (rate is overall a third-order function of concentration). The aqueous Fe^{II} produced has a high affinity for surfaces, so is quickly adsorbed. Therefore, Fe^{II} mobility in mid- to high-pH, low ionic strength groundwater (i.e., Ft. Lewis groundwater) is extremely limited, and iron is not expected to leach from sediments during the dithionite treatment. Aqueous iron measurements in previous studies have shown <1% iron leaching even after 600 pore volumes of groundwater through a sediment column. Corresponding solid iron measurements of sediments used in these columns showed 4% to 10% loss of iron. Iron mobility is somewhat higher during the actual dithionite injection, as a high ionic strength solution of other cations (0.06M Na^+ and 0.24M K^+ in this case) competes for the same adsorption sites as Fe^{2+}, causing some Fe^{2+} desorption. Previous experimental transport studies with dithionite injection into sediments have shown 0% to 12% iron loss after 40 pore volumes of dithionite treatment.

Experimental evidence from previous studies with Hanford sediments (Istok et al. 1999; Fruchter et al. 2000) have shown that two parallel reduction reactions are needed to describe iron reduction data (i.e., a fraction of sites are quickly reduced and a fraction more slowly reduced). This may be the result of the reduction of two or more major Fe^{III} phases. Based on this hypothesis, a second reduction reaction was added with a second ferric iron phase symbolized by $\equiv\equiv Fe^{3+}$:

$$S_2O_4^{-2} + 2 \equiv\equiv Fe^{3+} + 2H_2O \text{ <==> } 2 \equiv\equiv Fe^{2+} + 2(SO_3^{-2}) + 4H^+ \quad (2)$$

The total number of oxidized or reduced iron sites is the sum of sites in reaction 1 and 2. If the number of slowly reducing sites (Equation 2) is small, and the mass of iron is far in excess of the dithionite, reaction 1 can be reduced to a kinetic first-order reaction in which Fe^{3+} remains constant:

$$S_2O_4^{-2} \text{ <==> } 2\ Fe^{2+} + SO_3^{-2} \quad (3)$$

Equation 3 is not a balanced reaction, but is meant to illustrate the species upon which the reaction rate is dependent. Other studies of this chemical treatment have shown that reactions 1 and 2 can be approximated in some cases with reaction 3 with a pseudo-first order rate of ~5 h (half-life). Another reaction occurs in the system, which describes the disproportionation of dithionite in contact with sediment:

$$2S_2O_4^{-2} + H_2O \text{ <==> } S_2O_3^{-2} + 2(HSO_3^-) \quad (4)$$

that accounts for the mass loss of dithionite that cannot be used for iron reduction. Other studies have shown that this reaction has a half-life of ~27 h (basaltic sediments). The consequence of this

reaction is to limit how slowly dithionite can be reacted with (i.e., injected into) sediment in the field. If dithionite is injected too slowly, a significant amount of its mass is lost to disproportionation.

Although Fe^{III} phases are the most significant phases that react with dithionite, other mineral phases present in natural sediments may also be reduced and utilize some of the dithionite. Previous studies have shown that some Mn reduction occurs as a result of the dithionite treatment of Hanford sediment, although reduced Mn(II, 0) phases were about 3.4% of the mass of reduced iron phases.

2.2 Sediment Oxidation Mechanisms

The oxidation of the adsorbed and structural Fe^{II} in the sediments of the permeable redox barrier occurs naturally by the inflow of dissolved oxygen through the barrier, but can additionally be oxidized by contaminants that may be present such as chromate, TCE, nitrate, uranium, or other reducible species. If redox equilibrium completely defined the mechanism (i.e., no effects from activation energies), and contaminants are present in equal molar concentrations, they would be reduced faster in the following order:

$$\text{chromate} > \text{dissolved oxygen} > \text{nitrate} > \text{uranium} > \text{TCE} \qquad (5)$$

In relatively uncontaminated aquifers, dissolved oxygen in water is the dominant oxidant of reduced iron species, as contaminants are generally present in lower molar concentrations relative to dissolved oxygen. The oxidation of reduced iron in pure mineral phases is described by the following reactions first by dissolved oxygen, then with other contaminants. Fe^{II} species that are known to exist in the dithionite-reduced sediments include adsorbed Fe^{II} and siderite [$Fe^{II}CO_3$]. A single mole of electrons is consumed as a mole of these species is oxidized:

$$Fe^{2+} \text{ <==> } Fe^{3+} + e^- \qquad Eh = -0.77 \text{ v} \qquad (6)$$

$$Fe^{2+} + 3H_2O \text{ <==> } Fe(OH)_3(s) + 3H^+ + e^- \qquad Eh = -0.56 \text{ v} \qquad (7)$$

$$FeCO_3(s) + 3H_2O \text{ <==> } Fe(OH)_3(s) + 2H^+ + HCO_3^- + e^- \qquad (8)$$

The use of dissolved oxygen as an oxidant is generally divided into two electron sequences, and when combined, yields:

$$O_2 + 4H^+ + 4e^- \text{ <==> } H_2O, \qquad Eh = 1.23 \text{ v} \qquad (9)$$

which shows that 4 moles of electrons are needed per mole of O_2 consumed. The rate of this reaction (9) has generally been observed to be first-order at fixed pH, and the rate increases 100 fold for a unit increase in pH. Assuming one type of surface iron (adsorbed Fe^{II}) is oxidized by dissolved oxygen (reactions 5 and 8):

$$4\,Fe^{2+} + O_2 + 4H^+ \text{ <=> } 4\,Fe^{3+} + 2H_2O \qquad Eh = -1.85 \text{ v} \qquad (10)$$

yields 4 moles of Fe^{II} are oxidized per mole of O_2 consumed. At oxygen-saturated conditions (8.4 mg L^{-1} O_2, 1 atm, 25°C), 1.05 mmol L^{-1} Fe^{II} is consumed. Experimental evidence indicates that the oxygenation of Fe^{II} in solutions (pH >5) is generally found to be first order with respect to Fe^{II} and O_2 concentration and second-order with respect to OH-. The rate of oxidation of Fe^{II} in solution

by oxygen at pH 8 is a few minutes (Eary and Rai 1988, Buerge and Hug 1997). In contrast, the oxidation rate (as a half-life) observed in natural sediments (surface Fe^{II} thought to be adsorbed Fe^{II} and $Fe^{II}CO_3$) was found to be 0.3 h to 1.1 h.

The oxidation of reduced sediment appears to be more complex than can be described with a single oxidation reaction, and is likely controlled by both chemical and physical processes. Experimental evidence during iron oxidation experiments indicates that a second type of reduced iron species is present (siderite) in minor concentrations. In addition, a minor fraction of reduced iron sites (presumed to be siderite) appears to be more slowly oxidized, so a second oxidation reaction:

$$4\,FeCO_3(s) + O_2 + 4H^+ <=> 4Fe^{3+} + 2\,H_2O + 4\,CO_3^{2-} \qquad (11)$$

was considered in the reaction model used. Both of these reactions (10 and 11) show that 4 moles of Fe^{II} are consumed per mole of oxygen consumed. The Fe^{III} produced in reactions (10) and (11) quickly precipitates as $Fe(OH)_3$. The oxidation of redox barrier in an aquifer by dissolved oxygen is conceptually shown (Figure 1, 0.1 years to 50 years), in which the Eh remains negative but slowly increases over the same time period of no dissolved oxygen breakthrough.

2.3 TCE Degradation

At the Ft. Lewis site, the abiotic degradation of TCE and other organic contaminants is being tested using the In Situ Redox Manipulation treatment technology. In this case, the organic contaminants are electron acceptors. The degradation pathway of TCE by dithionite-reduced sediment has been investigated in other studies as well as in Ft. Lewis sediments. Degradation pathways for most organic compounds including TCE are complex, involving multiple and potentially parallel reaction steps. Of four possible abiotic degradation pathways for TCE, the two considered most common are reductive elimination and hydrogenolysis. Reductive elimination has been shown to be the major pathway in other studies using zero-valent and ferrous iron (Sivavec et al. 1996; Orth and Gillham 1996). Reductive elimination reactions include (Roberts et al. 1996):

TCE + $2e^-$ <=> chloroacetylene + $2Cl^-$;	Eh = 0.60 v	(12)
PCE - + $2e^-$ <=> dichloroacetylene + $2Cl^-$;	Eh = 0.63 v	(13)
cis-, trans-DCE + 2e- <=> acetylene + 2Cl-;	Eh = 0.56 v	(14)

which describes the destruction of TCE and polychloroethylene (PCE) to easily degraded (abiotically or biotically) chlorinated acetylene products. Abiotic degradation of these products by hydrogenolysis:

dichloroacetylene + H^+ + $2e^-$ <=> chloroacetylene + Cl^-;	Eh = 0.56 v	(15)
chloroacetylene + H^+ + $2e^-$ <=> acetylene + Cl^-;	Eh = 0.50 v	(16)
acetylene + $2H^+$ + $2e^-$ <=> ethylene;	Eh = 0.39 v	(17)

apparently proceeds rapidly as chlorinated acetylenes are unstable (Delavarenne and Viehe 1969). The degradation of TCE to ethylene by reductive elimination (or hydrogenolysis discussed below) involves the production of 6 moles of electrons, or 22 mg L^{-1} TCE needed to oxidize the equivalent mass of Fe^{II} as water saturated with dissolved oxygen (1.05 mmol L^{-1} Fe^{II}). Therefore, water containing partial oxygen saturation and ~1.0 mg L^{-1} TCE (as likely present in the Ft. Lewis aquifer with 0.3 mg/L in solution and 2x that mass adsorbed) means that TCE has an insignificant impact on Fe^{II} oxidation and remediation barrier lifetime. In the event that the reduced iron barrier is exhausted, previous laboratory studies with the Hanford 100D and 100H sediment have shown that sediment can be re-reduced with only a small (5% to 10%) loss in capacity. Hydrogenolysis reactions include:

$$TCE + H^+ + 2e^- \Leftrightarrow 1,1\text{-DCE (more likely) or cis-DCE} + Cl^-; \quad Eh = 0.51\ v \quad (18)$$
$$1,1\text{-DCE or cis-DCE} + H^+ + 2e^- \Leftrightarrow \text{vinyl chloride} + Cl^-; \quad Eh = 0.41\ v \quad (19)$$

which describes the degradation of TCE involving the production then destruction of dichloroethylene (DCE) and vinyl chloride intermediates (generally more difficult to degrade). These reduction potentials are lower than reductive elimination, indicating they are less likely to occur abiotically. Activation energies and the specific electron transfer mechanism, which does involve the Fe^{III} oxide surface, may also influence which reactions actually do occur. Studies of TCE degradation pathways using zero-valent iron and various Fe^{II} minerals (Roberts et al. 1996; Sivavec and Horney 1995; Thornton et al. 1998) indicate that reductive elimination is the major pathway, with minor amounts of DCE isomers and vinyl chloride produced from the hydrogenolysis pathway. One study also indicates that the DCE isomers and vinyl chloride slowly degraded to ethylene.

The TCE reaction pathway can be used to model the observed rate of TCE degradation. Because acetylene is the main reaction product observed, the combination of reactions (6), (12), and (16) described the major TCE degradation pathway:

$$TCE + H^+ + 4Fe^{2+} \Leftrightarrow \text{acetylene} + 3Cl^- + 4Fe^{3+} \quad (20)$$

A set of differential mass flux equations for (20) and (10) that describes iron oxidation by dissolved oxygen) for the 7 species can be written and simultaneously solved to define the rate of change of TCE. The mass flux equation for TCE:

$$\partial TCE/\partial t = -k_{f20}\,[TCE][H^+][Fe^{2+}]^4 + -k_{b20}\,[\text{acetylene}][Cl^-]^3\,[Fe^{3+}]^4 \quad (21)$$

describes mass fluxes as a function of each constituent concentration to each respective stoichiometric coefficient. The set of differential equations can be numerically solved (55 mixed equilibrium and kinetic reactions with 71 species described in Szecsody et al. [1995, 1998a, 1998b]), but this type of detailed modeling is useful only if extensive knowledge of the reaction parameters exists. In the case of TCE degradation, not enough information is known about the reaction pathways and reaction parameters to justify this approach.

Simpler models can be used to accurately describe the TCE degradation rate under specific conditions. The equation describing the TCE degradation rate can be greatly simplified assuming no backward mass flux and that the pH is buffered:

$$\partial TCE'/\partial t = -k'_{f20}[TCE][Fe^{2+}]^4 \quad (22)$$

which shows that the TCE degradation rate is a function of a rate coefficient (k'_{f20}), the TCE concentration, and the ferrous iron concentration (raised to a power >1). Therefore, as the sediment is slowly oxidized by both dissolved oxygen (reaction 10) and TCE (reaction 20), the observed overall TCE degradation rate ($\partial TCE'/\partial t$) will decrease. Over a small number of pore volumes, the Fe^{2+} concentration can be assumed constant, and the TCE degradation rate simplifies to a first-order reaction that can be integrated:

$$\partial TCE''/\partial t = -k''_{f20}[TCE] \quad (23)$$
$$TCE = TCE_{t=0}\, e^{-\lambda t} \quad (24)$$

Both the pseudo-first-order approach (reaction 23) and the fixed-pH approach (numerical solution to reactions (10) and (22) were used in this study to describe the TCE degradation data). As stated

earlier, because the actual TCE degradation rate is a function of Fe^{2+} and decreases over time, the first-order half-life will appear to decrease at progressively later points in time. As the overall TCE degradation rate decreases, the relative concentrations of degradation products change (Figure 1) during flow through a redox barrier in an aquifer. In general, final degradation products (ethylene, ethane) appear when all reactions are occurring at the fastest rates, and as reactions slow, intermediates (acetylene) and finally the initial degradation product of TCE dechlorination (chloroacetylene) appears.

2.4 Partial Iron Reduction and Temperature Effects on TCE Degradation

The electron-transfer mechanisms of TCE dechlorination by surface Fe^{II} phases are not completely understood, and as a consequence, there is a lack of ability to predict the TCE degradation rate with sediment that is only partially reduced. Two aspects of the electron transfer reactions are known: abiotic dechlorination of TCE and other chlorinated organic compounds requires both available Fe^{II} as an electron donor and the presence of an iron oxide or zero-valent iron surface. The surface is necessary for the electron transfer reaction as laboratory experiments have shown that TCE and carbon tetrachloride are not dechlorinated in the presence of only aqueous Fe^{II}. The role of the surface is not well understood, although may act as a catalyst, a semiconductor, or provide the necessary surface coordination for the electron transfer reactions (Scherer et al. 1999; Wehrli 1992).

The potential role of surface coordination of adsorbed Fe^{II} on the iron reduction/TCE dechlorination reaction is illustrated with an idealized example. The TCE dechlorination reaction is a two-electron transfer reaction in a single step (described in Section 2.4), so it is hypothesized that two adsorbed Fe^{II} molecules that are adjacent are needed for this reaction to occur. Assuming a single Fe^{III} oxide (goethite) that has orthorhombic crystal structure, adsorption sites are located in a rectangular grid, so a single site has 8 possible adjacent adsorption sites. The relationship between fraction of surface coverage of Fe^{II} on a goethite surface and the fraction of paired sites was developed from probability theory and verified with numerical simulations using a 200 by 200 grid of sites (Figure 1). The number of adjacent adsorbed Fe^{II} sites is a fraction of the number adsorbed sites at low surface coverage. For example, if 50% of the surfaces are occupied by Fe^{II}, only 25.2% of the sites are adjacent (solid line) and could promote TCE dechlorination. The implication of this surface area hypothesis is that partially reduced sediment will be significantly less effective at dechlorinating TCE than would be predicted assuming a linear relationship between fraction reduction and TCE dechlorination rate (dashed line, Figure 1).

The role of the iron oxide surface on TCE dechlorination was also experimentally investigated by developing a relationship between fraction-reduced iron and the resulting dechlorination ability of the sediment. In these experiments, sediment was reduced in batch systems and the mass of reduced iron measured by different types of iron extractions including oxygen breakthrough in columns. Batch time-course experiments were used to determine the resulting TCE dechlorination rate.

The potential role of the iron oxide surface as a catalyst for TCE dechlorination was investigated by batch TCE dechlorination time-course experiments over a temperature range. In contrast to a simple chemical reaction, a chemical reaction that requires a surface catalyst will likely show a more complex relationship between reaction rate and temperature, because the catalyst may cease to function as the temperature decreases beyond a specific value.

Iron reduction experiments were investigated over a temperature range to determine if the relative rates of iron reduction and disproportionation changed. Field-scale reductions take place at temperatures lower than laboratory studies, and these rate data are needed to design field-scale injection strategies. The ambient temperature of the Ft. Lewis aquifer is unusually cold at 11°C to 12°C (compared with many aquifers in the 16°C to 19°C range), and the time needed for reduction to be completed at 11°C results in additional density effects of the injection solution. Additional field-scale reductions will occur with the injection of heated water so that reduction occurs more quickly at higher temperature (20°C to 22°C), where density effects of the injection fluid are minimized. At 25°C, iron reduction has a ~5 h half-life and disproportionation a 27 h half-life. The rate at which a chemical reaction proceeds is a linear function, and will generally decrease in rate 2x-3x for each 10°C decrease. Because these two reactions are simple chemical reactions, it is expected that their relative rates would remain proportionally separated.

3.0 Experimental and Modeling Methods

3.1 Batch and Column Experiments

A series of batch and column experiments were conducted to determine the mass and rate of reduction of iron in sediment by the reduction solution (sodium dithionite pH buffered to 11.0). The batch experiments consisted of a single large septa-top glass bottle in which 14 g to 200 g of sediment was mixed with the dithionite solution for hundreds of hours. The experiment is then mixed on a linear shaker at slow rpm (to not cause particles to break up) and placed in a temperature-controlled chamber (2°C to 42°C) for the 10 different batch reduction experiments conducted (Table 1). At specific time intervals (minutes to tens of hours, a sample was withdrawn, filtered, and analyzed for dithionite remaining in solution. It is assumed that the sample volume withdrawn (0.2 mL) was small to the total system volume, and so the sampling did not affect the experimental conditions. The dithionite solution contained 0.001 mol L^{-1} to 0.10 mol L^{-1} sodium dithionite ($Na_2S_2O_4$), with 4x the dithionite concentration K_2CO_3, and 0.4x $KHCO_3$. These batch experiments were conducted inside an anaerobic chamber to prevent the dithionite from reacting with oxygen. The dithionite concentration was measured by UV absorption at 315 nm, as described below.

Sediment reduction studies conducted in 1-D columns consisted of injecting the dithionite solution at a steady rate into a sediment column and measuring the concentration of dithionite over time in the effluent for 48 h to 100 h (Table 2; 23 column reduction experiments). The flux rate was chosen to achieve specific residence times of the dithionite solution in the column (2 h to 14 h) relative to the reaction rates (Szecsody and Bales 1989). Column experiments involved measuring additional parameters to interpret dithionite results. The dry bulk density and porosity of the column was calculated from the dry and saturated column weight and column volume. The volumetric flow rate was calculated from the effluent volume and elapsed time. The electrical conductivity of the column effluent provided a second (dynamic) measure of the porosity, and was measured using a flow-through electrode and automatic data logging.

The dithionite concentration in the effluent was measured once per hour using an automated fluid system and data logging equipment. These measurements were taken with an HPLC injection valve with 15 µL to 52 µL loop that isolated a specified volume of the effluent. The contents of the loop were mixed with 5 mL to 10 mL of oxygen-free water, then injected into a UV-detector and absorbance measured at 315 nm. The sample injection took 2 minutes to flow the complete sample through the detector, and the absorbance over a 1-minute interval was averaged for a single dithionite concentration measurement. A triple-wash between injections prevented sample overlap. These fluid operations were controlled from one computer, and the dithionite concentration logged on a second computer. The concentration of the dithionite influent was measured with the same automated system by manually bypassing the column at approximately 24 h intervals over the multi-day experiments (Williams and Szecsody 1997). The fraction of reduced iron was calculated from dithionite breakthrough curves by determining the total mass loss (i.e., dithionite mass injected minus dithionite in the effluent) and the mass of dithionite used for disproportionation. The remaining dithionite mass loss was used for iron reduction. This dithionite breakthrough analysis assumes that dithionite has reached a steady state mass loss due to disproportionation and that all the iron has been reduced. The rate of iron reduction is also calculated from the steady state dithionite concentration during initial breakthrough (i.e., before the iron is all reduced).

Table 1. Summary of batch reduction experiments

				dithionite degradation analysis from simulations							
name	experiment	sediment	fraction < X mm	initial dithioite (mol/L)	sed/water	T (°C)	dispro[1] rate (1/h)	dispro half life (h)	Fe reduct. rate[3] ($L^2/hmol^2$)	Fe reduct. half life (h)	Fe reduced (µmol/g)
KF30	batch reduction	RM9, 60', < 4 mm	0.4037	0.110	0.500	2.0	0.00267	260	55	19.6	40.0
KF31	batch reduction	RM9, 60', < 4 mm	0.4037	0.080	0.500	42.1	0.05	14	1400	0.86	40.0
KF32a	batch reduction	RM9, 60', < 4 mm	0.4037	0.030	0.500	25.0	0.02567	27	350	3.1	40.0
KF32b	batch reduction	RM9, 60', < 4 mm	0.4037	0.018	0.500	25.0	0.02567	27	350	3.1	40.0
KF32c	batch reduction	RM9, 60', < 4 mm	0.4037	0.010	0.500	25.0	0.02567	27	350	3.1	40.0
KF32d	batch reduction	RM9, 60', < 4 mm	0.4037	0.0062	0.500	25.0	0.02567	27	1850*	0.74	40.0
KF32e	batch reduction	RM9, 60', < 4 mm	0.4037	0.0021	0.500	25.0	0.02567	27	6000**	0.62	40.0
KF35	batch reduction	RM9, 60', < 4 mm	0.4037	0.030	0.500	2.0	0.00267	260	55	19.6	40.0
KF36	batch reduction	RM9, 60', < 4 mm	0.4037	0.008	0.500	42.0	0.1024	6.8	1250	0.92	40.0
KF37	batch reduction	RM9, 60', < 4 mm	0.4037	0.008	0.500	10.1	0.00367	189	80	14	40.0

*dithionite was added to reduce only 62% of the iron

**dithionite was added to reduce only 21% of the iron

Table 2. Summary of reduction and oxidation column experiments

							Dithionite breakthrough curve analysis							Oxygen breakthrough curve analysis				
name	experiment	sediment	fraction < X mm	res. time (h/pv)	dith. (mol/L)	K_2CO_3 (mol/L)	injection mass (mol)	btc mass loss (mol)	dispro[1] loss (mol)	dl. oxidized by Fe[2] (mol)	Fe reduced[3] (mol)	Fe reduced (µmol/g)	red.rate half-life (h)	injection mass[4] (mol)	btc mass loss (mol)	Fe(II) oxidized[5] (mol)	iron ox/red	Fe oxidized (µmol/g)
												whole sediment						(< 4 mm)
KF1	reduction	LC149-40',<4mm	0.2084	1.96	0.09	0.36	4.80E-03	3.50E-03	2.30E-04	1.07E-03	2.14E-03	40.3	4.95					
KF2	reduction	LC149-40',<4mm	0.2084	2.06	0.09	0.36	2.42E-03	1.39E-03	1.30E-04	9.90E-04	1.98E-03	35.2	3.28					
KF3	oxidation of KF1	LC149-40',<4mm	0.2084	0.74										2.07E-04	8.30E-05	3.32E-04	0.155	
KF4	oxidation of KF2	LC149-40',<4mm	0.2084	0.58										4.55E-04	2.21E-04	8.84E-04	0.446	
KF5	reduction	LC133-40',<4mm	0.1683	4.94	0.09	0.36	1.58E-03	9.50E-04	1.89E-04	4.45E-04	8.90E-04	13.3	8.24					
KF6	reduction	LC133-40',<4mm	0.1683	4.02	0.09	0.36	2.00E-03	1.13E-03	2.00E-05	8.50E-04	1.70E-03	25.7	5.08					
KF7	oxidation of KF6	LC133-40',<4mm	0.1683	0.77										1.85E-04	1.08E-04	4.30E-04	0.506	
KF8	reduction	FL-6, <2mm	0.3035	12.03	0.09	0.36	2.57E-03	8.22E-04	6.83E-04	1.06E-03	2.12E-03	31.9	8.56					
KF9	reduction	FL-1, <2mm	0.4193	11.26	0.09	0.36	3.10E-03	1.62E-03	5.80E-04	9.00E-04	1.80E-03	40.7	7.93					
KF10	oxidation of KF8	FL-6, <2mm	0.3035	0.81										4.91E-04	4.30E-04	1.72E-03	0.808	
KF11	oxidation of KF9	FL-1, <2mm	0.4193	0.73										6.04E-04	4.58E-04	1.83E-03	1.018	
KF12	reduction	FL-6, <2mm	0.3035	4.94	0.09	0.36												
KF14	reduction	FL-3, <2mm	0.08891	12.77	0.09	0.36	3.52E-03	1.33E-03	9.82E-04	1.21E-03	2.42E-03	11.6	8.22					
KF15	reduction	FL-6, <2mm	0.3035	3.01	0.09	0.36												
KF16	oxidation of KF14	FL-6, <2mm	0.3035	3.01										7.62E-04	4.88E-04	1.95E-03	0.807	
KF18	reduction	rm4,53',<2mm	0.1525	4.30	0.09	0.36	6.41E-03	1.67E-03	6.70E-04	4.07E-03	8.14E-03	107.2	3.95					
KF19	reduction	rm1, 62',<2mm	0.3463	3.37	0.09	0.36	6.65E-03	3.82E-03	5.50E-04	2.28E-03	4.56E-03	126.2	6.14					
KF20	reduction	rm2, 62'<2mm	0.2476	9.62	0.09	0.36	1.23E-03	4.78E-04	2.69E-04	4.83E-04	9.66E-04	18.9						
KF21	reduction	rm9, 60',<2mm	0.4037	7.89	0.06	0.24	1.66E-03	5.90E-04	3.04E-04	7.66E-04	1.53E-03	51.4	6.90					
KF22	reduction	rm9, 60',<2mm	0.4037	6.98	0.03	0.12	1.25E-03	3.43E-04	2.04E-04	6.99E-04	1.40E-03	46.8	11.80					
KF41	oxidation	rm1, <4mm	0.3461	2.89			batch reduced (dithionite/iron = 3.0, actual 100% reduced)					28.7						83.0
KF43	oxidation	Istok mix, <4mm	0.3793	2.64			batch reduced (dithionite/iron = 4.0, actual: 100% reduced)					60.3		2.98E-03	1.91E-03	4.40E-03		159.0
KF45	oxidation	Istok mix, <4mm	0.3793	2.64			batch reduced (dithionite/iron = 0.41, actual: 27.4% reduced)					16.5*		1.01E-03	6.28E-04	1.21E-03		43.6
KF47	oxidation	Istok mix, <4mm	0.3793	2.64			batch reduced (dithionite/iron = 0.30, actual: 11.1% reduced)					6.68*		3.13E-04	2.32E-04	4.87E-04		17.6
KF48	oxidation	Istok mix, <4mm	0.3793	2.64			batch reduced (dithionite/iron = 0.71, actual: 52.6% reduced)					31.7*		1.49E-03	1.12E-03	2.31E-03		83.6
KF49	reduction	Istok mix, <4mm	0.3793	2.53	0.09	0.36	2.51E-03	8.79E-04	1.57E-04	7.22E-04	1.44E-03	66.5	5.21					
KF50	reduction	Istok mix, <4mm	0.3793	3.30	0.09	0.27	1.80E-03	7.10E-04	1.46E-04	5.64E-04	1.13E-03	76.4	4.87					
KF51	oxidation of KF49	Istok mix, <4mm	0.3793	0.32										6.26E-04	3.82E-04	2.15E-03	1.060	137.0
KF52	oxidation of KF50	Istok mix, <4mm	0.3793	0.33										5.35E-04	2.63E-04	1.05E-03	0.930	79.2
KF53	reduction	Istok mix, <4mm	0.3793	2.14	0.09	0.27	2.73E-03	5.65E-04	1.46E-04	4.19E-04	8.38E-04	55.6	4.53					
KF54	reduction	Istok mix, <4mm	0.3793	2.18	0.09	0.18	2.58E-03	3.78E-04	1.42E-04	2.36E-04	4.72E-04	58.1	6.77					
KF55	oxidation of KF53	Istok mix, <4mm	0.3793	0.34										2.97E-04	1.90E-04	7.60E-04	0.920	76.3
KF56	oxidation of KF54	Istok mix, <4mm	0.3793	0.27										2.46E-04	1.03E-04	4.10E-04	0.882	58.2
KF57	reduction	Istok mix, <4mm	0.3793	4.31	0.09	0.18	7.94E-03	1.37E-03	8.32E-04	5.38E-04	1.08E-03	18.6	5.68					
KF58	reduction	Istok mix, <4mm	0.3793	4.27	0.09	0.09	4.32E-03	1.87E-03	5.63E-04	1.31E-03	2.61E-03	11.5	6.02					
KF58x	reduction	Istok mix, <4mm	0.3793	4.28	0.09	0.09	2.63E-03											
KF59	reduction	Istok mix, <4mm	0.3793	2.88	0.09	0.045	4.75E-03	1.91E-03	3.42E-04	1.57E-03	3.14E-03	14.2	7.56					
KF60	oxidation of KF59	Istok mix, <4mm	0.3793	0.54										4.90E-04	2.97E-04	1.19E-03	0.835	41.5
KF61	reduction	Istok mix, <4mm	0.3793	4.27	0.09	0.045	3.54E-03	1.59E-03	4.23E-04	1.17E-03	2.33E-03	10.4	8.79					

[1] disproportionation mass loss = [inj. mass - [(inj. mass)*e^(-0.02567*residence time)]] (27 h half life assumed)

[2] injection mass - btc mass loss - disproportionation mass loss

[3] 2 mol Fe/mol dithionite

[4] oxygen injected = 256umol/L x mL/h x 1L/1000mL x total h

average 6.82±2.46

average all FL sediments: 45.6±33.3 µmol/g for the whole sediment

average all rm sediments: 62.8±39.7 µmol/g for the whole sediment

average rm-9: 49.1±3.25 µmol/g for the whole sediment

Sediment oxidation studies were also conducted in 1-D columns to determine the rate at which the dithionite-reduced sediments are oxidized and to provide an additional measure of the mass of reduced iron. These experiments (Table 2; 16 experiments) consisted of injecting oxygen-saturated (8.4 mg/L^{-1}) water at a steady rate into a reduced sediment column and measuring the concentration of dissolved oxygen over time in the effluent for 100 h to 800 h. The flux rate was chosen to achieve specific residence times of the dissolved oxygen in the column relative to the oxidation rate(s) of the sediment. The water used in experiments approximated the major ions found in the aquifer (consisting of 15 mg/L NaCl, 8.2 mg/L KCl, 67 mg/L $CaSO_4$, 13 mg/L $MgCO_3$, 150 mg/L $CaCO_3$, 15.3 mg/L H_2SiO_3, and the pH adjusted to 7.7 to 8.2). A series of in-line micro-electrodes were used to monitor geochemical changes during oxidation and included dissolved oxygen (2 electrodes), Eh, pH, and electrical conductivity. Electrode measurements were continuously monitored, averaged, and data logged at 2-minute to 5-minute intervals. Two point calibration was conducted on the in-line electrodes at 4 h to 8 h intervals (oxygen-free and oxygen-saturated solution for oxygen) using an automated fluid system. Electrode data from calibrations were also data logged. The mass of reduced iron that was oxidized was calculated from the oxygen breakthrough curves. The difference in the total mass of dissolved oxygen injected minus dissolved oxygen in the effluent is that consumed by ferrous iron. This oxygen breakthrough analysis assumes dynamic equilibrium, or that all of the reduced iron has been oxidized in the column. In many cases, there is a fraction of the sediment that has not been oxidized, so some error in estimating the fraction not reduced is introduced.

Additional analysis was conducted on sediment and water samples to establish additional information about the redox geochemistry of the Ft. Lewis sediment during reduction and oxidation cycling. To establish the mobility of trace metals during sediment reduction and oxidation, liquid effluent samples from some column reduction experiments and oxidation experiments were analyzed for trace metals by ICP-MS. Geochemical analysis of sediment samples was conducted to determine the amounts of various $Fe^{II/III}$ phases, which included seven different types of iron extractions (Heron and Christensen 1995; Chao and Zhou 1983; Heron et al. 1994a,b).

The TCE and other organic contaminant degradation studies were conducted in batch systems and in 1-D columns. Batch TCE experiments consisted of reacting Ft. Lewis groundwater containing 1 ppm to 2 ppm TCE with reduced Ft. Lewis sediment in individual vials with no headspace for times from minutes to 240 h (Table 3, 22 experiments). Water was then extracted and organic solutes analyzed by gas chromatograph (GC) or gas chromatograph mass spectrometry (GC-MS). To more clearly discriminate the reaction pathway of TCE, in some batch studies deionized water containing only TCE was reacted with reduced sediment. This eliminated the effects of reaction products of PCE, TCA, and DCE interfering with determining the masses of TCE degradation products. All batch TCE experimental vials were placed on low rpm rotary mixers and placed in chambers (2°C to 42°C) for temperature studies. Water and sediment for these temperature studies were pre-equilibrated at the appropriate temperature before the experiment started. Sediment reduction was generally accomplished in columns to control the amount of reduction. Mixing of the sediment, water, and TCE was accomplished in an anaerobic chamber to minimize the oxidation of ferrous iron by atmospheric oxygen.

Column experiments consisted of injecting Ft. Lewis groundwater into reduced Ft. Lewis sediment at a steady flow rate and collecting effluent water for measurement of degradation products. As with other column studies discussed, the flow rate was chosen to achieve specific residence times that would be similar to the TCE degradation rate (5 h to 50 h range). Seven TCE column experiments were conducted with residence times ranging from 5.8 h to 102 h (Table 4). Most experiments were initiated with 100% reduced sediment. Because the degradation rate was expected to slow as the sediment was oxidized, in one column, the TCE degradation rate was additionally measured at 100 and 230 to pore volumes after oxygen-saturated water was flushed through the column to partially

Table 3. Summary of batch TCE experiments

name	sediment	fraction < x mm	reduction	water source	initial TCE conc. (ppm)	initial TCE conc. (µmol/L)	T (°C)	adsorption Kd (cm^3/g)	adsorption TCE rem. by ads.	total TCE removed (fraction)	acetylene generated (fraction)	TCE dechlorination rate rate** (1/h))	TCE dechlorination rate half life (h)	analysis	# points	degradation products	other compounds
KF13	FL6 < 2 mm	0.3035	100% reduced	Ft .L groundwater	2.700	20.50	25.0	0.53	0.21	0.995		0.200	3.46	GC-MS	22	c.acet., acet, eth.	DCE, vinyl chloride
KF24	RM9, 60', < 4 mm	0.4037	100% reduced	Ft .L groundwater	1.005	7.66	23.8	1.13	0.36	0.96		0.144	4.8	GC-MS	7	acetylene	vinyl chloride
KF25	RM9, 60', < 4 mm	0.4037	100% reduced	Ft .L groundwater	0.836	6.25	17.1	0.94	0.32	0.56		0.050	13.9	GC-MS	7	acetylene	vinyl chloride
KF26	RM9, 60', < 4 mm	0.4037	100% reduced	Ft .L groundwater	1.080	8.22	10.0	0.97	0.33	0.86		0.030	23.1	GC-MS	7	acetylene	vinyl chloride
KF33	RM9, 60', < 4 mm	0.4037	100% reduced	Ft .L groundwater	1.320	10.08	2.5	1.03	0.34	0.56		0.005	140	GC-MS	7	acetylene	vinyl chloride
KF34	RM9, 60', < 4 mm	0.4037	100% reduced	Ft .L groundwater	2.150	16.41	42.0	0.82	0.29	0.70		0.050	13.9	GC-MS	7	acetylene	vinyl chloride
KF40a	RM9, 60', < 4 mm	0.4037	reduced (0.82)*	TCE in di water	1.760	13.41	25.0	0.90	0.31	0.62		0.0062	110	GC	3	acetylene	
KF40b	RM9, 60', < 4 mm	0.4037	reduced (0.65)*	TCE in di water	1.760	13.41	25.0	-		0.49		0.0047	147	GC	3	acetylene	
KF40c	RM9, 60', < 4 mm	0.4037	reduced (0.49)*	TCE in di water	1.760	13.41	25.0	-		0.71		0.00044	1400	GC	3	acetylene	
KF40d	RM9, 60', < 4 mm	0.4037	reduced (0.33)*	TCE in di water	1.760	13.41	25.0	-		0.62		0.00008	>2000	GC	3	acetylene	
KF40e	RM9, 60', < 4 mm	0.4037	reduced (0.16)*	TCE in di water	1.760	13.41	25.0	-		0.63		none	--	GC	3	acetylene	
KF42a	RM1, 60', <4 mm	0.3875	100% reduced	TCE in di water	1.540	11.76	25.0	1.123	0.36	0.89	0.825	0.161	4.3	GC	8	acetylene	
KF42b	Istok mix, < 4 mm	0.3793	4.0% reduced	TCE in di water	1.041	7.92	25.0	5.512	0.73	0.42	0.000	none	--	GC	5	acetylene	
KF42c	Istok mix, < 4 mm	0.3793	11.1% reduced	TCE in di water	1.270	9.67	25.0	5.512	0.73	0.45	0.017	0.0006	1100	GC	5	acetylene	
KF42d	Istok mix, < 4 mm	0.3793	27.4% reduced	TCE in di water	1.041	7.92	25.0	5.512	0.73	0.61	0.167	0.0028	250	GC	5	acetylene	
KF42e	Istok mix, < 4 mm	0.3793	27.4% reduced	TCE in di water	2.000	15.2	25.0	5.512	0.73	0.53	0.056	0.0032	216	GC	4	acetylene	
KF42f	Istok mix, < 4 mm	0.3793	33.4% reduced	TCE in di water	1.270	9.67	25.0	5.512	0.73	0.70	0.204	0.0058	120	GC	5	acetylene	
KF42g	Istok mix, < 4 mm	0.3793	38.7% reduced	TCE in di water	2.000	15.2	25.0	5.512	0.73	0.54	0.091	0.0107	65	GC	4	acetylene	
KF42h	Istok mix, < 4 mm	0.3793	38.7% reduced	TCE in di water	2.000	15.2	25.0	5.512	0.73	0.44	0.080	0.0139	50	GC	2	acetylene	
KF42i	Istok mix, < 4 mm	0.3793	43.8% reduced	TCE in di water	1.041	7.92	25.0	5.512	0.73	0.91	0.911	0.036	19.2	GC	5	acetylene	
KF42j	Istok mix, < 4 mm	0.3793	52.6% reduced	TCE in di water	1.270	9.67	25.0	5.512	0.73	0.95	0.594	0.043	16	GC	5	acetylene	
KF42k	Istok mix, < 4 mm	0.3793	100% reduced	TCE in di water	0.813	6.19	25.0	5.512	0.73	0.999	0.750	0.578	1.2	GC	3	acetylene	
KF62a	Istok mix, < 4 mm	0.3793	0.09M buffer	TCE in di water	12.100	90.5	25.0	5.512	0.73	0.55	0.069	0.043	200	GC	4	acetylene	
KF62b	Istok mix, < 4 mm	0.3793	0.045M buffer	TCE in di water	12.100	90.5	25.0	5.512	0.73	0.490	0.012	0.0005	1400	GC	4	acetylene	

* stoichiometric (calculated) fraction of iron that should be reduced. Actual reduction is less, but was not measured in these experiments.
**first order model fit to the acetylene (degradation product) data. TCE removal from solution is additionally affected by adsorption, so not a clear indication of dechlorination.

Table 4. Summary of TCE column experiments

name	sediment	fraction < x mm	reduction	res. time (h)	total time (h)	pore vol.	water source	initial TCE conc. (ppm)	initial TCE conc. (µmol/L)	T (°C)	adsorption Kd (cm^3/g)	adsorption TCE lag by ads.	total TCE removed (fraction)	acetylene generated (fraction)	TCE dechlorination rate rate* (1/h))	TCE dechlorination rate half life (h)	analysis	# points	degradation products	other compounds
KF17a	FL6 < 2 mm	0.3035	100% reduced	73	0 - 235	0 - 3	Ft .L groundwater	0.571	4.36	25.0	0.53	3.5 pv	0.982	>1.0**	0.087	8	GC-MS	5	c.acet., acet, eth.	DCE, vinyl chloride
KF17b	FL6 < 2 mm	0.3035	80% reduced	67	427-622	102-105	Ft .L groundwater	1.200	9.10	25.0	0.53	3.5 pv	0.92	>1.0**	0.036	19	GC-MS	5	c.acet., acet, eth.	DCE, vinyl chloride
KF17c	FL6 < 2 mm	0.3035	55% reduced	102	808-1055	230-234	Ft .L groundwater	1.490	11.35	25.0	0.53	3.5 pv	0.80	1.000	0.025	28	GC-MS	6	c.acet., acet, eth.	DCE, vinyl chloride
KF17d	FL6 < 2 mm	0.3035	50% reduced	83	1100-1400	234-238	Ft .L groundwater	2.040	15.53	25.0	0.53	3.5 pv	0.40	1.000	0.080	88	GC-MS	4	c.acet., acet, eth.	DCE, vinyl chloride
KF23	RM9 <4mm	0.4037	100% reduced	5.8	0 - 216	0-37	Ft .L groundwater	3.090	23.51	25.0	0.90	6.1 pv	0.85	not meas.	0.025	28	GC-MS	4		1,1DCE, 1,2DCE, TCA***
KF38	RM9 <4mm	0.4037	~25% reduced	10.7	0 - 380	0 - 35	Ft .L groundwater	0.951	7.24	10.0	0.966	5.2 pv	0.45	0.000	0.039	18	GC	8	acetylene	DCE
KF39	RM9 <4mm	0.4037	(1/4)100% reduced	12.4	0 - 380	0 - 35	Ft .L groundwater	0.951	7.24	10.0	0.966	5.2 pv	0.13	0.007	0.0140	51	GC	8	acetylene	DCE

* TCE breakthrough data after the lag caused by adsorption used for calculation of the TCE dechlorination rate.
** a value of > 1.0 may represent degradation of other chlorinated compounds in addition to TCE dechlorination
***TCA degradation rate 2.1 h half life; 1,1-DCE not degraded; some evidence that cis-1,2-DCE is degraded

oxidize the sediment. The sediment was expected to remain anoxic for ~450 pore volumes. Two experiments were conducted with 25% reduced sediment and additionally at 10°C to be similar to field-scale conditions of early dithionite injections.

The column experimental system for the TCE degradation studies was designed to minimize mass losses to volatilization and diffusion, because TCE and degradation products had moderate to high vapor pressures. The column influent, consisting of groundwater containing TCE, DCE, and PCE, was contained in a 5-L metalized bag. Influent monitoring over experiments ranging from 200 h to 1400 h showed <3% mass loss of this influent. Effluent was collected in 154 mL anaerobic vials with 10-mm-thick septa tops. The flow rate was measured from the sample volume and elapsed time. An automated switching valve was used to collect the samples over 24 h or 48 h intervals over the 500 h experiment. Materials used in the column system were stainless steel or PEEK, both of which have extremely low permeabilities to organic compounds. Dissolved oxygen was monitored during this experiment with in-line electrodes, as described earlier. Organic compounds were measured in the inlet and effluent samples by GC-MS.

3.2 Experimental Data Quality Control

To ensure the accuracy of the data collected in these bench-scale studies, a percentage of the experiments and sample analysis within experiments were duplicated. In some cases, different types of experiments were used to ultimately determine the same parameter (reducible iron, for example) to ensure the validity of the information obtained.

Batch time-course reduction studies were generally conducted with duplication of dithionite analysis for 10% to 15% of the samples. In addition, measurement points close in time show accuracy of the dithionite analysis. Three model parameters were determined from batch reduction studies: reduction rate, disproportionation rate, and reducible iron. The reducible iron (same value for all experiments as the same sediment was used) was determined from simulation fit to five data sets. The mass of reducible iron was fixed for all other experiments in which reduction and disproportionation rates were determined by simulation fit to one or more data sets.

Column reduction studies were conducted with 20% duplication. Parameters determined from reduction studies included the reducible iron and the reduction rate. Dithionite measurements were made with an automated system at a rate of one per hour, and the point-to-point reproducibility provides an indicator of sample precision. Sediment oxidation studies in columns were conducted with 10% duplication, where the reducible iron was determined from oxygen breakthrough. Because dissolved oxygen breakthrough analysis requires fewer assumptions, it was considered a more accurate method to determine reducible iron than analysis of reduction column experiments.

Sediment oxidation studies conducted in column experiments relied upon accurate dissolved oxygen measurements, which were used to calculate the mass of reduced iron (duplicate measurement of reduction studies). Two in-line dissolved oxygen electrodes connected to separate meters were used with automated 2-point calibration (at 4 h to 8 h intervals) to ensure dissolved oxygen accuracy. Previous experimental studies with these in-line electrodes showed that manual calibrations (likely at a different and variable flow rate) are not considered as accurate as using the automated fluid control system, which injected calibration solutions at the same flow rate as the column effluent. So, to ensure accurate dissolved oxygen measurements over the course of several weeks, an automated system to collect effluent measurements and recalibrate every 4 h to 8 h was used. The calibration from other in-line electrodes (pH, electrical conductivity, Eh) was also achieved with the same fluid system. The two calibration solutions consisted of: 1) oxygen-free water (with continuous He

bubbling through the solution) with an electrical conductivity of 200 μS and a pH of 8.3, and 2) oxygen-saturated water (initial air bubbling, left open to the atmosphere) with an electrical conductivity of 420 μS and a pH of 9.4.

Additional analysis was conducted on sediment and water samples to establish additional information about the redox geochemistry of the Ft. Lewis sediments. Four different types of iron extractions were conducted with duplicate samples for 10% of the samples. For one type of extraction, duplicate analysis was also conducted for all samples. Liquid effluent samples from column reduction and oxidation studies were analyzed for trace metals by Inductively Coupled Plasma Mass Spectrometry (ICP-MS). For 10% of these samples, duplicate analysis and duplicate with a spike of all metals was conducted (duplicate shown in Tables 3 and 4).

Batch and column TCE degradation studies were conducted with duplicate GC or GC-MS analysis of 10% to 15% of the samples. TCE and degradation products were used to determine the TCE degradation rate and relationship between barrier longevity and TCE degradation rate. Because TCE also undergoes adsorption, positive confirmation of TCE dechlorination was not determined from TCE mass loss, but acetylene production (the main degradation product observed). Therefore, quality control of samples used for acetylene analysis were the most important component to assess degradation. For each sample collected from an experiment, duplicate acetylene analysis was conducted on 50% or more of the samples. The concentration of TCE and 1,2-trans-DCE was measured from the liquid effluent, and accuracy was established with an internal standard that had similar volatility. The concentration of the lighter organic compounds such as acetylene was measured in the gas phase in the headspace effluent vials with separate gas standards used to establish calibration.

4.0 Results - Iron Reduction

Batch and column reduction studies were used to develop an understanding of how: 1) iron oxide phases in sediment are reduced by the sodium dithionite/potassium carbonate solution, 2) TCE is dechlorinated by ferrous iron phases, and 3) the reduced sediment reactivity evolves over time as the barrier is slowly oxidized by dissolved oxygen. Batch experimental data and simulations were used to quantify the reduction mechanism (Section 4.1) and reaction rates at different temperatures (Section 4.2). Column experiments were used to assess the spatial variability of iron reduction in different sediment samples in a small-flow system at constant pH (Section 4.3), and in pH varying conditions (Section 4.4). Changes in iron surface chemistry and mobility of other metals during reduction and oxidation were quantified with liquid and solid extraction analysis of metals (Section 4.5). Results of TCE dechlorination studies are discussed in Section 5.

4.1 Sediment Reduction in Batch Systems

The rate of iron reduction and quantity of reduced iron was determined in batch experiments mainly from observations of the rate of disappearance of dithionite. Because dithionite is used for iron reduction (a reaction with a ~5 h half-life) and disproportionation (reaction 4, half-life 27 h), specific proportions of dithionite/iron are needed, and observations of dithionite use at specific time intervals are used. Given that iron reduction is approximately 5x faster than disproportionation, dithionite is used entirely for iron reduction at short times (<5 h), but with greater contact time, dithionite is destroyed proportionally more from disproportionation. To reduce all the iron in the system, dithionite must be added in excess of the reducible iron because of disproportionation use. Sediment reduction experiments can be qualitatively observed from the visual change in sediment color from tan to gray (<0.1 M dithionite) to black (using >0.1 M dithionite). As described in Section 5.5, amorphous and some crystalline Fe^{III} oxide phases that are dissolved and reduced during reduction produce mainly adsorbed Fe^{II} with minor amounts of siderite ($Fe^{II}CO_3$). At high dithionite/pH buffer concentrations in contact with sediment for long periods of time, FeS (black precipitate observed) forms presumably because the high ionic strength prevents Fe^{II} adsorption and provides a source of S-.

A typical experiment at high dithionite concentration (Figure 2a, data points) shows dithionite use for iron reduction with a shallow slope for the first 100 h (iron reduction and some disproportionation), then a much steeper dithionite use slope at >100 h from disproportionation. In contrast, an experiment using low dithionite concentration relative to reducible iron (Figure 2b) shows a single slope of dithionite use, and is not useful to determine the disproportionation rate or the total mass of reducible iron, but can be used to determine the iron reduction rate. During reduction, the sediment visually changes color from tan to gray to black with increasing amount of reduction, so visual inspection shows reduction occurring within hours.

Simulation of the third-order reduction (Equation 1) and first-order disproportionation (Equation 4) over time were used to quantify reducible iron mass and disproportionation/iron reduction rates. Simulation of the experiment at high dithionite concentration (Figure 2a, lines) matches the two slopes of the data. A simulation was additionally made with the disproportionation reaction turned off, which shows the fraction of dithionite used for iron reduction only. Simulations of the low dithionite concentration experiment (Figure 2b) with and without disproportionation are nearly the same because the dithionite is all used up at short times for reduction. The experiment at

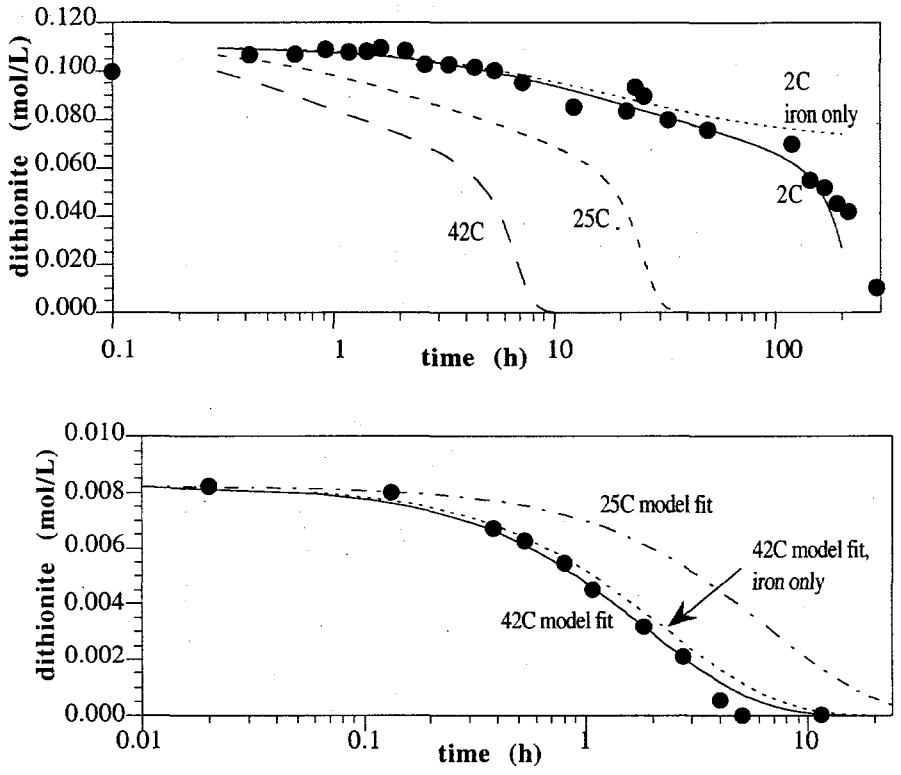

Figure 2. Batch experiment of Ft. Lewis sediment reduction by dithionite at different concentrations. Dithionite use at short time (<100 h) is mainly due to iron reduction and at >100 h is mainly due to disproportionation. Experiments conducted starting with 0.11 mol/L sodium dithionite a) and 0.008 mol/L sodium dithionite b).

low concentration can be visually shown by data and simulations of the first 50 h of the high concentration experiment (Figure 2a). There is little use of dithionite for disproportionation in this time range. The mass of iron in all these batch reduction experiments was determined from a series of experiments varying the relative dithionite/iron proportions (Appendix A, experiment KF32) and simulation fit to these five experiments with a single mass of reducible iron. These experiments were also useful to indicate that iron reduction is somewhat more dynamic than can be described with a single reduction reaction. One experiment with very low dithionite concentration reduced only 10% of the reducible iron and that reduction rate was much faster than when all the iron was reduced. This observed range of reduction rate may be caused by a range of Fe^{III} phases: amorphous iron oxides being more easily reduced and crystalline iron oxides being reduced more slowly.

An understanding of the dynamics of iron reduction and disproportionation is useful to upscale the process to the field scale. The iron reduction reaction (rxn 1) is a third-order reaction theoretically (solid line, Figure 3a), but a first-order reaction (rxn 3) can approximate dithionite use in some cases (i.e., over the first half of the reduced iron, dashed line in Figure 3a).

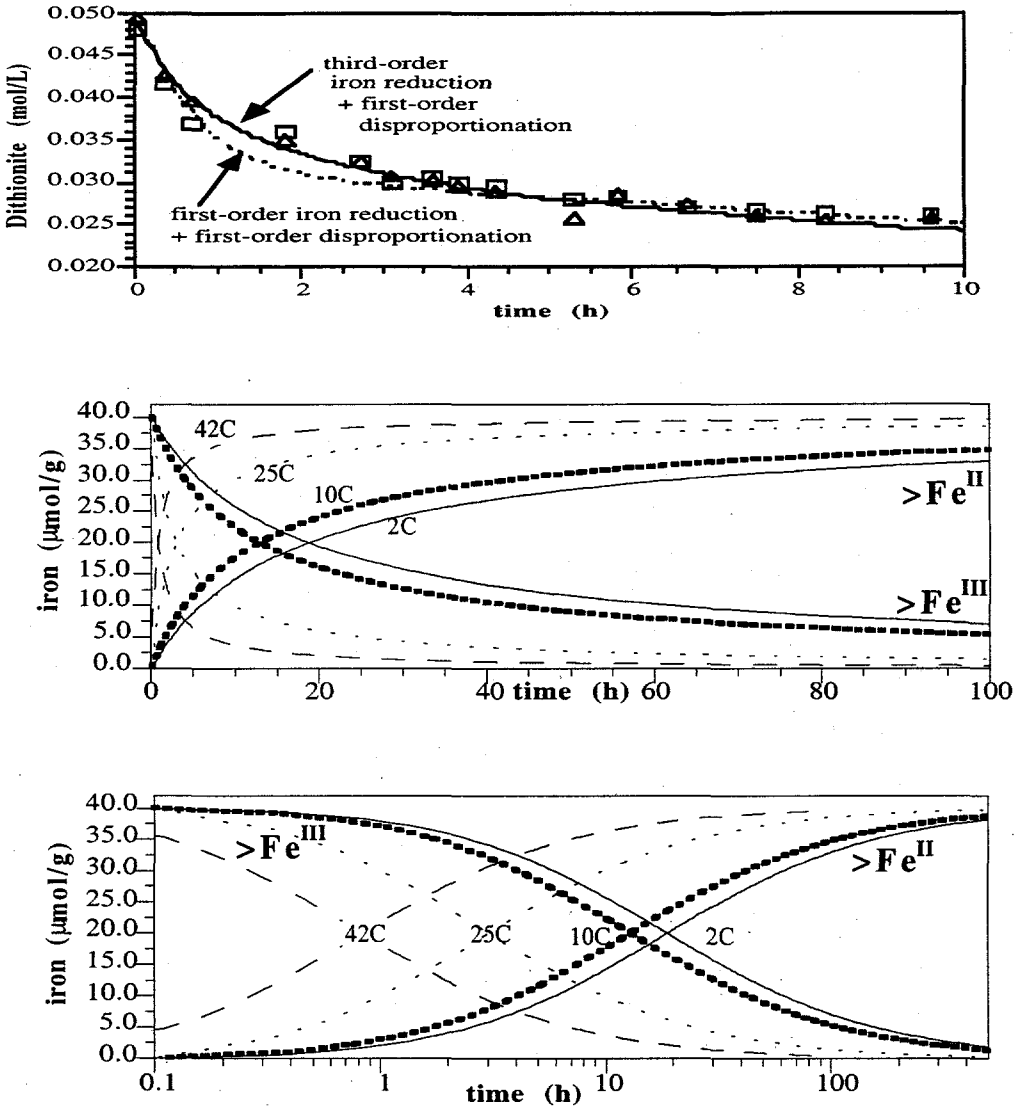

Figure 3. Simulation of iron reduction with: a) third versus first-order iron reduction fit to data, b) simulated iron reduction fraction at different temperatures with linear time, and c) log time.

Although the short time scale (<2 h) can be fit with a first-order reduction reaction, the model overall underpredicts dithionite use (and overpredicts the amount of reduction) over long periods of time. This data set (Hanford 100D area sediment) was initially fit with third-order reduction (4.5 h half-life) and disproportionation (27 h half-life) reactions. The data were then fit with first-order reduction (2 h half-life, dashed line) without allowing the disproportionation rate to change. This can be incorrectly compensated for by increasing the disproportionation reaction rate to an 18-h half-life. The result is an artificially low mass of reducible iron, as the actual third-order iron reduction dynamics continue to reduce iron even in tens of hours Figure 2a). Based on simulations of experiments at different temperature (described below), the fraction of reduced iron is predicted in experiments (Figures 3b and 3c). These simulations show that at 25°C, the iron reduction half-life is 3.1 h, but 10% of the iron is still not reduced after 50 h. The implication is that enough reaction time is needed in the field to allow for the dithionite to reduce sediment.

4.2 Temperature Effects on Iron Reduction

Batch iron reduction experiments were conducted at temperatures from 2°C to 42°C to be able to predict iron reduction and disproportionation rates in different aquifer conditions. Simulation of reactions made to 10 data sets (Appendix A) show that iron reduction (Figure 4a) and disproportionation (Figure 4b) rates changed in a predictable relationship with temperature. Iron reduction averaged 2.27x decrease with a 10°C decrease, or reduction is 4.37x slower at 10°C than at 25°C. The change in the disproportionation rate over temperature was 3.04x decrease in rate for each 10°C decrease (7.00x slower at 10°C versus 25°C). The third-order reduction rates and first-order disproportionation rate parameters shown (Figure 4a and 4b) were used to simulate iron reduction and disproportionation at different temperatures (Figure 3b and 3c).

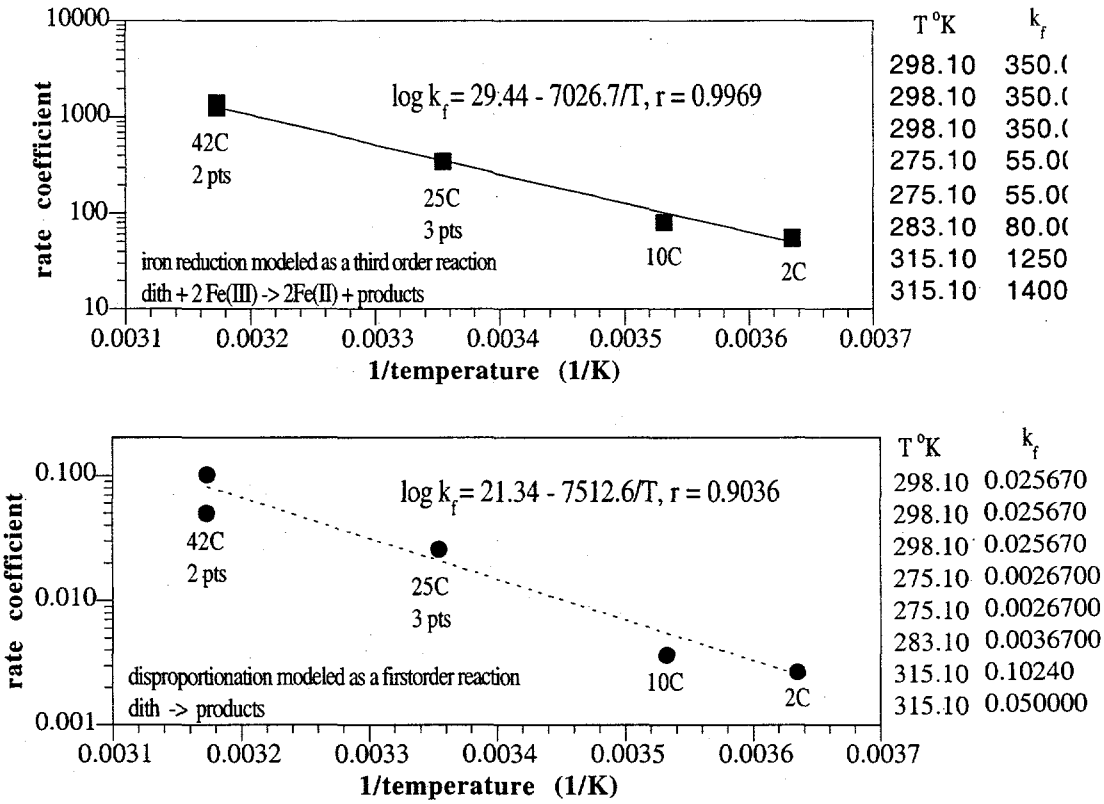

Figure 4. Change in a) iron reduction, and b) disproportionation over temperature from 2°C to 42°C

Contact time between dithionite and sediment needed at different temperatures is needed to balance against other field-scale problems such as dense plume settling. For the purpose of the field-scale injections, to achieve 80% reduction of iron, 20 h of contact time is needed at 25°C, but 100 h is needed at 12°C (ambient aquifer temperature). Because 100 h of reaction time is difficult to achieve due to fast advective flow and dense plume sinking (of a high dithionite concentration), it is recommended that injections at Ft. Lewis be heated (18°C to 21°C).

In addition to the reaction time, the proportions of dithionite needed for iron reduction and disproportionation at specific temperatures and contact times are needed at the field scale due to the cost of chemicals. Over time, a greater fraction of dithionite is used for disproportionation, as previously shown (Figure 2a). The additional amount of dithionite needed for disproportionation

was calculated (Table 5) at 10°C and 25°C, based on reaction rates in experiments (Table 1, Appendix A, Figure 4a and 4b). A value greater than 1.0 for the multiplier for disproportionation is the additional fraction of dithionite mass needed for disproportionation. These values range from 1.10 when 50% of the iron is reduced to over 4.00 to reduce 99+% of the iron. The competition between iron reduction and disproportionation for dithionite mass can be clearly seen on a log time plot (Figure 2a), which clearly shows that the first 80% of the iron can be efficiently reduced with little dithionite lost to disproportionation (multiplier is 1.3, regardless of temperature). It is increasingly less efficient to reduce >80% of the iron, due to the large dithionite use for disproportionation.

Table 5. Fraction of dithionite use for iron reduction and disproportionation at 10°C and 25°C

10°C			25°C		
contact time (h)	fraction iron reduced	multiplier for disprop.*	contact time (h)	fraction iron reduced	multiplier for disprop.*
20	0.43	1.10	7	0.516	1.09
30	0.55	1.19	10	0.656	1.12
50	0.67	1.20	15	0.749	1.19
75	0.80	1.24	20	0.879	1.21
100	0.86	1.33	25	0.908	1.26
150	0.937	1.60	30	0.937	1.37
200	0.966	2.30	35	0.948	1.56
250	0.989	2.90	40	0.966	1.94
300	0.992	4.30	50	0.995	2.42

* multiplier = dithionite used to reduce iron plus disproportionation, where 1.00 is defined at each contact time for iron reduction only. Assumes dithionite is in excess of the reducible iron.

4.3 Sediment Reduction and Oxidation in Columns

Column experiments in which Ft. Lewis sediment is reduced with the dithionite/pH buffer solution then oxidized with oxygen-saturated water were conducted to determine reducible iron mass and reduction/oxidation rates. Reduction information determined in columns is more applicable to the field scale than to results of batch experiments. Reaction rates in column and field systems are typically slower than rates observed in batch systems, due to some particle breakup in batch systems (i.e., artifacts), and some slow physical access to sites in columns that does not occur in batch. Although column experiments incorporate some aspects of the field scale such as the advective flow of mobile solutes through the reactive immobile surfaces, these small systems are not representative of all aspects of the field scale, as discussed in this section.

Calculation of the reducible iron from column reduction experiments involves mass balance calculations of both iron reduction and disproportionation reactions. The differing time scales of the reactions can be observed from dithionite breakthrough (Figure 5a and 5b). By injecting dithionite at a flow rate such that the residence time (4 h, Figure 5a) of dithionite is similar to the reduction rate half-life (5 h) results in approximately half of the dithionite consumed in the reduction of iron (Figure 5a). If the iron mass is large relative to the dithionite concentration, the dithionite concentration in the effluent would remain constant. However, with the limited number of reducible iron oxides in natural sediments used, the dithionite concentration increases over time as less iron is reduced (Figure 5a). At a slower flow rate (i.e., longer residence time, Figure 5b), more dithionite is consumed. However, disproportionation (half-life 27 h) consumes enough mass in this 5-day experiment to result in decreasing long-term dithionite concentration.

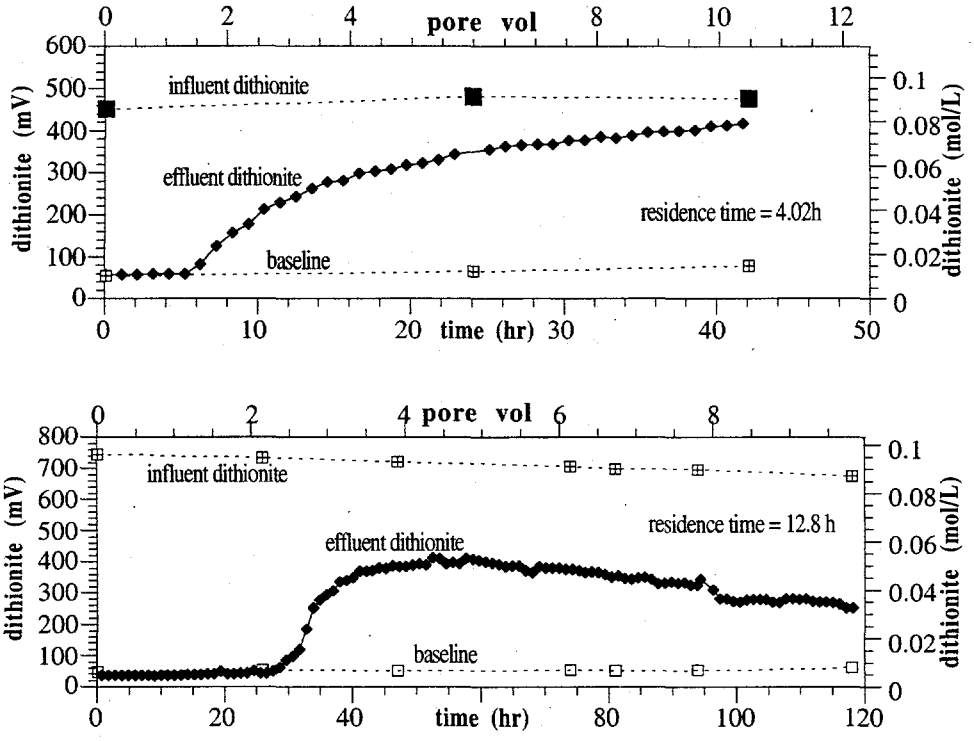

Figure 5. Dithionite influent and effluent in a reactive sediment column with a sediment-dithionite contact time of: a) 4.0 h, and b) 12.8 h.

Reduction experiments (27) showed that the sediments from the Ft. Lewis reduction field site averaged 62.8 ± 39.7 μmol/g (0.351 ± 0.222%) of reducible iron (Table 2). This 63% standard deviation is large, and indicates locations within the aquifer with very little iron and other areas with ~2x the average amount of reducible iron. Well RM-9 averaged 49.1 ± 3.25 μmol/g (0.274%) of reducible iron (3 experiments). Column experiments were also conducted with sediment samples from six U.S. Geological Survey wells. All 14 reduction experiments averaged 45.6±33.3 μmol/g (0.255 ± 0.186%) of reducible iron (Appendix B), meaning that the location where the reduction experiment is taking place averages 30% greater iron than the field experimental site.

The rate of iron reduction in columns can be calculated from dithionite breakthrough curves and was compared with batch iron reduction. The rate of iron reduction is calculated using the steady-state concentration of dithionite in the effluent before the system is site limited, meaning the dithionite concentration at the time between steep and shallow dithionite breakthrough. At a residence time of 4.0 h, this occurred at 10 h (Figure 5a), and with a 12.8 h residence time, this occurred at 36 h (Figure 5b). The column reduction experiments averaged 6.82 ± 2.46 h for the reduction half-life, as opposed to 3.1 h for six batch experiments (25°C). Reduction in columns is likely slightly slower due to physical access limitations to sites, which does not occur in batch systems.

Reduced sediment columns are then oxidized with oxygen-saturated water to provide an additional measure of the amount of reduced iron as well as a measure of the oxidation rate of the reduced iron. The reducible iron mass from these oxidation experiments is considered the most accurate at reflecting the mass of reduced iron because only iron oxidation reactions (rxn 10 and 11) are occurring. Oxidation column experiments were also used to test the prediction of reduced barrier longevity and quantify sediment oxidation rates. A total of 11 oxidation experiments were conducted on reduced Ft. Lewis sediment that ranged in time from 70 h to 500 h. In some cases, the

experiments were conducted long enough to completely oxidize the sediment, while other experiments were stopped before the sediment was completely oxidized. In all cases, the oxygen breakthrough curves were used to calculate the mass of reduced iron in the column that consumed the oxygen. These values were compared with the mass of reduced iron calculated from dithionite breakthrough curves indicated that 50% to 100% of the iron was oxidized in the experiments.

The size and shape of the oxygen breakthrough data from columns is used to calculate the mass of reduced iron and provide oxidation rate information (all experiments in Appendix C). In one experiment (Figure 6a), although oxygen saturated water is being injected into the column, the effluent is oxygen free for the first 260 pore volumes due to oxygen consumption by the ferrous iron. In this case, the oxygen breakthrough curve shape is can be modeled with a single type of site being oxidized (i.e., the shape of the breakthrough curve has a single shape). In contrast, a different experiment run at faster velocity reveals a change in slope (Figure 6b). The rapid rise in

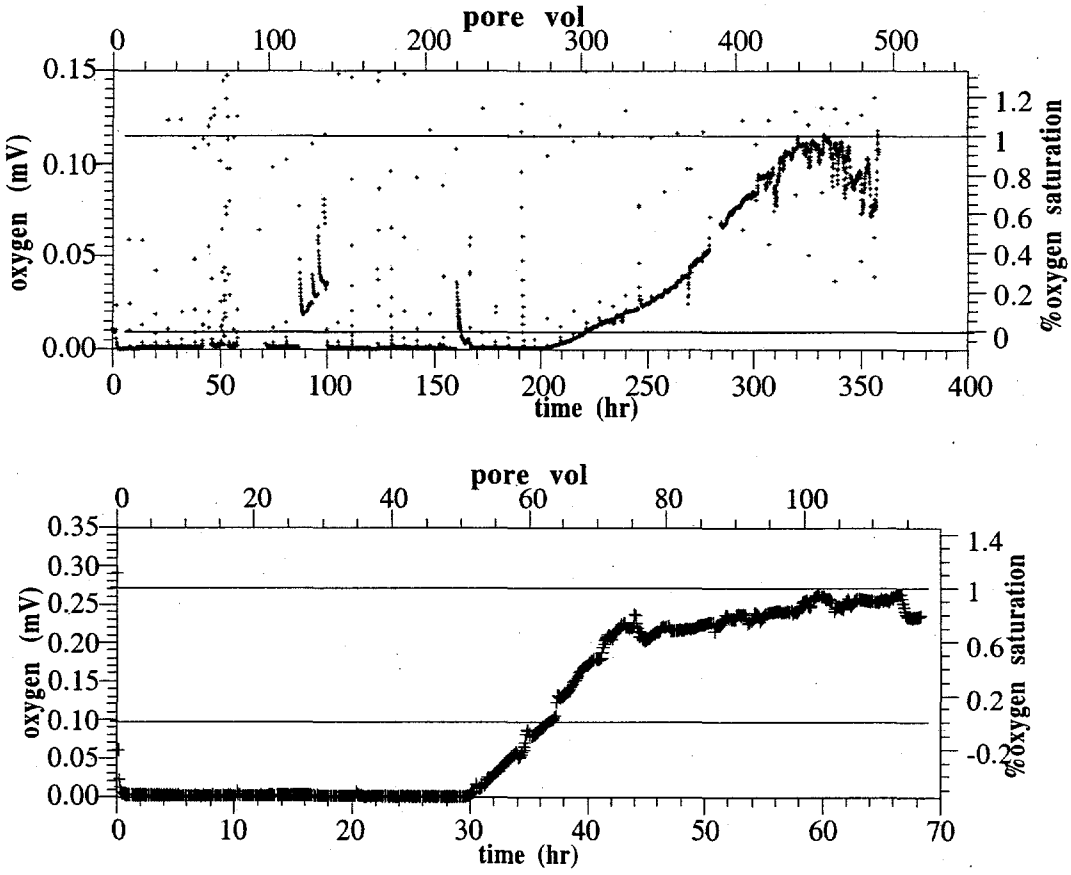

Figure 6. Oxidation of a reduced sediment column with dissolved oxygen in water with residence time of: a) 0.72 h in a highly reduced sediment column, and b) 0.58 h in a partially reduced sediment column.

oxygen levels through 3/4 of saturation, then a fairly slow increase to saturated levels indicate a fraction of sites that are slow to oxidize in the relatively short time scale of this experiment (i.e., 70 h). The oxidation of reduced iron in the natural sediment appears to be more complex than a single oxidation reaction, and is likely controlled by both chemical and physical processes, as shown by results of a different redox study in the Hanford 100D sediments. Physical rate limitations were shown by breakthrough curve tailing of dissolved oxygen in nonreduced sediment, indicating diffusional limitations accessing a fraction of the pore volume. Oxygen breakthrough data at shorter residence times in that study showed multiple slope changes, indicating quickly and slowly oxidizing sites. It is hypothesized that the fast oxidizing sites represent adsorbed ferrous iron, and the slowly oxidizing sites represent siderite, as discussed in the next section for the Ft. Lewis sediments.

The applicability of batch and column studies to the field scale depends upon accounting for large-scale chemical and physical variability. Although column experiments incorporate some aspects of the field scale such as the advective flow of mobile solutes through the reactive immobile surfaces, these small systems are not representative of all aspects of the field scale. Groundwater systems contain: a) natural physical and chemical heterogeneities, b) unique flow fields, c) different temperature, and d) a wide range of porous media size that are not represented in column experiments. Because of the small (1 cm diameter x 10 cm length; up to 10 cm diameter x 50 cm length) size of columns, natural sediment from cores is sieved and repacked, so does not incorporate natural heterogeneity patterns (but rather point samples). The chemical spatial variability of the sediment was addressed in this study by statistical variability in experiments with sediments from different boreholes. Because of the small size of column systems, natural sediment was sieved, and the <2 mm or <4 mm fraction was used in experiments. It was assumed that the surface area of larger particles was minimal and nonreactive, which may slightly underestimate the fraction of reducible iron in the sediment. Intermediate-scale experiments currently in progress use <2.5 cm fraction, so will be much closer to field sediment. Because some cobbles in the gravel units are >10 cm, a fully representative experiment would have to include sediment from a large borehole (>10 cm diameter), which is not cost effective. Some column experiments were conducted at groundwater temperatures (11°C), but most were conducted at 25°C. Differences in reduction over temperature were discussed previously in Section 4.2.

4.4 Sediment Reduction and pH Change

To determine the concentration of pH buffer needed to efficiently reduce sediment without resulting in significant iron mobility, the pH and effluent iron was measured during reduction in columns. The relationship between the pH buffer concentration used during dithionite treatment and the resulting reactivity of sediment was examined in a series of column experiments in which the potassium carbonate concentration was varied (4x, 3x, 2x, 1x, 0.5x) relative to the dithionite concentration. During reduction in columns, the pH and aqueous iron concentration were measured in the effluent water. The influent pH (dithionite solution) is 10.5 to 11.0, and with a high buffer concentration (i.e., 4x or 3x times the 0.09 mol/L sodium dithionite), the effluent pH is typically constant at 9.5 to 10.0 (Figure 7a). At lower pH buffer concentrations, reduction and disproportionation reactions (reactions 1, 2, 4) produce H^+ that is beyond the sediment and solution pH buffering capacity, so the pH drops at the reactive front. With Ft. Lewis sediments, with 0.18 mol/L K_2CO_3 (2x dithionite) the pH dipped to 8.8, with 0.09 mol/L K_2CO_3 (1x) the pH dipped to 7.7, and at 0.045 mol/L K_2CO_3 (0.5x) the pH dipped and stayed at 2.3. In a previous study with Hanford 100D sediments, 4x and 2x buffer concentrations showed no pH change, but the 1x buffer experiment showed a pH drop to 3.3. By itself, the pH data indicates little effect of changing buffer concentration except at very low (0.5x) buffer concentration. However, the effect on the mobility of iron and the amount of iron reduced was significant.

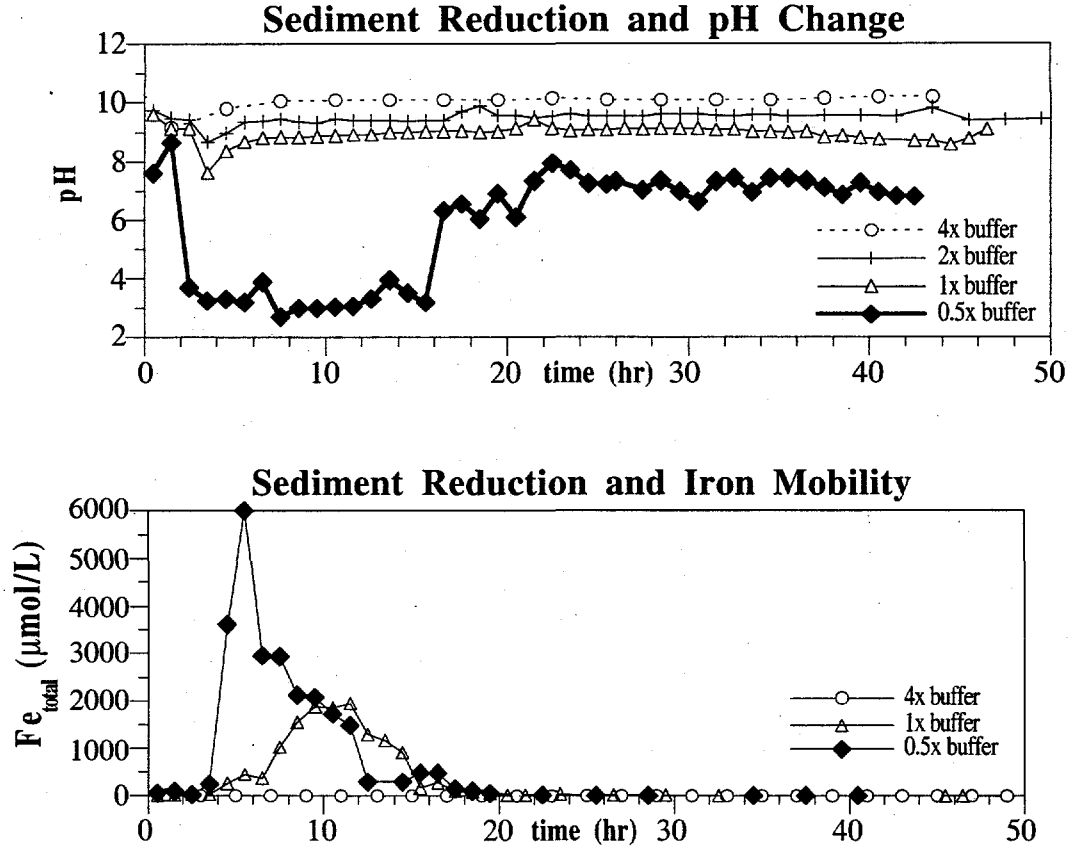

Figure 7. Sediment reduction column experiments at different potassium carbonate concentrations relative to sodium dithionite concentration with the resulting pH and the total aqueous iron concentration measured in effluent samples.

Iron mobility out of the column was a direct function of how low and how long the pH of the sediment remained acidic (Figure 7b). With 0.36 mol/L K_2CO_3 (4x dithionite), the total aqueous iron in the effluent (Fe^{II}) averaged 0.036 mg/L with the first sample at 1.25 mg/L. The total mass of iron in the effluent was 0.021% of the iron in the column. This result was consistent with iron extractions of the sediment, showing very little movement of iron in these highly pH buffered systems where any Fe^{II} produced is highly adsorbed to sediment surfaces. However, because Fe^{II} is stable in solution at a pH below 8.0, experiments in which the pH dropped showed some iron mobility. With 0.09 mol/L K_2CO_3 (1x dithionite; triangles in Figure 7b), where the pH dipped briefly to 7.7 (Figure 7a), the aqueous Fe^{II} was 0.94% of the reducible iron in the column. Finally, with 0.045 mol/L K_2CO_3 (0.5x dithionite; diamonds in Figure 7b), where the pH remained <3.0 for 12 h, the advection and reduction process removed 3.3% of the reducible iron in the column. There was significant precipitate forming in the tubing of the low pH experiment, as iron was oversaturated and was oxidizing to insoluble Fe^{III} oxides. The use of injecting aqueous Fe^{II} species at the field scale at low pH has been observed ineffective due to iron mobility (Seaman et al. 1999).

The effectiveness of the reduction at different pH buffers was measured by oxidizing columns (to measure reduced iron) and conducting TCE degradation experiments. In all the reduction experiments, sediment columns were treated with the same concentration of sodium dithionite (0.09 mol/L)

at the same flow rate for 45 h (i.e., differed only in the buffer concentration). Although the pH drop was small in most cases, and the mass of iron removed from columns was small, there was a significant difference in the mass of reduced iron in columns. Using the maximum buffer (4x), 85% of the reducible iron was reduced (i.e., more is reduced with longer contact time), but even with slightly less buffer (3x), only 50% of the iron was reduced. The resulting TCE degradation half-life indicated even worse performance, with a 200-h half-life for the 0.09 mol/L buffer (1x) and a 1400-h half-life for the 0.045 mol/L (0.5x) buffer (Appendix D, KF62a and 62b). Comparing results to those of the partial reduction studies, these low degradation rates indicate the 1x buffer reduction was <27% reduced, and the 0.5x buffer reduction was ~11% reduced (Table 6). The general conclusion is that a high buffer concentration is needed to efficiently reduce iron species for TCE dechlorination.

Table 6. Summary of reduction experiments with different pH buffer concentration

buffer concentration (mol/L)	iron reduced (μmol/g)	iron reduced (fraction)*	TCE degradation half-life (h)
0.36 (4x dithionite conc.)	137.0	85	<16**
0.27 (3x)	79.2, 76.3	49, 47	–
0.09 (1x)	58.2	37	200
0.045 (0.5x)	41.5	26	1400

*based on 159 μmol/g as the maximum reducible iron measured for this sediment (Table 2).
**16-h half-life was measured with 53% reduced sediment, and a 1.2-h half-life was measured with 100% reduced sediment (Table 12).

4.5 Geochemical Changes During Redox

In addition to monitoring dithionite concentration during reduction and dissolved oxygen concentration during oxidation, other solution and surface constituents were monitored to address specific issues related to the impact of the redox manipulation of sediments: 1) changes in solid phase iron mineralogy, and 2) solution phase metals mobility. Iron extractions were conducted on unreduced, reduced, and reduced/oxidized sediments to specifically determine the changes in iron phases that occur during reduction and subsequent oxidation of the sediment. This information was used to determine if the dithionite treatment would leach significant iron mass from one area to another and if sediment can be effectively re-reduced. To assess the potential migration of heavy metals that could occur as the natural (oxic) sediment is reduced, the mobility of metals was monitored during sediment reduction and oxidation in columns.

Iron extractions conducted on the unaltered Ft. Lewis aquifer sediment (Table 7) had an average of 0.40 ± 0.29% iron oxides and carbonates, with a range of 0.05% to 1.05% for 22 sediment samples from boreholes. The Fe^{III} phases accounted for 58% to 90% of the total, with the remainder Fe^{II} phases. Measurable Fe^{III} phases included 25% amorphous and ~60% crystalline, whereas measurable Fe^{II} phases appeared to be siderite ($Fe^{II}CO_3$). As a check of the accuracy of the total Fe^{III} + Fe^{II} extractant method (with ferrozine analysis), the extractant water was analyzed for Fe and Mn by ICP-MS (Heron et al. 1994). Results indicated the iron values measured by ferrozine were accurate and that only 3.7% of the reduced phases were Mn (i.e., iron phases were by far the dominant redox phases). The extraction for total Fe^{II} oxides showed that 50% to 60% of the phases were not accounted for in the amorphous and crystalline Fe^{III} oxide extractions (Table 8). Unaccounted for phases may include Fe^{III} in clay. Samples were submitted for identification of clay phases by x-ray diffraction, but the mass of clay was too small for analysis. Phase separations concentrating the clay phases would have to be conducted, followed by Mossbauer spectroscopy to identify iron mass and oxidation states.

Table 7. Iron analysis of sediment samples

sediment name	%<xmm	redox treatment		Iron (II) Extractions 1 1M CaCl2 (µmol/g)	2 0.5M HCl (µmol/g)	3 5.0M HCl (µmol/g)	Iron (III) Extractions 2 0.5M HCl (µmol/g)	3 5.0M HCl (µmol/g)	4 NH2OH.HCl (µmol/g)	6 DCB (µmol/g)	7 Ti-EDTA (µmol/g)	Fe^{II} in sediment sample: Fe^{II} CO$_3$ + FeS [#2-#1] (µmol/g)	Fe^{II} ion exch. [#1] (µmol/g)	total Fe^{II} [#3] (µmol/g)	%Fe g Fe/g sed	Fe^{III} in sediment sample: am.-Fe^{III} oxides [#2] (µmol/g)	cryst.-oxides [#4-#2] (µmol/g)	reducible Fe^{III} [#7] (µmol/g)	total Fe^{III} [#3] (µmol/g)	%Fe (g Fe/g sed)	total Fe^{II} + Fe^{III}: sediment sample (µmol/g)	%Fe (g Fe/g)	whole sediment (µmol/g)	%Fe (g Fe/g)
				-for < 2 mm sediment fraction-			--------for < 2mm sediment fraction---------					--------for < 2mm sediment fraction--------				---------- for < 2mm sediment fraction ----------							for whole sediment	
FL-1, <2mm	0.4093	untreated			16.1	48.2		32.8	410.4		0.0	16.1		48.2	0.269	32.8		0.0	410.4	2.29	458.6	2.56	187.7	1.05
FL-6, <2mm	0.3035	untreated			13.8	52.4		37.9	439.9		0.0	13.8		52.4	0.293	37.9		0.0	439.9	2.46	492.3	2.75	149.4	0.83
FL-3, <2mm	0.0889	untreated			15.8	72.5		38.4	506.8		0.0	15.8		72.5	0.405	38.4		0.0	506.8	2.83	579.3	3.24	51.50	0.29
FL-4b<2mm	0.1315	untreated			13.4	64.4		34.2	468.5		0.0	13.4		64.4	0.360	34.2		0.0	468.5	2.62	532.9	2.98	70.10	0.39
149, 40', <2mm	0.2084	untreated			14.5	80.7		47.9	677.1		0.0	14.5		80.7	0.451	47.9		0.0	677.1	3.78	757.8	4.23	157.9	0.88
133, 40', <2mm	0.1683	untreated		0.02	13.3	22.2 81.5	85.7	42.5	573.2	23.9	170.1 0.0	17.7	0.0	81.5	0.455	85.7	106.0	0.0	573.2	3.20	654.7	3.66	110.2	0.62
133, 40', <2mm	0.1683	reduced	9 pv; 0-5 cm	0.03	31.9	39.9 60.5	47.6	38.3	464.7			35.9	0.0	60.5	0.338	47.6			464.7	2.60	525.2	2.93	88.39	0.49
133, 40', <2mm	0.1683	reduced	9 pv; 5-10 cm		64.3	60.2	15.3	22.2		27.1	134.6	62.3					115.9							
133, 40', <2mm	0.1683	reduced	9 pv; 10-15 cm	0.04	53.2	56.1 83.4	45.4	38.3	492.8			54.6	0.0	83.4	0.466	45.4			492.8	2.75	576.2	3.22	97.0	0.54
133, 40', <2mm	0.1683	reduced	5 pv; 0-1 cm	154.8									154.8											
133, 40', <2mm	0.1683	reduced	5 pv; 5-6 cm	70.43									70.4											
133, 40', <2mm	0.1683	reduced	5 pv; 10-11 cm	77.44									77.4											
133, 40', <2mm	0.1683	reduced	5 pv; 14-15 cm	82.00									82.0											
133, 40', <2mm	0.1683	untreated	5 pv; 10-15 cm																					
133, 40', <2mm	0.1683	reduced/oxidized	5 pv; 10-15 cm								806.7							806.7						
133, 40', <2mm	0.1683	reduced/oxidized	300 pv, 0-2 cm	0.028	38.6	68.8 56.9	75.0	73.8	474.6			53.7	0.028	56.9	0.318	75.0			474.6	2.65	531.5	2.97	89.45	0.50
133, 40', <2mm	0.1683	reduced/oxidized	300 pv, 11-15 cm		24.3	31.1	72.2	61.2		64.1	216.8	27.7		72.2	150.1									
133, 40', <2mm	0.1683	reduced/oxidized	600 pv, 0-5 cm	0.015	30.7	37.1 64.8	69.6	60.4	526.7			33.9		64.8	0.362	69.6			526.7	2.94	591.5	3.30	99.55	0.56
133, 40', <2mm	0.1683	reduced/oxidized	600 pv, 10-15 cm	0.026	27.2	33.3 90.1	52.8	44.1	541.8							52.8			541.8	3.03				
RM1, 59', <2 mm	0.4909	untreated			12.8	36.6		5.00	46.6	5.2	7.9	12.8		36.6	0.204	5.0	2.9		46.6	0.260	83.2	0.46	40.84	0.23
RM1, 59', <2 mm	0.3463	untreated			21.5	32.8		27.2	52.6	13.3	22.6	21.5		32.8	0.183	27.2	0.0		52.6	0.294	85.4	0.48	29.57	0.17
RM1, 59', <2 mm	0.4468	untreated			40.5	38.7		45.1	57.2	22.7	21.1	40.50		38.7	0.216	45.1			57.2	0.319	95.9	0.536	42.85	0.24
RM2, <2 mm	0.3198	untreated			22.6	33.4		23.8	85.8	16.5	21.6	22.60		33.4	0.187	23.8	0.0		85.8	0.479	119.2	0.666	38.12	0.21
RM2, <2 mm	0.2476	untreated			20.6	28.7		28.7	57.2	13.3	15.3	20.60		28.7	0.160	28.7	0.0		57.2	0.319	85.9	0.480	21.27	0.12
RM2, <2 mm		untreated			23.7	20.6		11.3	37.0	14.4	18.5	23.70		20.6	0.115	11.3	7.2		37.0	0.207	57.6	0.322		
RM3, <2 mm	0.226	untreated		0.305	38.6	56.5		0.0	8.8	9.5	16.6	38.30	0.305	56.5	0.316	0.0	16.6		8.8	0.049	65.3	0.365	14.76	0.08
RM3, <2 mm		untreated		0.327									0.327											
RM4, <2 mm	0.1978	untreated			23.3	34.0		15.4	61.8	13.0	21.4	23.30		34.0	0.190	15.35	6.05		61.8	0.345	95.8	0.535	18.95	0.11
RM4, <2 mm	0.1525	untreated			14.1	23.2		30.3	31.6	14.9	24.0	14.10		23.2	0.130	30.3	0.0		31.6	0.176	54.8	0.306	8.36	0.05
RM4, <2 mm		untreated, anerobic		0.335	26.6	37.4		34.7	46.2	16.0	23.6	26.27	0.335	37.4	0.209	34.7	0.0		46.2	0.258	83.6	0.467		
RM4, <2 mm		untreated, anerobic		0.402	19.7	30.5		35.6	48.7	16.0	18.9	19.30	0.402	30.5	0.170	35.6	0.0		48.7	0.272	79.2	0.442		
RM4, <2 mm	0.2832	untreated			16.9	31.0		25.0	53.6	16.1	20.3	16.90		31.0	0.173	25.0	0.0		53.6	0.299	84.6	0.472	23.96	0.13
Istok mix, < 4 mm	0.3793	0.0% reduced		0.017	7.88	93.0		10.3	143.3			7.86	0.017	92.97	0.519	10.35			143.3	0.800	236.3	1.320	89.63	0.50
Istok mix, < 4 mm	0.3793	4.0% reduced		1.66									1.66											
Istok mix, < 4 mm	0.3793	4.0% reduced		2.64									2.64											
Istok mix, < 4 mm	0.3793	4.0% reduced		2.05									2.05											
Istok mix, < 4 mm	0.3793	4.0% reduced		2.79									2.79											
Istok mix, < 4 mm	0.3793	11.1% reduced		2.73									2.73											
Istok mix, < 4 mm	0.3793	11.1% reduced		2.88									2.88											
Istok mix, < 4 mm	0.3793	11.1% reduced		2.52	51.3	104.0		0.04	56.0			48.76	2.52	104.0	0.581	0.04			56.0	0.313	160.0	0.894	60.69	0.34
Istok mix, < 4 mm	0.3793	27.4% reduced		3.53									3.53											
Istok mix, < 4 mm	0.3793	27.4% reduced		3.31									3.31											
Istok mix, < 4 mm	0.3793	27.4% reduced		3.41									3.41											
Istok mix, < 4 mm	0.3793	27.4% reduced		3.18									3.18											
Istok mix, < 4 mm	0.3793	33.4% reduced		4.59									4.59											
Istok mix, < 4 mm	0.3793	33.4% reduced		4.47									4.47											
Istok mix, < 4 mm	0.3793	38.7% reduced		4.50	53.66	150.7		0.00	68.40			49.16	4.50	150.68	0.842	0.00			68.4	0.382	219.1	1.224	83.10	0.46
Istok mix, < 4 mm	0.3793	43.8% reduced		5.08									5.08											
Istok mix, < 4 mm	0.3793	43.8% reduced		7.01									7.01											
Istok mix, < 4 mm	0.3793	43.8% reduced		4.81									4.81											
Istok mix, < 4 mm	0.3793	43.8% reduced		6.90									6.90											
Istok mix, < 4 mm	0.3793	52.6% reduced		10.57									10.57											
Istok mix, < 4 mm	0.3793	52.6% reduced		11.62									11.62											
Istok mix, < 4 mm	0.3793	52.6% reduced		11.04									11.04											
Istok mix, < 4 mm	0.3793	52.6% reduced		9.80									9.80											
Istok mix, < 4 mm	0.3793	52.6% reduced		9.08	60.49	194.2		0.11	84.10			51.41	9.08	194.20	1.085	0.11			84.1	0.470	278.3	1.554	105.56	0.59
RM1, 51', < 4 mm	0.3354	100% reduced		36.05									36.05											
RM1, 51', < 4 mm	0.3354	100% reduced		33.14									33.14											
RM1, 51', < 4 mm	0.3354	100% reduced		33.40									33.40											

Table 8. Summary of iron oxide phases changes during reduction and oxidation

sediment	total Fe^{II}	total Fe^{III}	Fe lost	ads. Fe^{II}	$Fe^{II}CO_3$	am-Fe^{III}	crystalline Fe^{III}	Other Fe^{III}
untreated	12%	88%	0%	0%	3%	13%	16%	59%
reduced 9pv	21%	75%	3%	15%	6%	7%	17%	50%
red./ox 600pv	9%	80%	10%	6%	6%	10%	23%	58%

Detailed iron extractions conducted on a fully reduced sediment showed a decrease in Fe^{III} phases (~15%) and an increase in Fe^{II} phases (~12%), although there was considerable variability in the results. One sediment (well 133, 40 ft depth) showed that the dithionite reduction resulted in the amorphous Fe^{III} oxides decreasing by half (~40 μmol/g), but showed no measurable decrease in the crystalline Fe^{III} oxides. The corresponding increase in Fe^{II} oxides was greater, with siderite increasing by 30 μmol/g and ion exchangeable (i.e., adsorbed) Fe^{II} increasing by 154 μmol/g. This was not unexpected, as not all Fe^{III} phases are accounted for in extractions. Corresponding reduction from column experiments in which sediments were oxidized indicated 153 μmol/g for this sediment, so it appears that adsorbed Fe^{II} was the main Fe^{II} phase created by dithionite reduction (80% to 100%), with minor amounts of siderite (Table 8).

Iron extractions conducted on sediment that was reduced, then oxidized indicated a general increase in Fe^{III} phases (~5%) and a decrease in Fe^{II} phases (11%; Table 8). The adsorbed Fe^{II} appeared to decrease significantly, although siderite did not decrease or decreased to some extent for some sediments. The decrease in Fe^{II} phases (11%) was greater than the corresponding increase in Fe^{III} phases (5%), although there was considerable variability at these low iron concentrations. Extractions also indicated that there may have been a 3% loss in total iron during reduction and a 10% during 600 pore volumes of subsequent oxidation (relative to the iron in untreated sediment. These values for iron mass loss are considerably greater (and suspect) compared to the accurate analysis of iron in aqueous samples during reduction (Section 4.4) in which 0.021% iron was present in the effluent for most reductions (4x buffer concentration). The iron phase changes reported for Ft. Lewis sediments are similar to that observed for Hanford sediments. Re-reduction experiments have been conducted with Hanford sediments confirmed similar mass of reducible iron when re-reduced, indicating little overall migration of iron and zones can be re-reduced with nearly the same efficiency.

Detailed iron extractions were also conducted on sediments that were partially reduced for comparison to reduced iron measurements by dissolved oxygen column experiments. Results showed that the various iron extractions generally showed a trend of increasing Fe^{II} phases and decreasing Fe^{III} phases, but these were not as accurate as the column experimental data. Although the total Fe^{II} increased linearly with greater reduction, the total Fe^{III} did not linearly decrease (Figure 8a), and the total Fe^{II} + Fe^{III} did not remain constant. In addition, while the ion exchangeable Fe^{II} extractions (24) linearly increased with increasing reduction, the values of the adsorbed Fe^{II} were too small (Figure 8b). The conclusion that can be drawn from these extractions is similar to what other researchers have suggested: extractions on natural sediments with multiple phases present in small quantities can only be qualitatively assessed with this method. It still appears that the time-consuming process of slowly oxidizing sediment with dissolved oxygen in a column experiment yields the most accurate and consistent results of the mass of reduced iron in dithionite-treated sediments.

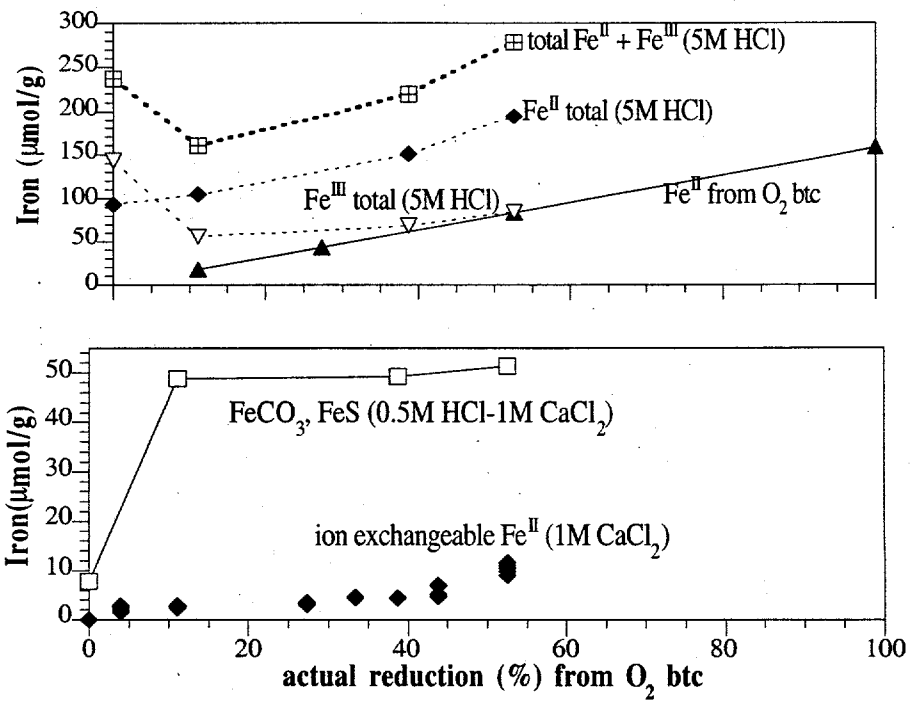

Figure 8. Changes in Fe^{II} and Fe^{II} phases as sediment is partially reduced, as characterized by: a) 5M HCl extractions that measure total Fe^{II} and Fe^{II} phases, and b) 1M $CaCl_2$ for extracting adsorbed Fe^{II} and the difference of a 0.5M HCl and 1M $CaCl_2$ to measure $FeCO_3$ and FeS.

The mobility of major and trace metals during sediment reduction and oxidation was measured in effluent samples during reduction (10 pore volumes) and oxidation (550 pore volumes) to assess the potential migration of heavy metals that could occur as the redox conditions of the natural (oxic) sediment have been reduced. Metals that increased due to the reducing conditions created (Table 9) included Fe, Mn, and As, as reduced species of these metals are more mobile under low Eh conditions. The concentrations of Sn, Sb, Zn, and Pb also increased, but these metals may have leached from the sediment regardless of the Eh. For example, there is no thermodynamic correlation of Pb mobility with redox. Metals that decreased due to the reducing conditions created included Mg, Al, and U. The concentrations of Na, K, Si, Ba, and Cr increased, but these were from the injection solution. All of these changes are not considered significant because the highly reducing conditions during dithionite injection that mobilized these metals only occur over 2 to 3 days during a field injection experiment. Analysis of metals mobility during sediment oxidation shows which metals are mobile under reduced conditions, then are immobile under oxic conditions. Of significance are the slight mobility of Fe and Mn in the reducing conditions, which become immobilized as the column becomes oxic (Table 10). There were no metals that increased in concentration during the 550 pore volumes of oxidation. Metals that were in the dithionite solution (Na, K, Mg, Si, Ba, Cr) decreased during oxidation as species were advected out of the column. The potassium concentration was 25% of the injection concentration at 1.9 pore volumes, 5% by 4.8 pore volumes, and 1.8% by 7.2 pore volumes, which may roughly indicate the remaining carbonate and sulfate from the injection water.

Table 9. Metal mobility during sediment reduction in columns

pore volumes	*Na µg/ml	*Mg µg/ml	Al µg/ml	Si µg/ml	*K µg/ml	Ca µg/ml	Fe µg/ml	Cr ng/ml	Mn ng/ml	Ni ng/ml	Cu ng/ml	Zn ng/ml	As ng/ml	Se ng/ml	Mo ng/ml	Ag ng/ml	Cd ng/ml	Sn ng/ml	Sb ng/ml	Ba ng/ml	Pb ng/ml	U ng/m
dithionite inj. soln	3440	0.3	0.6	16.2	30300	3.43	<1	407	<10	<5	49.2	<10	<20	300	10±5	<2	<2	<2	<2	89.4	<2	<2
0.5	1840	97.6	0.09	13.2	12600	6.08	2.3	288	2840	62±7	<5	502	74.5	30±14	73.3	<2	8.0±3	<2	3	9.4	154	6.2C
2	2900	87.4	0.093	12.1	19800	8.4	4.5	330	740	26.1	<5	47.9	536	47±17	252	<2	<2	10.3	18±2	279	9.8	6.7
4.98	3780	9.38	0.047	23.0	25900	22.4	3.88	190	18±2	13.3	<5	26.9	947	<50	143	<2	<2	27±4	17.9	149	3±1	7±3
4.98	3960	9.2	0.051	23.0	25500	23.8	4.38	191	16.4	12.9	<5	17.9	1010	<50	151	<2	<2	20.1	16.9	144	<2	4±1
8	3760	3.99	0.023	19.6	25300	19.9	3.18	186	33.1	5.3	<5	23.1	718	<50	93.4	<2	<2	28±7	13±2	188	<2	3±1
9.5	3050	3.2	<0.02	12.2	29300	5.80	2.50	419	6.6	<5	<5	12±5	419	44±13	87.4	<2	<2	16.0	10±1	196	<2	<2

Table 10. Metal mobility during sediment oxidation in columns

pore volumes	*Na µg/ml	*Mg µg/ml	Al µg/ml	Si µg/ml	*K µg/ml	Ca µg/ml	Fe µg/ml	Cr ng/ml	Mn ng/ml	Ni ng/ml	Cu ng/ml	Zn ng/ml	As ng/ml	Se ng/ml	Mo ng/ml	Ag ng/ml	Cd ng/ml	Sn ng/ml	Sb ng/ml	Ba ng/ml	Pb ng/ml	U ng/ml
dithionite inj. soln	3440	0.3	0.6	16.2	30300	3.43	<1	407	<10	<5	49.2	<10	<20	300	10±5	<2	<2	<2	<2	89.4	<2	<2
oxidation inj. soln.	1.30	<0.2	<0.02	0.538	<1	4.09	<1	<10	<10	<5	<5	3.82	<20	<20	<10	<2	<2	<2	<2	<2	<2	<2
0.62	3360	2.28	0.047	11.3	28700	7.74	4.36	436	221	5.5	<5	16±2	260	30±17	49±7	<2	<2	12±2	6.3	180	<2	2±1
1.87	722	0.57	0.0413	6.30	7560	1.71	<1	100	<10	<5	<5	5±3	86.7	<20	26±4	<2	<2	3.8	3.99	37.1	<2	<2
4.8	181	0.290	0.054	3.41	1400	10.4	0.171	12±2	3.5	2.5	<5	14.4	32±7	<50	7±1	<2	<2	4±1	<2	14±2	<2	<2
7.2	78.3	0.189	0.043	3.07	565	10.4	0.098	12.6	3±1	3±1	<5	12.9	21±7	<50	4.0	<2	<2	<2	<2	10.7	<2	<2
9.1	40.3	0.172	0.046	3.38	337	11.7	0.142	9±1	2±1	3±1	<5	14.9	20±3	<50	<2	<2	<2	<2	<2	12.3	<2	<2
21.6	7.24	0.138	0.066	3.10	92.8	12.0	0.147	5.8	2.9	2±1	<5	11.9	11.9	<50	<2	<2	<2	<2	<2	13.8	<2	<2
50	4.31	0.134	0.081	2.69	69.9	11.3	0.149	5±1	4±1	3±2	<5	8.9	11±4	<50	<2	<2	<2	<2	<2	15.1	<2	<2
170	1.76	0.197	0.038	0.9	36.8	7.19	0.058	2±1	13.4	2±1	<5	7.1	<5	<50	<2	<2	<2	<2	<2	13.1	<2	<2
550	0.396	0.133	0.203	1.5	9.99	12.2	0.13	2.3	19.7	3.8	<5	4.1	<5	<50	<2	<2	<2	<2	<2	15.4	<2	<2

*injected with dithionite

Reactive transport modeling of the general problem of Fe and Mn transport from reduced zones (Smith and Jaffe 1998) confirms the laboratory results of limited Mn^{II} movement from the reduced zone. In these simulations, the Fe^{II} was generated biotically, and although Fe^{II} was highly adsorbed, the mass generated exceeded the number of adsorption sites and Fe^{II} migrated downgradient (a process that would not occur with the dithionite injection). Arsenic speciation over a range of redox conditions was also simulated. The As^{V} species that dominated oxic waters was arsenate [H_3AsO_4] and the As^{III} species that dominate anoxic waters was arsenite [H_3AsO_3]. Simulations showed that the $As^{V/III}$ species change was sharp during the transport across the redox interface. Although these simulations were not conducted under the specific conditions of a dithionite injection, they do show that species that are mobile in a reduced environment are not mobile outside the localized reduced zone.

5.0 Results – TCE Dechlorination

Batch experiments in this study were conducted in fully reduced sediment to determine the major reaction pathway for TCE dechlorination, reaction products, and dechlorination rate of TCE and various degradation products (Section 5.1). Batch studies were additionally conducted in partially reduced sediment to understand the mechanism at the field scale, where dithionite treatment through wells would result in varied reduction spatially (Section 5.2) and at different temperature (Section 5.3). Finally, reactive transport experiments in 1-D columns were conducted to assess TCE dechlorination during advective transport at field-scale temperatures in fully and partially reduced sediment (Section 5.4).

5.1 TCE Dechlorination Pathway and Rate

The pathway by which TCE was degraded by dithionite-reduced sediments was determined in batch experiments. Previous research using Hanford sediments and research by others (see Section 2.3) have shown that TCE is degraded by two major pathways: 1) reductive elimination (TCE -> chloroacetylene -> acetylene -> ethylene -> ethane), and 2) hydrogenolysis (TCE -> cis-DCE -> vinyl chloride), with all the mass accounted for by reductive elimination and with possibly a minor (0.3%) amount of mass accounted for by hydrogenolysis.

The major pathway for TCE degradation by dithionite-reduced Ft. Lewis sediments was clearly shown to be reductive elimination, which accounted for 99.5% to 100% of degraded TCE mass (Figure 9 with detailed plots in Appendix D). A typical batch experiment consisted of a series of vials containing Ft. Lewis groundwater (with 2.7 ppm TCE, Table 6) mixed with Ft. Lewis sediments that were fully reduced with no headspace. Initially all the TCE was in the water, and over time, TCE adsorbed and was degraded. At different time intervals, TCE and degradation products in the water were measured by GC or GC-MS analysis. One experiment (Figure 9) shows TCE decreasing in solution with a half-life of 3.5 h, which corresponds almost exactly to the increase in acetylene mass. There was a slight increase, then decrease, in chloroacetylene at 1 h to 4 h, indicating that any chloroacetylene produced was quickly degraded to acetylene.

Evidence for the lack of importance of the hydrogenolysis pathway for TCE degradation is shown by the lack of change in the DCE and vinyl chloride data. DCE is present in the Ft. Lewis groundwater at 40% of the molar concentration of TCE (see Appendix D), and over the course of a 70 h experiment (KF13), the DCE concentration did not change. Vinyl chloride (2.4 ppb) is initially present in the Ft. Lewis groundwater at approximately 1% of the TCE mole fraction. During the TCE degradation experiment, vinyl chloride in contact with reduced sediment is rapidly removed from solution within minutes (see Appendix D), leaving 0.18 ppb vinyl chloride in solution initially in this experiment. There is a slight increase in vinyl chloride concentration to 0.46 ppb at 10 h to 20 h, which may represent evidence of a reaction pathway, although these concentrations are below the detection limits (0.5 ppb) of vinyl chloride. If these data are real, they indicate hydrogenolysis could account for 0.3% of the degraded TCE mass. The vinyl chloride concentrations decreased to 0.14 ppb by 30 h, which (if real) represent vinyl chloride degradation by the reduced sediment. Column experiments provided similar evidence of the lack of importance of hydrogenolysis (Appendix E, discussed in Section 5.4), in which the vinyl chloride concentration increased to 0.8% of the TCE mass, in contrast to acetylene, which was >100% of the TCE mass (i.e., reductive elimination is the major reaction pathway).

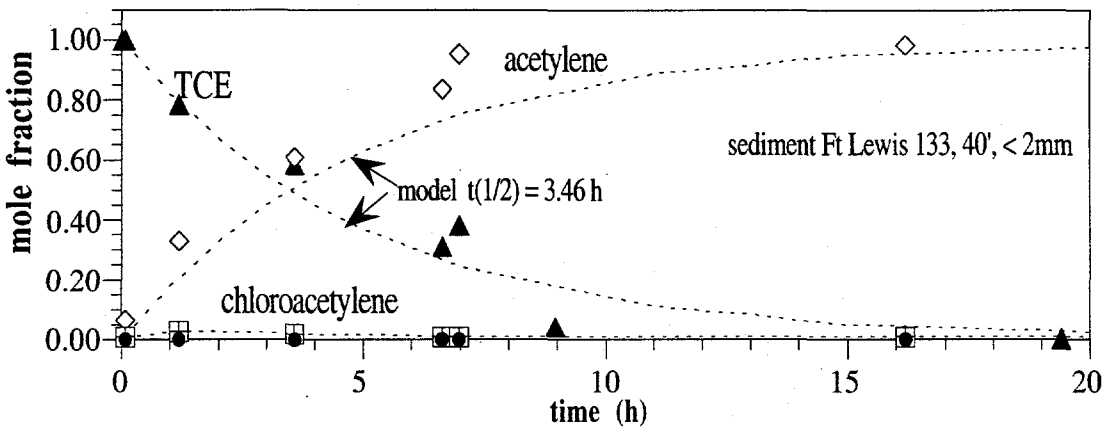

Figure 9. Degradation of 2.7 ppm TCE present in Ft. Lewis groundwater by reduced sediment to chloroacetylene and acetylene indicating reductive elimination is the major reaction pathway.

Although the intrinsic rate of TCE reduction on an iron oxide surface with adsorbed Fe^{II} at the molecular scale is the same for different sediments, the observed TCE degradation rate for different sediments varies with the mass of reduced iron. Given that the theoretical mass flux rate for TCE via reductive elimination (Equation 21) is a first-order function of TCE, a third-order function of H^+, and a third-order function of Fe^{II}, the observed rate for different sediments should vary considerably. For the experiments in this study at fixed pH, the H^+ term becomes constant. TCE degradation rate data with varying iron content (this and other studies) was used to determine the intrinsic TCE reduction rate and functional dependence on Fe^{II}. The observed TCE degradation rate (reported as first-order half-life, Table 11) varied over an order of magnitude from 0.013/h (low iron content Hanford sediment) to 0.2/h (high iron content Ft. Lewis sediment). Assuming a first-order dependence of Fe^{II} on the intrinsic TCE degradation rate, the rate variability was reduced to 3x (0.0018 to 0.0054), so is likely the correct dependence:

$$k_{f,\ intrinsic} = 0.0034 \pm 0.0014\ 1/[\text{h } \mu\text{mol } Fe^{II}]$$

Assuming a second-order dependence of Fe^{II}, intrinsic rate values that varied 2.5 orders of magnitude (Table 10), and assuming a third-order dependence of Fe^{II}, intrinsic rate values that varied 4 orders of magnitude, so were highly likely not the correct dependence of Fe^{II} on the intrinsic TCE degradation rate.

Table 11. Dependence of the TCE degradation rate on reduced iron mass

experiment name, type	TCE half-life (hr)	Fe^{II} (μmol)	first-order k_f(intrinsic)	second-order k_f(intrinsic)	third-order k_f(intrinsic)
Hanford, KE, column	53.0	3.16	0.0041	1.31E-3	4.14E-4
Ft. Lewis, KF13, batch	3.46	37.0	0.0054	1.46E-4	3.95E-6
Moffett, M12, column	9.4	40.9	0.0018	4.41E-5	1.08E-6
Ft. Lewis, KF24, batch	5.78	46.0	0.0026	5.67E-5	1.23E-6
Ft. Lewis,KF17, column	19.0	80.6	0.0045	5.62E-6	6.97E-8
Ft. Lewis,KF23, column	4.2	86.4	0.0019	2.21E-5	2.56E-7
Ft. Lewis, KF42, batch	1.2	333.	0.0036	5.21E-6	1.57E-8

The presence of a permeable reduced iron barrier in the groundwater system at Ft. Lewis is capable of degrading organic compounds in addition to TCE. Laboratory studies with reduced Hanford and other sediments have demonstrated that carbon tetrachloride and trinitrotoluene (TNT) are degraded. In this study, there were indications that compounds other than TCE that are present in the Ft. Lewis groundwater were degraded. Column experiment KF23 (Appendix E) clearly showed that TCA was degraded with a half-life of 2.1 h. In this same experiment, GC-MS analysis was used to separate DCE isomers. Although cis-1,2 DCE had an apparent degradation rate of 14 h, the 1,1 DCE (present in trace quantities) did not appear to be degraded. As described earlier in this section, chloroacetylene, acetylene, and ethylene were clearly degraded, and vinyl chloride appeared to be degraded. Although the evidence shows apparent loss of some of these compounds in the reduced sediment, separate degradation experiments of each compound are needed to identify a clear reaction pathway by measurement of one or more reaction products.

5.2 Influence of Partial Iron Reduction on the TCE Degradation Rate

Because TCE degradation requires both an electron donor (adsorbed Fe^{II}) and a surface (iron oxide or clay), the rate of dechlorination may not be a simple function of the mass of reduced iron. This fact is significant at the field scale because sediments cannot be uniformly reduced, so studies were conducted to determine the rate of TCE degradation as the reduced iron mass was varied. The mass of reduced iron was measured by oxidizing sediments in columns with dissolved O_2 (Section 4.3), and the TCE degradation rates (Table 12) were based upon the acetylene data because the TCE mass loss from solution is also affected by adsorption (details in Table 3). A plot of acetylene concentrations of all 15 experiments (Figure 10a, details of each experiment in Appendix D) shows the change in TCE degradation rate with partially reduced sediment.

The TCE degradation rate is highly dependent on the fraction of reduced iron in sediment and varied from >1000 h or 11% reduced to 1.2 h for 100% reduced iron. The intrinsic TCE degradation rate varied two orders of magnitude (Table 12), and there appeared to be a significant increase in the TCE degradation rate between 30% and 45% reduced sediment (Figure 10a). The intrinsic degradation rate had a second-order dependence on the fraction of reduced iron (line in Figure 10b), which may be caused by the influence of the surface on the TCE degradation rate. These results are consistent with a long-term (4-month) column study with Hanford sediments in which the TCE degradation rate decreased significantly when the sediment was <50% reduced.

Table 12. Dependence of the TCE degradation rate on the fraction of reduced iron

sediment color	reduction (%)	TCE half-life (hours)	k_f, intrinsic, first-order (1/[h μmol Fe^{II}])
tan	0.0	–	–
*gray	4.0	–	–
**	11.1	1100	0.000034
***	27.4	250, 216	0.000069
****	33.4	120	0.00011
*****	38.7	65, 50	0.00021
*****	43.8	19.2	0.00052
*****	52.6	16.	0.00052
black	100.	1.2	0.0036

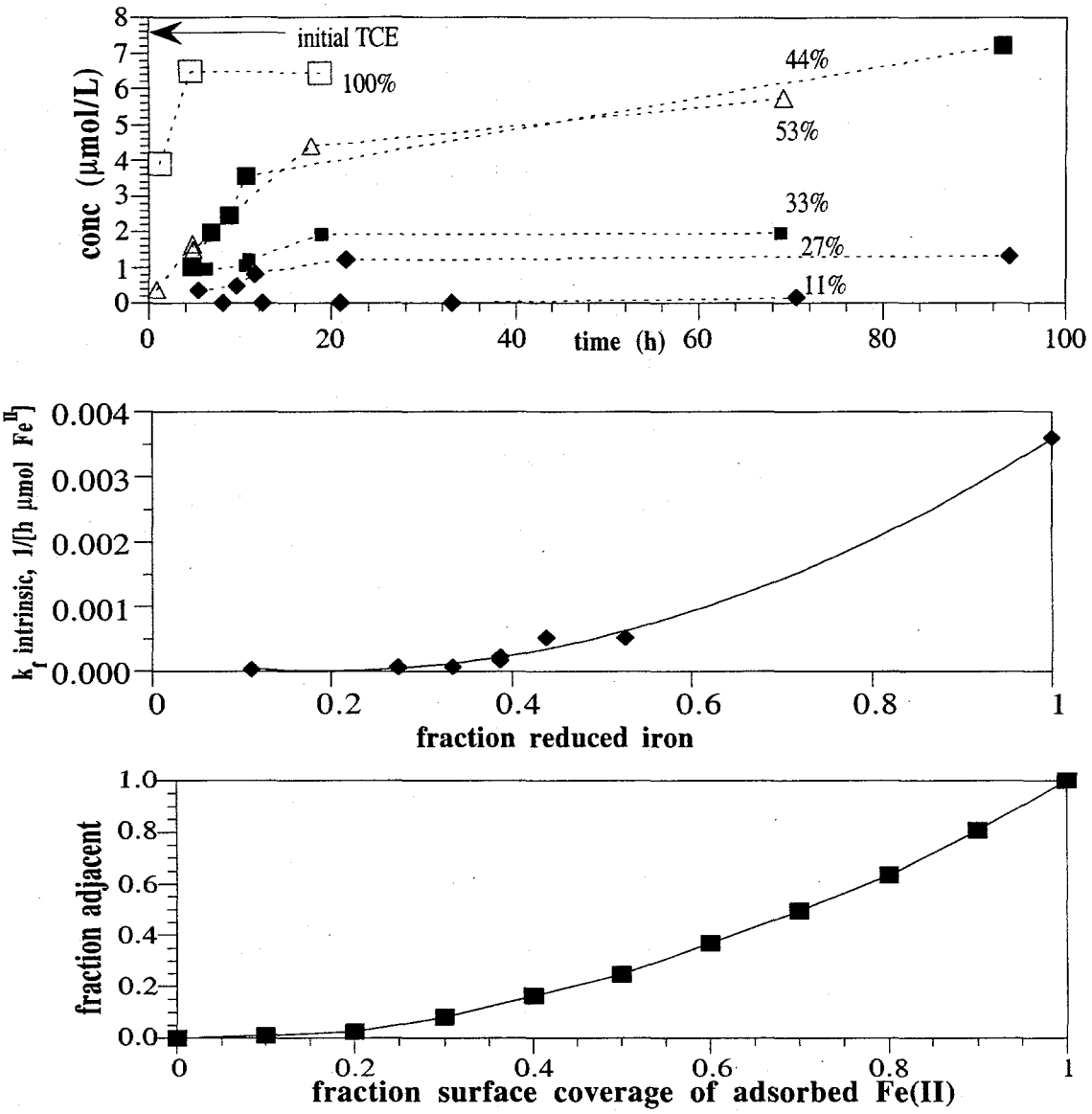

Figure 10. TCE dechlorination rate in partially reduced sediment, as shown by: a) acetylene production rate with differing fraction reduced iron, b) intrinsic TCE dechlorination rate dependence on the fraction of reduced iron, and c) theoretical dependence of adsorbed Fe^{II} that are adjacent on a goethite surface as a function of the fraction surface coverage.

The surface coordination of adsorbed Fe^{II} on the iron oxide surface is a possible cause of the dependence of the TCE degradation rate on the fraction of iron reduction (see Section 2.4). Because two electrons are needed for TCE dechlorination to chloroacetylene (rxn 12), it was assumed that two adsorbed Fe^{II} that were adjacent on a goethite (orthorhombic structure) are needed for the reaction to occur. This surface coordination hypothesis was assessed by probability theory and numerical studies. Results indicated that adjacent sites were a second-order function of the fraction coverage, so at low coverage, there were fewer adjacent sites. For example, if 25% of the sites were occupied with Fe^{II}, only 8% were adjacent and might catalyze TCE dechlorination. In contrast, if 75% of the sites were occupied with Fe^{II}, 55% were adjacent. These theoretical results were consistent with and may explain the second-order dependence of the TCE dechlorination rate on sediment reduction fraction, although additional proof is needed.

5.3 Temperature Effects on the TCE Dechlorination Rate

The effect of temperature on the TCE dechlorination rate was investigated because the Ft. Lewis aquifer temperature was significantly colder (12°C) than laboratory experiments (25°C). It was hypothesized that because TCE dechlorination was surface catalyzed, the dechlorination rate may not be a simple function of temperature. Batch experiments (2°C to 42°C) with fully reduced Ft. Lewis sediment (Appendix D, Table 3) showed TCE mass decreasing faster than acetylene increased, due to adsorption. The dechlorination rate based on acetylene data (Figure 11a) indicated a regular decrease with lower temperature. In some cases, the acetylene mass produced was greater than the TCE mass consumed. This may be caused by the degradation of other compounds in the Ft. Lewis groundwater. The dependence of the TCE dechlorination rate was 4.00x slower at 10°C compared with 25°C (Figure 11b). Therefore, although TCE dechlorination involves multiple surface reactions, it is apparently a fairly regular function of temperature over the range studied. TCE dechlorination can occur at aquifer temperature at a predictable rate.

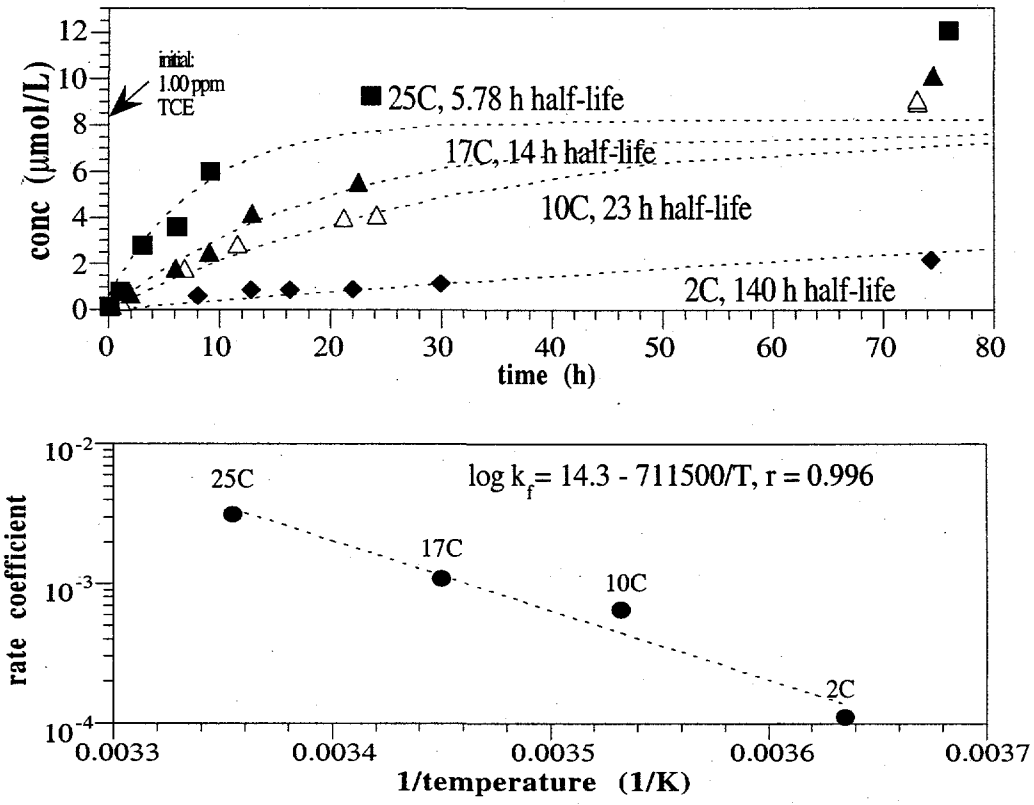

Figure 11. Dechlorination of TCE at different temperature as shown by: a) acetylene production rate over time in experiments at different temperature, and b) regular dependence of the intrinsic TCE dechlorination rate coefficient with temperature.

5.4 TCE Dechlorination During Reactive Transport

The degradation of TCE in Ft. Lewis groundwater was also studied in column experiments to determine if there were additional rate limitations caused in a reactive transport system compared to batch studies. These column experiments were conducted with fully and partially reduced sediment,

and 10°C and 25°C, to confirm temperature and partial reduction effects quantified in batch systems on TCE dechlorination in flowing systems. A previous long term studies (4000 h; Thornton et al. 1998) with Hanford sediment showed: a) the TCE degradation rate slowly decreased as fully reduced sediment was slowly oxidized, b) TCE degradation stopped when the sediment was ~50% oxidized. Those results are consistent with the partial reduction results of this study (Section 5.2), in which a significant dependence of the fraction-reduced iron on the TCE degradation rate was observed.

One long-term (1500 h) column experiment was conducted in which the TCE degradation rate was measured as the fully reduced sediment was oxidized. Given that the sediment contains sufficient reducible iron to require 500 pore volumes to fully oxidize the sediment, it is estimated that TCE will be degraded for ~250 pore volumes. To achieve residence times similar to aquifer conditions, slow flow rates were used. Given these 50-h to 100-h residence times for one pore volume in a column, it was not economic to conduct experiments at this rate for 500 pore volumes. Therefore, the flow rate was varied in the column (Figure 12), alternating between slow flow rates to measure the TCE dechlorination (70-h to 100-h residence times), and fast flow rates to oxidize sediment (0.3-h residence time).

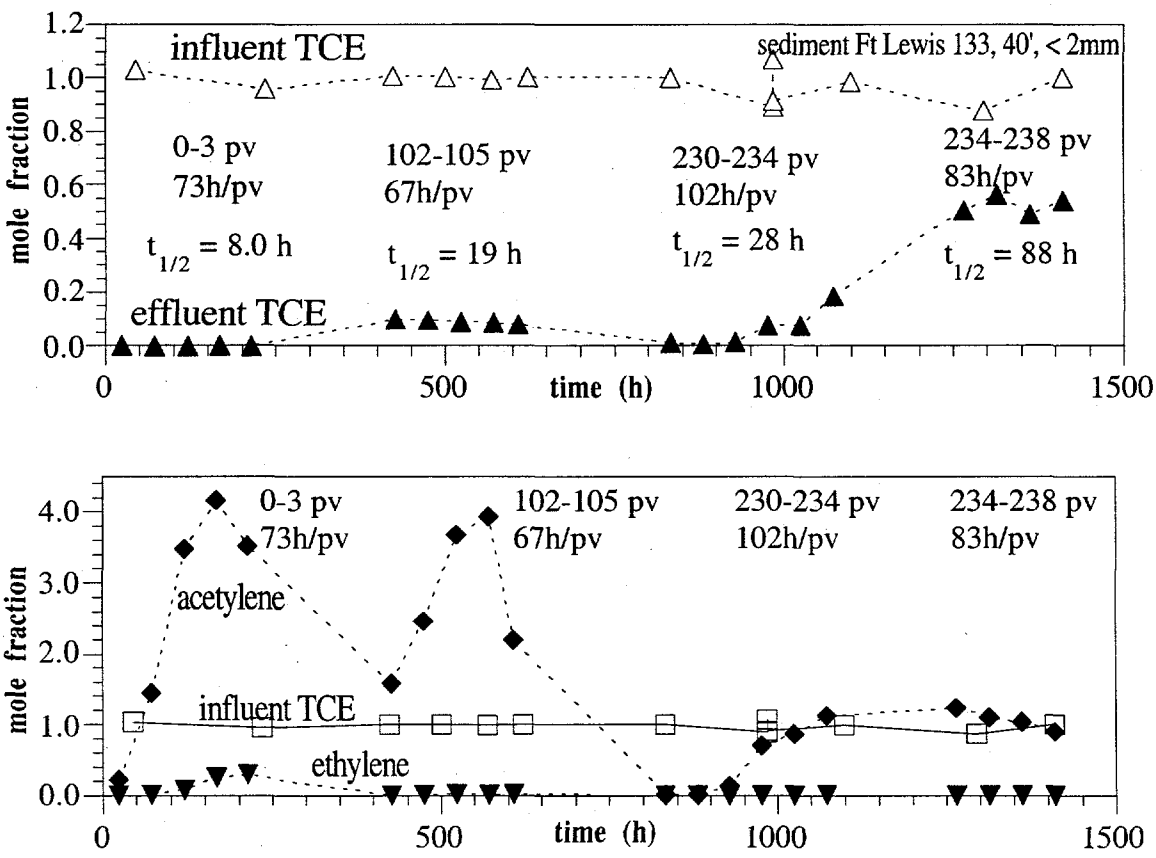

Figure 12. TCE dechlorination in a long-term column experiment as sediment is slowly oxidized, as shown by: a) TCE influent and effluent, and b) acetylene and ethylene.

Results of this long-term experiment indicate that TCE dechlorination rates achieved in flowing porous media systems are equal or slower than in batch systems. TCE was dechlorinated for 1000 h (230 pore volumes, Figure 12a) at rates that were initially the same as batch experiments, but slowly decreased (Table 10). The acetylene data in this experiment peaked at 4x the molar concentration of TCE, indicating degradation of other compounds and suggested that the transport of acetylene involved additional processes other than advection in water (Figure 12b). Integration of the area of produced acetylene with ~1.8x the area of TCE consumed clearly indicated that other compounds were being dechlorinated. It was hypothesized that significant acetylene can be transported in bubbles, which may have contributed to the peak acetylene concentrations observed. The dechlorination rate decreased significantly by 235 pore volumes (Figure 12a) as sediment became partially oxidized. An additional column experiment conducted with Ft. Lewis sediment with significantly higher iron content (KF23, Appendix E) also had a slightly slower TCE dechlorination rate relative to batch experiments (Table 11).

Column experiment results showed considerable TCE mass loss with a corresponding increase in degradation products clearly illustrated the importance of reductive elimination was the major (and essentially only) reaction pathway. Reductive elimination was evident from the significant masses of acetylene and ethylene (and traces of chloroacetylene) in the long-term experiment. The lack of importance of the hydrogenolysis reaction pathway was shown by only a trace increase in vinyl chloride concentration (Appendix E, KF23), and the decrease in 1,2-DCE concentration in reduced sediment (instead of an increase).

To determine the effect of partial reduction on TCE dechlorination under aquifer conditions (flowing system, 10°C), two column experiments were conducted that differed in the spatial distribution of reduced iron. In one experiment (KF39, Appendix E), 10 g of fully reduced sediment was mixed with 30 g of untreated sediment to achieve "25% reduced" sediment. At the molecular scale, particles that contained adsorbed Fe^{II} were adjacent, so this sediment should be able to dechlorinate TCE. In a second experiment (KF 38, Appendix E), sediment was 25% partially reduced, so would likely not contain sufficient adjacent adsorbed Fe^{II} (see Figure 10 and associated text). Subsequent batch studies showed that the stoichiometric proportions of dithionite to iron used in this experiment would have yielded <10% reduced iron. Results of these two column experiments both removed some TCE from solution, although only the experiment with a fraction of fully reduced iron (KF39) produced any acetylene. These results confirmed results of batch experiments that partially reduced sediment is significantly less efficient at degrading TCE. The effect of temperature was small (4x slower at 10°C) relative to the effect of the partial reduction.

6.0 Conclusions

Bench-scale studies were conducted to ascertain how effectively Ft. Lewis sediments can be chemically reduced, and how efficiently the reduced sediment can degrade TCE. The effects of temperature, partial iron reduction, and flow on these redox reactions were also studied to ascertain how to achieve viable TCE dechlorination rates at the field scale.

The fraction of reducible iron in Ft. Lewis sediments was more than sufficient to create an effective reduced zone in the aquifer. The average reducible iron for aquifer sediments at the field site was 63 ± 40 μmol/g or 0.35 ± 0.22%, which indicates that the reduced zone would last for 300 pore volumes of oxygen-saturated water (assuming O_2 is the only electron acceptor) or longer in the sub-oxic water present at Ft. Lewis. The reduced iron was mainly (80% to 100%) adsorbed Fe^{II}, with the remainder $Fe^{II}CO_3$. Iron was reduced rapidly at short times (half-life 3.5 h in batch, 6.8 h in columns) and more slowly at later times because the reaction is a third-order function of dithionite and iron concentrations. First-order modeling of reduction would well predict the first half of reduction, but underpredict dithionite use for high fractions of reduction. The relative rates of iron reduction and disproportionation controlled the sediment-dithionite contact times needed to efficiently reduce 80% of the iron in sediment: 32 h at 25°C; 100 h at 12°C (ambient aquifer temperature), and 140 h at 10°C. Reduction of >80% of the iron is highly inefficient because of dithionite use for disproportionation at long contact times. To reduce 80% of the iron, 30% extra dithionite is needed for disproportionation at any temperature. At the field scale, dense (concentrated) dithionite solutions were slumping and not allowing sufficient contact times for reduction. The combination of heated injections at higher velocity and lower dithionite concentration are currently being evaluated at the field scale to achieve aquifer zone reductions.

There was a significant effect of altering the pH buffer concentration used in dithionite treatment on reduction efficiency, iron mobility, and pH change. Although 4 moles of H^+ are generated per mole of dithionite consumed (and the K_2CO_3 buffer is typically 4x the dithionite concentration), the sediment may contribute some buffering capacity. With the same dithionite concentration and contact time, sediment reduced in 3x buffer had 40% less reduced iron, and sediment reduced in 0.5x buffer had 70% less reduced iron. Less pH buffer resulted in a low pH front in columns, which dipped from 9.5 to 3.3 (0.5x buffer) and mobilization of iron: 3.3% with the 0.5x buffer compared with 0.02% with the 4x buffer. These results indicate the K_2CO_3 concentration should be 4x the dithionite concentration to create an immobile reduced iron zone.

Dithionite-reduced Ft. Lewis sediments have been shown to degrade TCE in Ft. Lewis groundwater at a sufficiently fast rate during reactive transport that a successful permeable barrier could be made at the field scale. Degradation rates observed with different sediments ranged from 1.2 h to 19 h (expressed as a half-life for TCE). The TCE degradation rate can be calculated for all sediments from the product of the intrinsic degradation rate (0.0034/h μmol) and the mass of reduced iron (range of 12 to 126 μmol/g; average = 63 μmol/g). Products of TCE dechlorination clearly show that 99.5% to 100% is occurring via reductive elimination, producing acetylene, ethylene, and chloroacetylene. The 2.4 ppb vinyl chloride in Ft. Lewis groundwater quickly decreased in contact with reduced sediment, then increased slightly at 10 h (0.18 ppb to 0.46 ppb; below detection limits) which may represent the hydrogenolysis reaction pathway. If real, hydrogenolysis could account for, at most, 0.3% of the TCE mass degraded. Experiments also showed that the reduced sediment degraded other compounds (TCA, chloroacetylene, acetylene, and ethylene), and possibly cis-1,2 DCE and vinyl chloride, although further studies are needed.

The TCE degradation rate decreased three orders of magnitude in partially reduced sediment, which has significant implications because uniform full sediment reduction is not possible at the field scale. Although minimally reduced sediment had nearly no TCE reactivity, >40% reduced sediment resulted in TCE reduction rates that were viable at the field-scale (<65 h). The second-order dependence of the TCE dechlorination rate on the fraction of reduced iron demonstrates the significant role of the iron oxide surface (as a catalyst or for surface coordination) in addition to Fe^{II} as the electron donor for TCE dechlorination. Calculation of the fraction of adjacent Fe^{II} atoms (providing the two electrons needed for TCE dechlorination) on an iron oxide surface resulted in a second-order dependence which was consistent with the trend in the TCE degradation rate data change over fraction of reduced iron. Although the TCE dechlorination is surface catalyzed, the dependence on temperature was predictable, with a 4x slower rate at 10°C compared with 25°C.

Advection resulted in a small decrease in the TCE degradation rate relative to batch experimental results, likely due to diffusional (mixing) limitations in porous media systems. Reduced sediment barrier longevity was demonstrated in a column in which TCE was degraded for over 230 pore volumes. The design of a field-scale reduced iron barrier should be wide enough to allow the TCE to be degraded to below the MCL during the groundwater transport time through the barrier (>10 half-lives or 50 h to 100 h), assuming no physical or chemical heterogeneities. Because few sites are homogeneous, barriers are typically designed wider than needed to account for the spatial variability in the iron content and the velocity variability resulting from hydraulic conductivity variability and temporal changes.

7.0 References

Balko, B., and P. Tratnyek. 1998. Photoeffects on the Reduction of Carbon Tetrachloride by Zero-Valent Iron, J. Phys. Chem. 102(8):1459-1465.

Blowes, D., C. Ptacek, and J. Jambor. 1997. In Situ Remediation of Cr(VI) Contaminated Groundwater Using Permeable Reactive Walls: Laboratory Studies, Env. Sci. Technol. 31(12):3348-3357.

Buerge, I. J., and S. J. Hug. 1997. Kinetics and pH Dependence of Chromium(VI) Reduction by Iron(II), Environ. Sci. Technol. 31(5):1426-1432.

Chao, T. T., and L. Zhou. 1983. Extraction Techniques for Selective Dissolution of Amorphous Iron Oxides from Soils and Sediments, J. Soil Science Society of America, 47:225-232.

Delavarenne, S., and H. Viehe. 1969. Chemistry of Acetylenes, Marcel Dekker, New York, p 651-750.

Eary, L., and D. Rai. 1988. Chromate Removal from Aqueous Wastes by Reduction with Ferrous Ion, Environ. Sci. and Technol. 22:972-977.

Fruchter, J., C. Cole, Williams, M., V. Vermeul,, J. Amonette, J. Szecsody, J. Istok and M. Humphrey, Creation of a Subsurface Permeable Treatment Barrier Using In Situ Redox Manipulation, 2000, Groundwater Monitoring Review, in press.

Genin, J., G. Bourrie, F. Trolard, M. Amdelmoula, A. Jaffrezic, P. Refait, V. Maitre, B. Humbert, and A. Herbillon. 1998. Thermodynamic Equilibria in Aqueous Suspensions of Synthetic and Natural Fe^{II}-Fe^{III} Green Rusts: Occurrences of the Mineral in Hydromorphic Soils, Environ. Sci. Technol. 32:1058-1068.

Heron, G., and T. H. Christensen. 1995. Impact of Sediment-Bound Iron on Redox Buffering in a Landfill Leachate Polluted Aquifer. Environ. Sci. Technol. 29:187-192.

Heron, G., C. Crouzet, A. C. Bourg, and T. H. Christensen. 1994a. Speciation of Fe^{II} and Fe^{III} in Contaminated Aquifer Sediments Using Chemical Extraction Techniques. Environ. Sci. Technol. 28:1698-1705.

Heron, G., T. H. Christensen, and J. Tjell. 1994b. Oxidation Capacity of Aquifer Sediments. Environ. Sci. Technol. 28:153-158.

Istok, J.D., Amonette, J.E., Cole, C.R., Fruchter, J.S., Humphrey, M.D., Szecsody, J.E., Teel, S.S., Vermeul, V.R., Williams, M.D., and Yabusaki, S.B. 1999. In Situ Redox Manipulation by Dithionite Injection: Intermediate-Scale Laboratory Experiments. Groundwater, 37:884-889.

Johnson, T., W. Fish, Y. Gorby, and P. Tratnyek. 1998. Degradation of Carbon Tetrachloride: Complexation Effects on the Oxide Surface, J. Cont. Hyd. 29:379-398.

Orth, W., and R. Gillham. 1996. Dechlorination of Trichloroethene in Aqueous Solution Using Fe^{o}, Environ. Sci. Technol. 30(1):66-71.

Roberts, A., L. Totten, W. Arnold, D. Burris, and T. Campbell. 1996. Reductive Elimination of Chlorinated Ethylenes by Zero-Valent Metals, Environ. Sci. Technol. 30(8):2654-2659.

Seaman, J. C., P. M. Bertsch, and L. Schwallie. 1999. In Situ Cr(VI) Reduction within Coarse-Textured, Oxide Coated Soil and Aquifer Systems Using Fe^{II} Solutions, Environmental Science and Technology 33(6):938-944.

Scherer, M., B. Balko, and P. Tratnyek. 1999. The Role of Oxides in Reduction Reactions at the Metal-Water Interface, in Kinetics and Mechanisms of Reactions at the Mineral/Water Interface, eds D. Sparks and T. Grundl, ACS Symposium Series #715, American Chemical Society, Atlanta, Georgia, p 301-322.

Sivavec, T., and D. Horney. 1995. Reductive Dechlorination of Chlorinated Ethenes by Iron Metal and Iron Sulfide Minerals, in Emerging Technologies in Hazardous Waste Management VII, p. 42-45. American Chemical Society, Atlanta, Georgia.

Sivavec, T., P. Mackenzie, D. Horney, and S. Baghel. 1996. Redox-Active Media for Permeable Reactive Barriers, research report, General Electric Research and Development Center, Schenectady, New York, p. 753-759.

Smith, S., and P. Jaffe. 1998. Modeling the Transport and Reaction of Trace Metals in Water-Saturated Soils and Sediments, Water Res. Res. 34(11):3135-3147.

Szecsody, J., and R. C. Bales. 1989. Sorption Kinetics of Hydrophobic Organic Compounds on Surface Modified Silica: J. Contaminant Hydrol. 4:181-203.

Szecsody, J., A. Chilikapati, J. Zachara, and A. Garvin. 1998a. Influence of Iron Oxide Lens Shape on CoII/IIIEDTA Reactive Transport Through Spatially Heterogeneous Sediment, Water Res. Res. 25(10):2501-14.

Szecsody, J., A. Chilikapati, J. Zachara, P. Jardine, and A. Ferrency. 1998b. Importance of Flow and Particle-Scale Heterogeneity on CoII/IIIEDTA Reactive Transport, J. Hydrology 209(1-4):112-136.

Szecsody, J., K. Cantrell, K. Krupka, C. Resch, M. Williams, and J. Fruchter. 1998c. Uranium Mobility during In Situ Redox Manipulation of the 100 Areas of the Hanford Site. PNNL-12048, Pacific Northwest National Laboratory, Richland, Washington.

Szecsody, J. E., A. Chilakapati, J. M. Zachara, K. M. Salvage, and G. T. Yeh. 1995. Experimental and simulation results of reactive transport of Co(II/III)EDTA at variable pH, EOS, American Geophysical Union, 76(46):221

Thornton, E., J. Szecsody, K. Cantrell, C. Thompson, J. Evans, J. Fruchter, and A. Mitroshkov. 1998. Reductive Dechlorination of TCE by dithionite, in Physical, Chemical, and Thermal Technologies for Remediation of Chlorinated and Recalcitrant Compounds, ed. G. Wickromanayake and R. Hinchee, p. 335-340.

Wehrli, B. 1992. Redox Reactions of Metal Ions at Mineral Surfaces, in Aquatic Chemical Kinetics, ed. W. Stumm, Wiley Interscience, New York.

Williams, M., Szecsody, J., 1997. Chemical/Physical Controls on the Chemical Reduction and Oxidation Rates of Fe-containing Sediments, American Geophysical Union, EOS, 78(46):H322.

Appendix A

Batch Reduction Experiments

KF30: Iron Reduction at 2C, 0.11 mol/L Dithionite

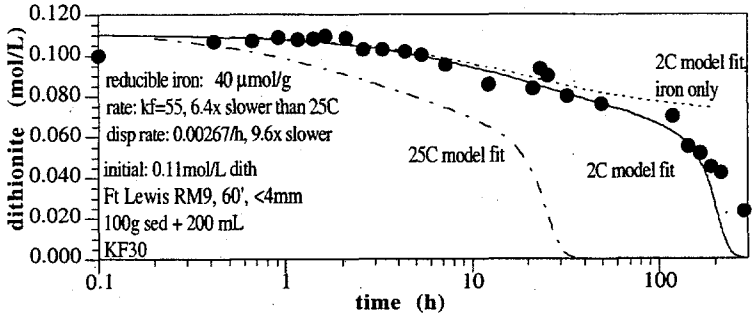

KF30 Simulation: Iron Reduction at 2C

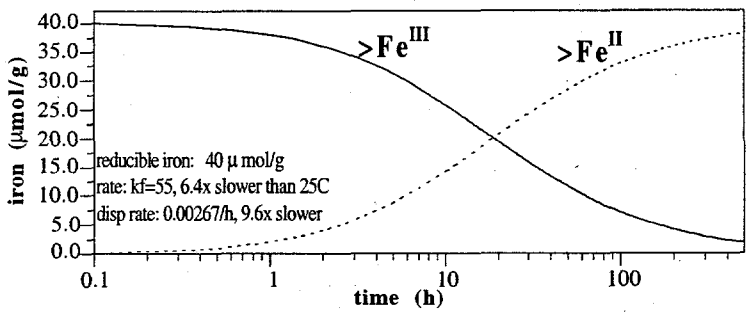

KF31: Iron Reduction at 42C, 0.08mol/L Dithionite

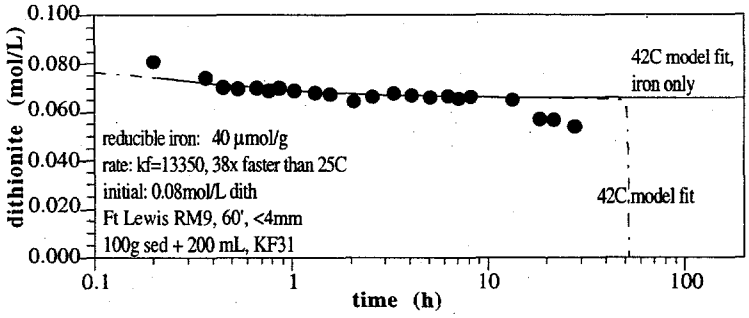

KF32: Iron Reduction vs Dithionite Concentration

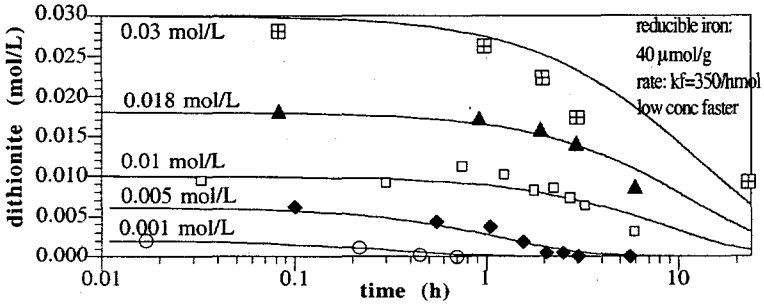

KF35: Iron Reduction at 2C, 0.03mol/L Dithionite

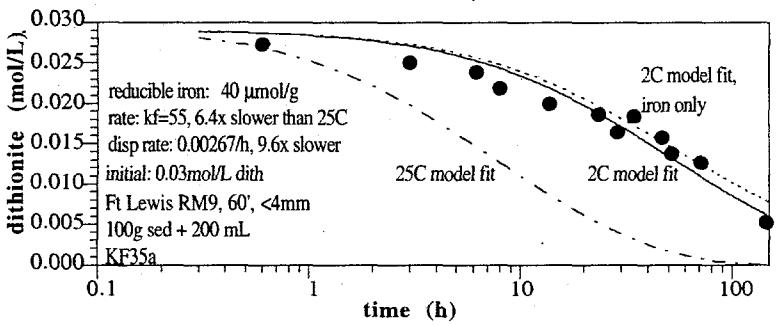

KF36: Iron Reduction at 42C, 0.008 mol/L Dithionite

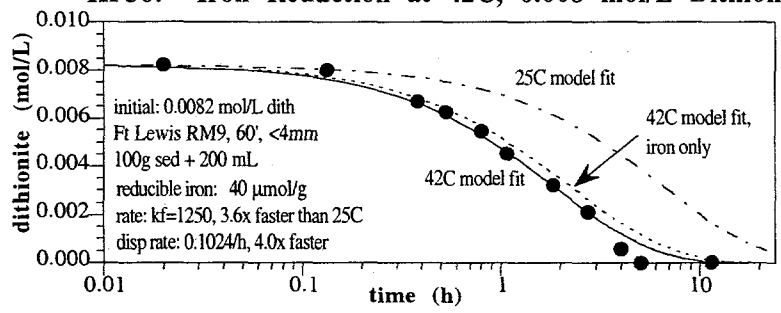

KF37: Iron Reduction at 10C, 0.008mol/L Dithionite

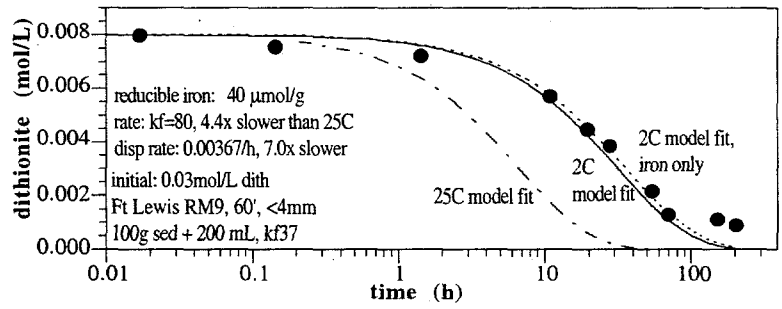

KF30-37: Iron Reduction Rate vs Temperature

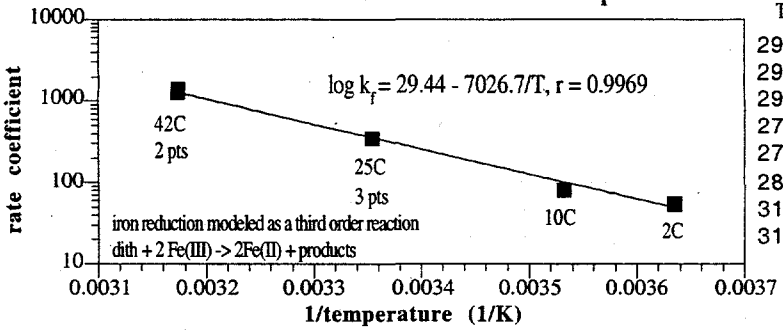

T °K	k_f
298.10	350.00
298.10	350.00
298.10	350.00
275.10	55.000
275.10	55.000
283.10	80.000
315.10	1250.0
315.10	1400.0

KF30-37: Disproportionation Rate vs Temperature

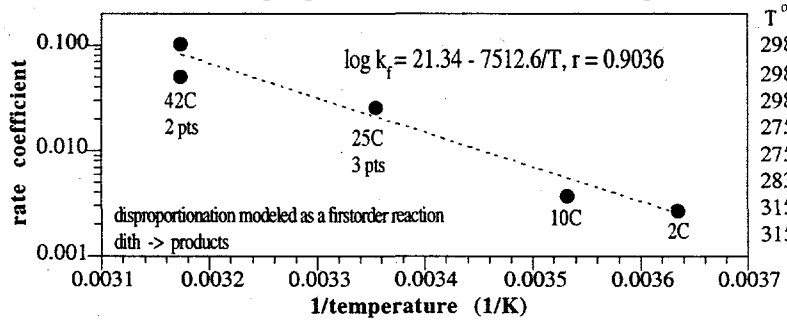

T °K	k_f
298.10	0.025670
298.10	0.025670
298.10	0.025670
275.10	0.0026700
275.10	0.0026700
283.10	0.0036700
315.10	0.10240
315.10	0.050000

Simulation of Dithionite Removal from Iron Reduction, 2 to 42C

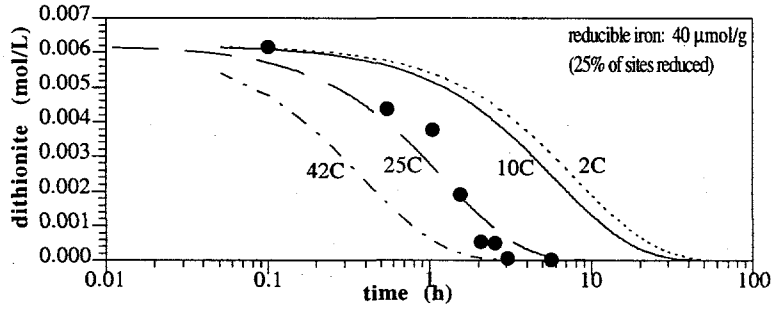

Iron Reduction at 2C to 42C

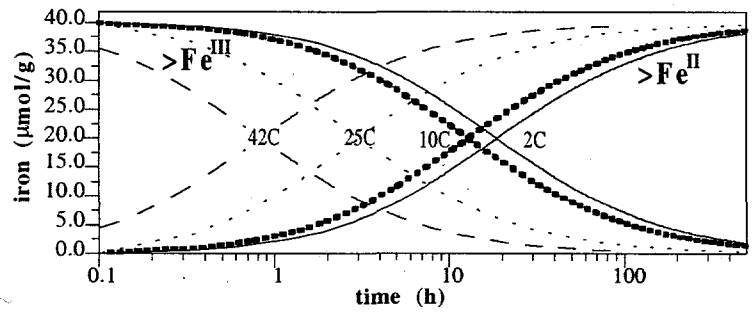

Appendix B

Column Reduction Experiments

Ft Lewis KF1: Dithionite for 0.09M dith + 0.36M K_2CO_3 inject

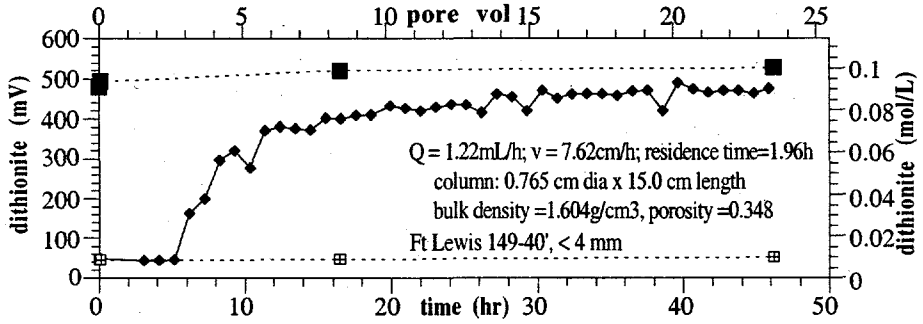

Ft Lewis KF2: Dithionite for 0.09M dith + 0.36M K_2CO_3 inject

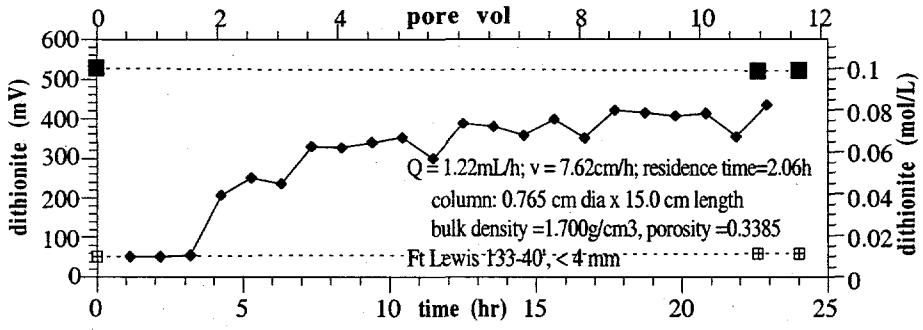

Ft Lewis KF5: Dithionite for 0.09M dith + 0.36M K_2CO_3 inject

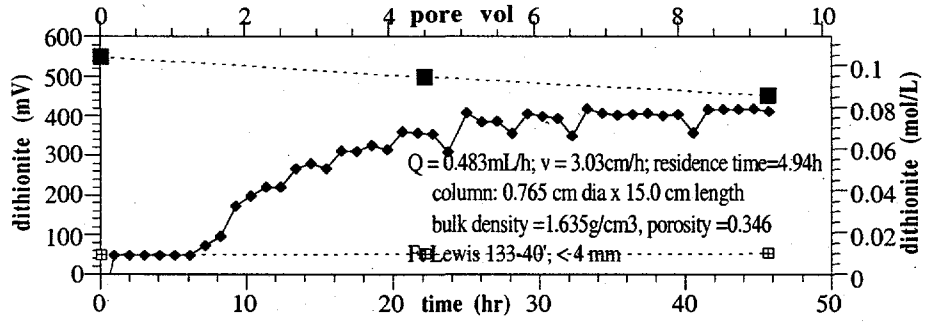

Ft Lewis KF6: Dithionite for 0.09M dith + 0.36M K_2CO_3 inject

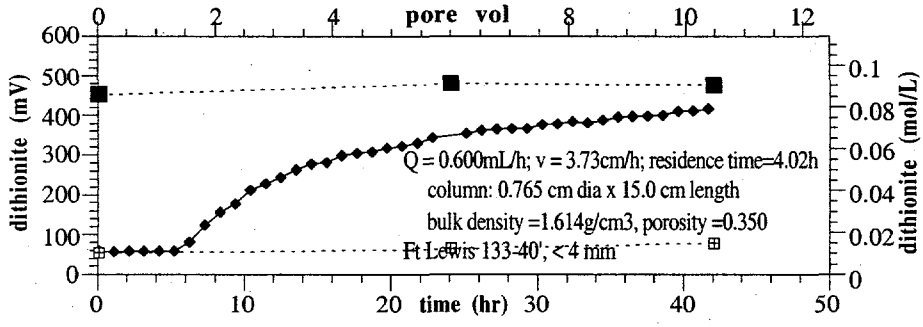

Ft Lewis KF8: Dithionite for 0.09M dith + 0.36M K_2CO_3 inject

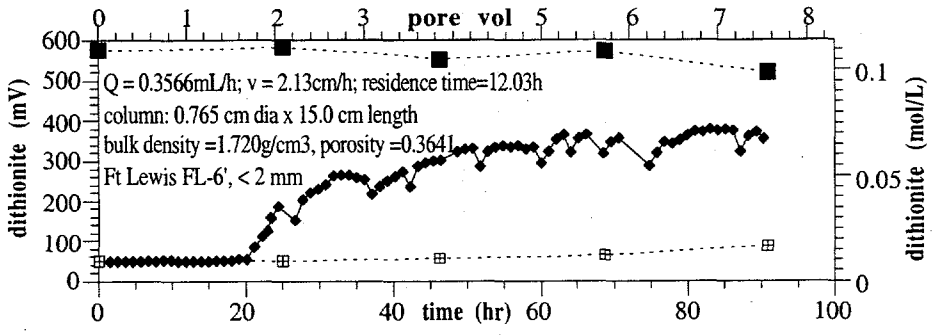

Ft Lewis KF9: Dithionite for 0.09M dith + 0.36M K_2CO_3 inject

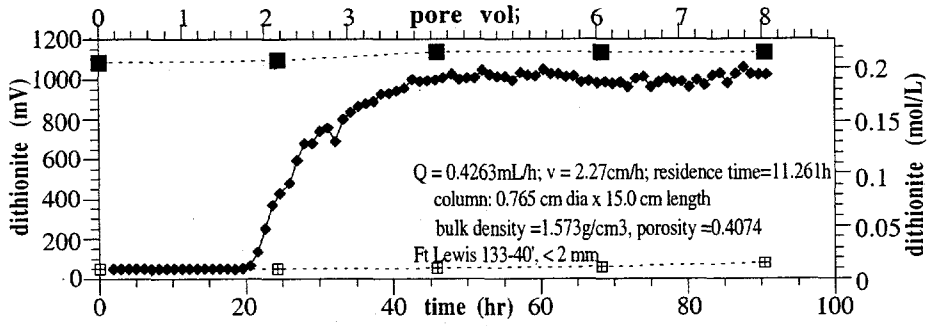

Ft Lewis KF14: Dithionite for 0.09M dith + 0.36M K_2CO_3 inject

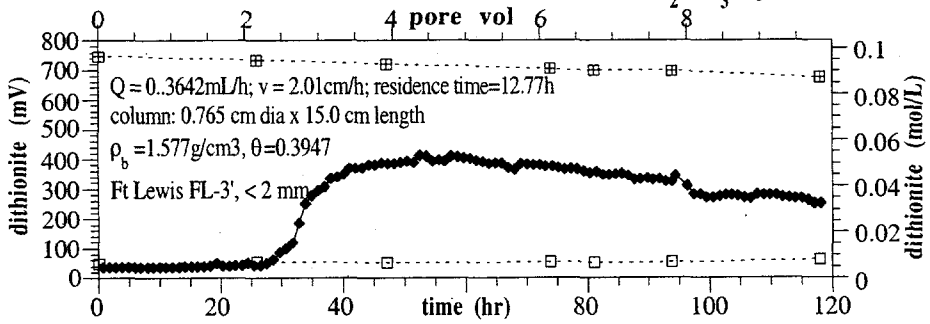

Ft Lewis KF18: Dithionite for 0.09M dith + 0.36M K_2CO_3 inject

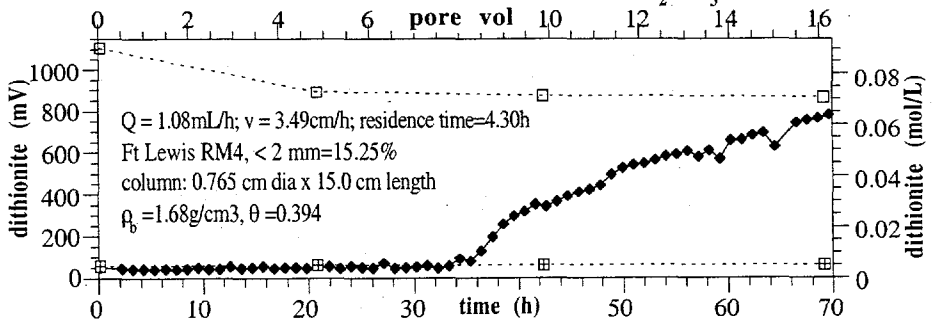

Ft Lewis KF19: Dithionite for 0.09M dith + 0.36M K_2CO_3 inject

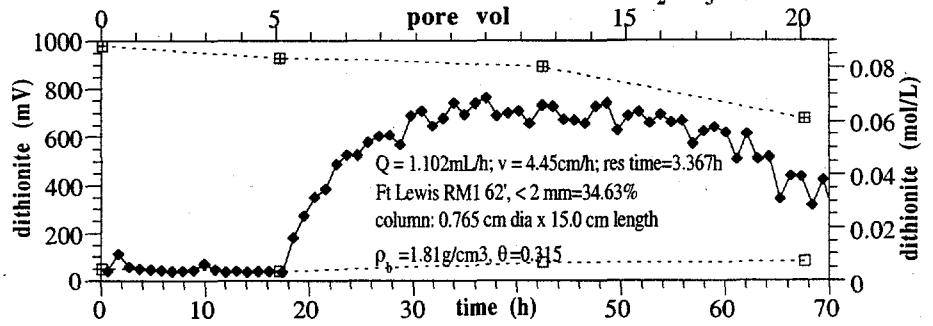

Ft Lewis KF20: Dithionite for 0.09M dith + 0.36M K_2CO_3 inject

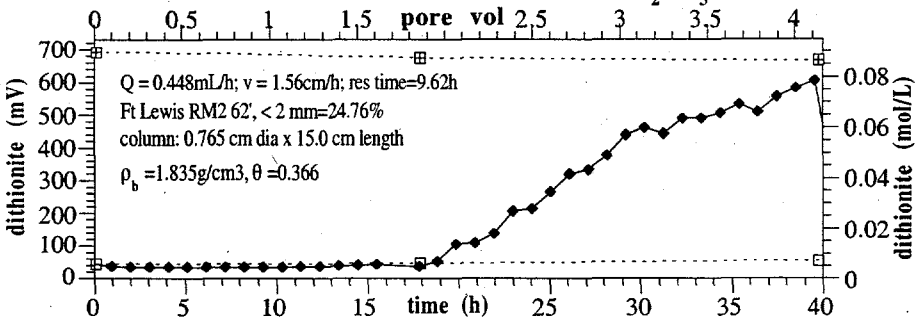

Ft Lewis KF21: Dithionite for 0.06M dith + 0.24M K_2CO_3 inject

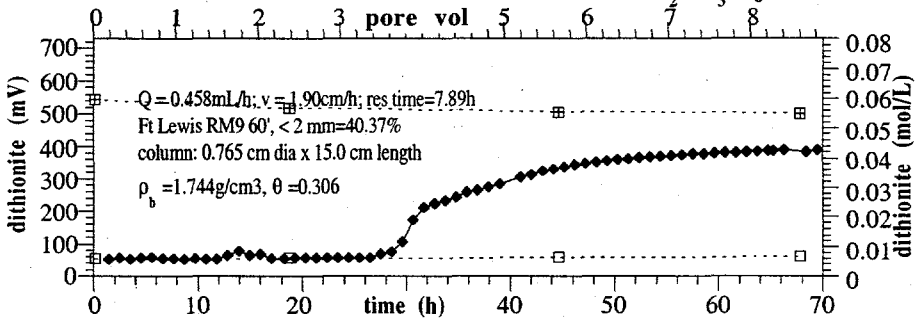

Ft Lewis KF22: Dithionite for 0.03M dith + 0.12M K_2CO_3 inject

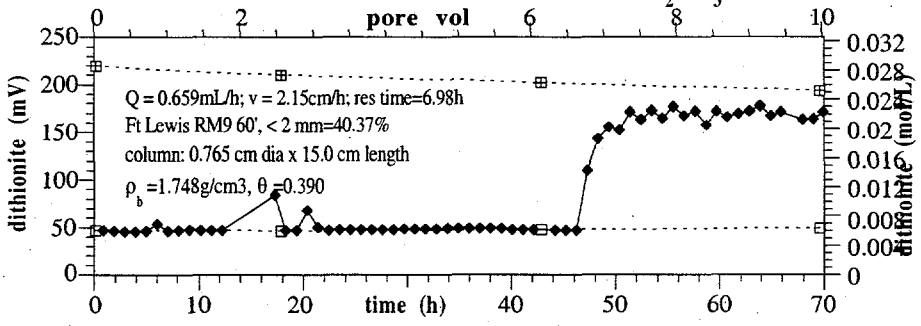

KF49: Dithionite for 0.09M dith + 0.36M K_2CO_3 inject

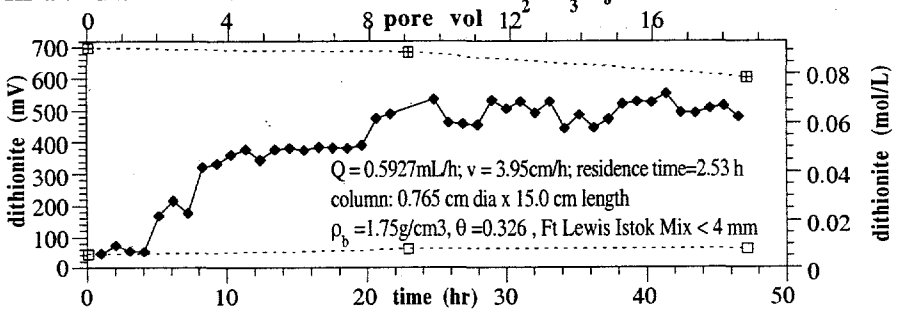

KF49: pH for 0.09M dith + 0..36M K_2CO_3 inject

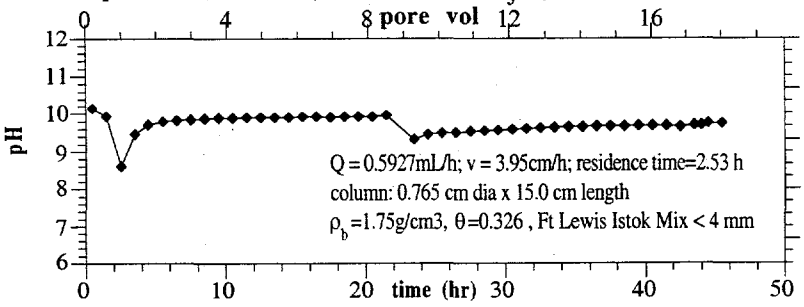

KF50: Dithionite for 0.09M dith + 0.27M K_2CO_3 inject

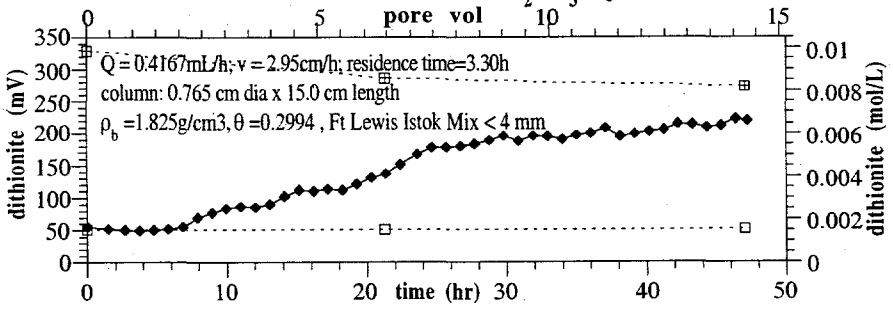

KF50: pH for 0.09M dith + 0.27M K_2CO_3 inject

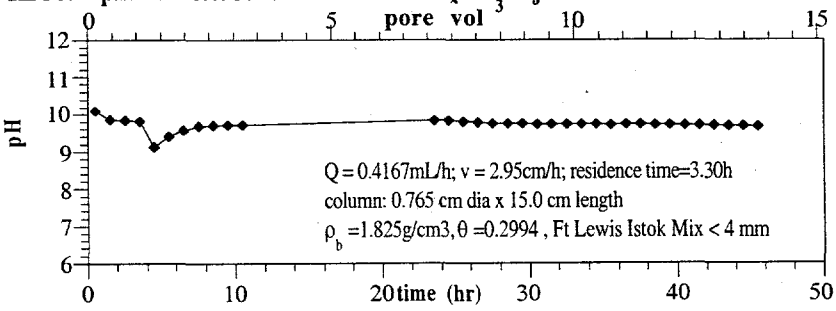

KF53: Dithionite for 0.09M dith + 0.27M K_2CO_3 inject

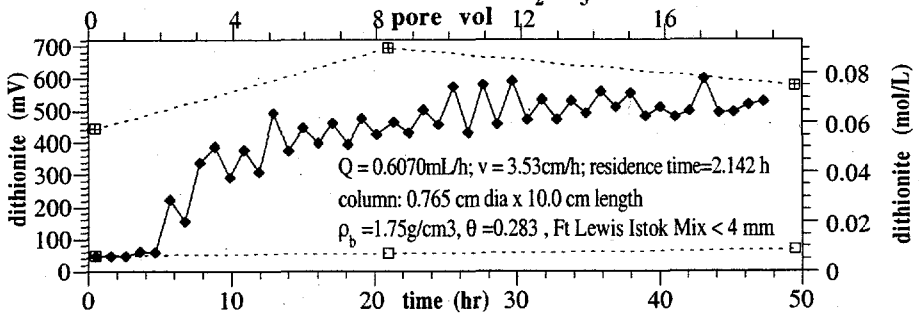

KF53: pH for 0.09M dith + 0.27M K_2CO_3 inject

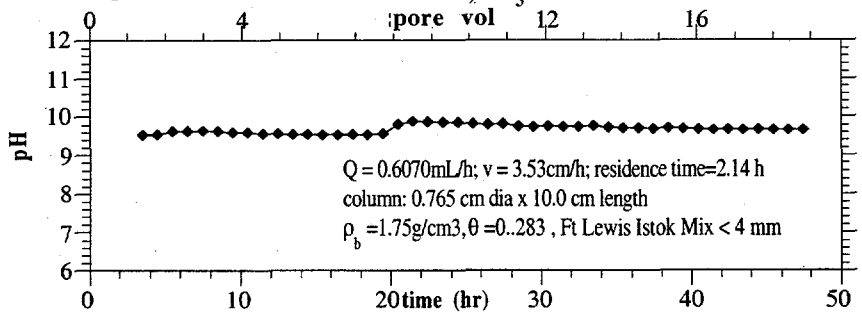

KF54: Dithionite for 0.09M dith + 0.18M K_2CO_3 inject

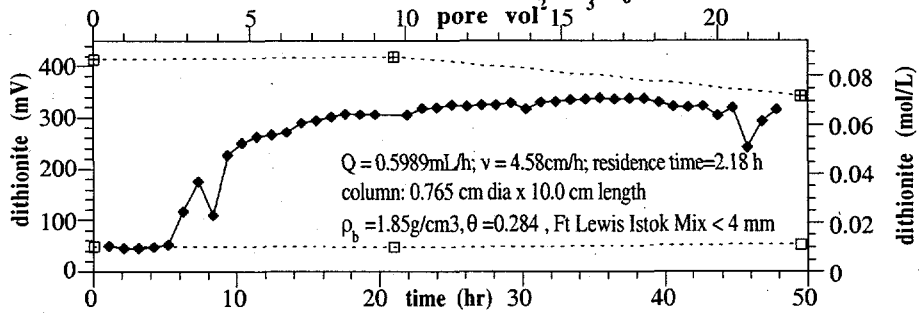

KF54: pH for 0.09M dith + 0.18M K_2CO_3 inject

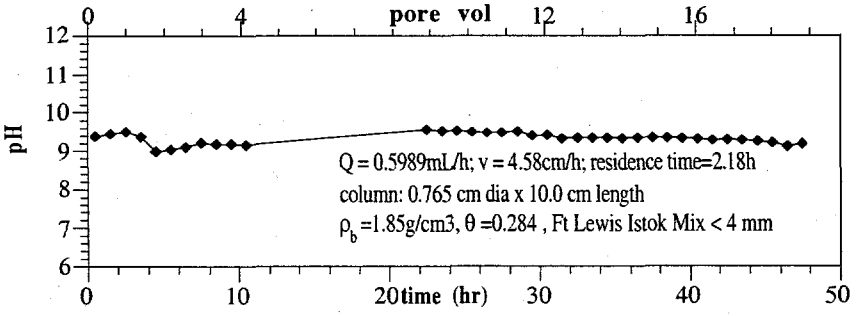

KF57: Dithionite for 0.09M dith + 0.18M K_2CO_3 inject

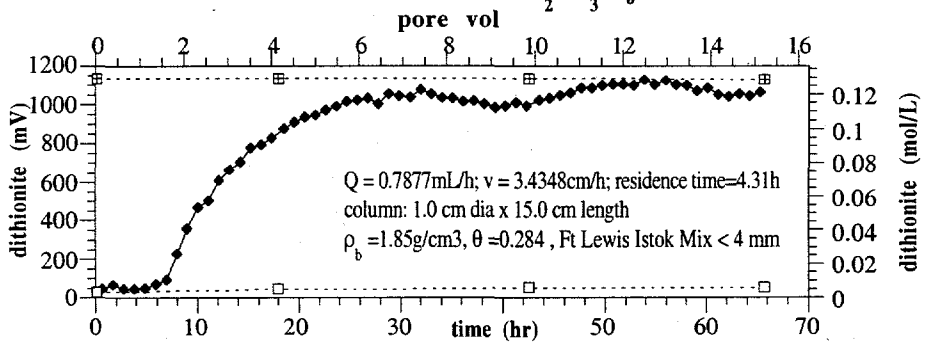

KF57: pH for 0.09M dith + 0.18M K_2CO_3 inject

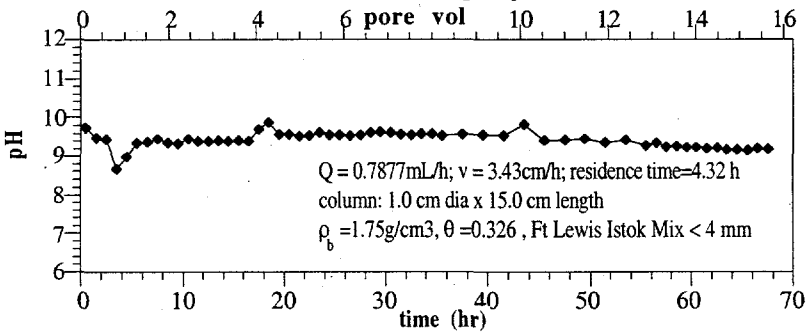

KF61: Dithionite for 0.09M dith + 0.045M K_2CO_3 inject

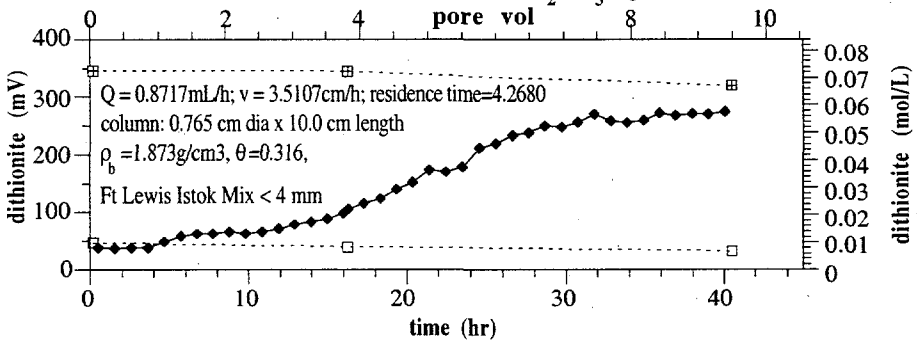

KF61: pH for 0.09M dith + 0.045M K_2CO_3 inject

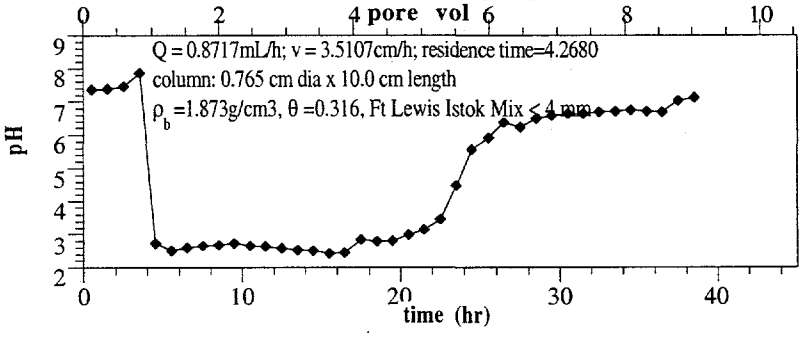

KF58: Dithionite for 0.09M dith + 0.09M K_2CO_3 inject

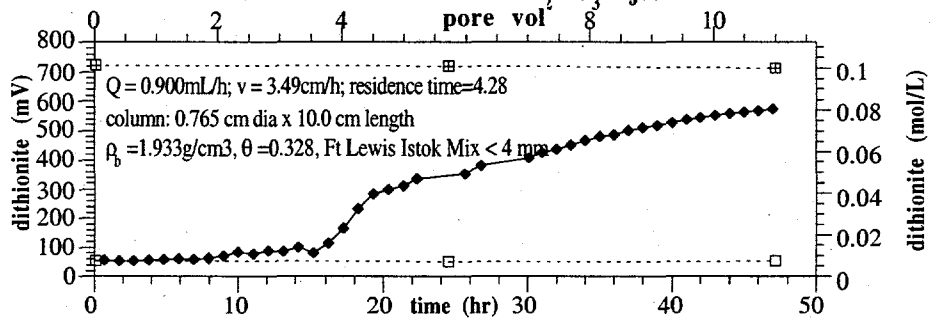

KF58: pH for 0.09M dith + 0.09M K_2CO_3 inject-two separate experiments

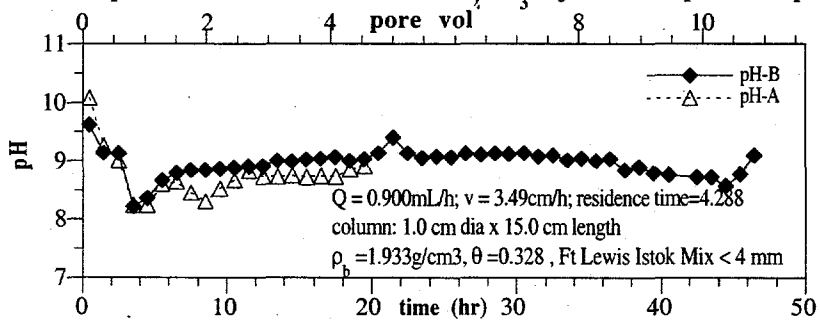

KF58: Total Fe for 0.09Mdith+0.09MK_2CO_3 inject

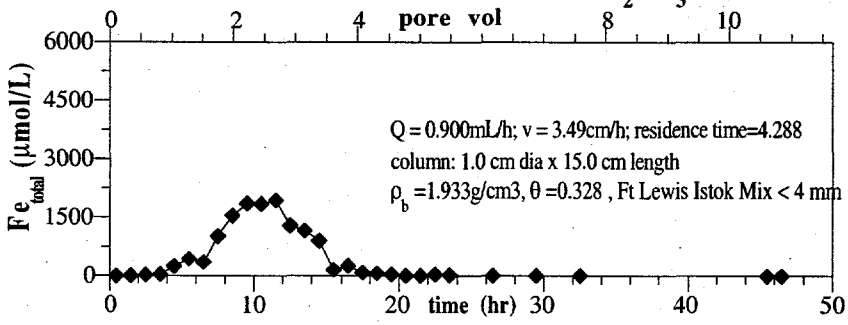

KF59: Dithionite for 0.09M dith + 0.045M K_2CO_3 inject

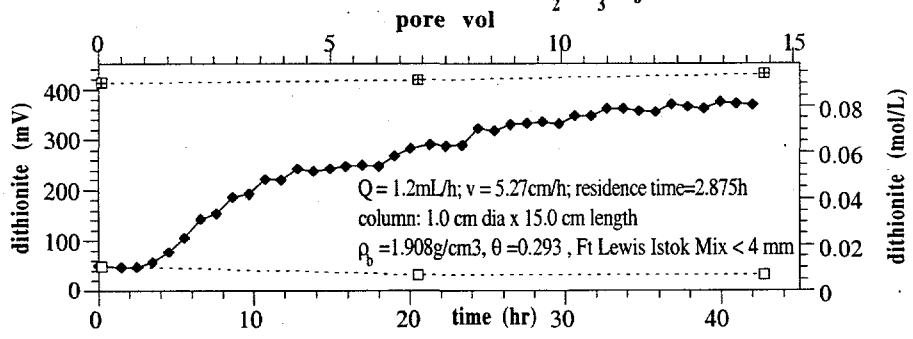

KF59: pH for 0.09M dith + 0.045M K_2CO_3 inject

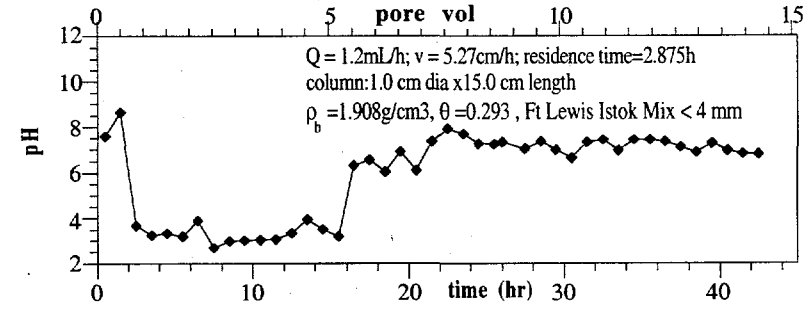

KF59: Total Fe 0.09M dith + 0.045M K_2CO_3 inject

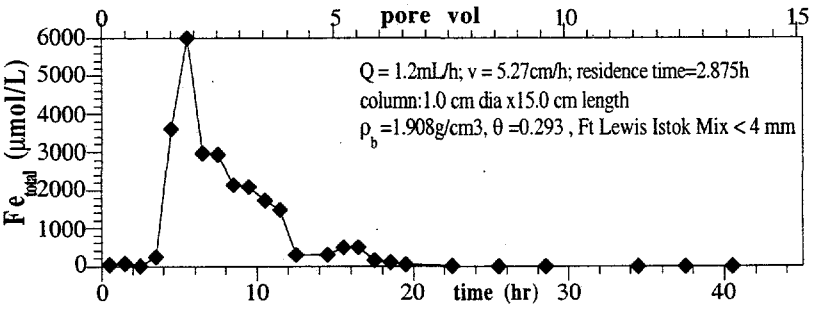

Appendix C

Column Oxidation Experiments

kf3: Oxygen 2, column effluent

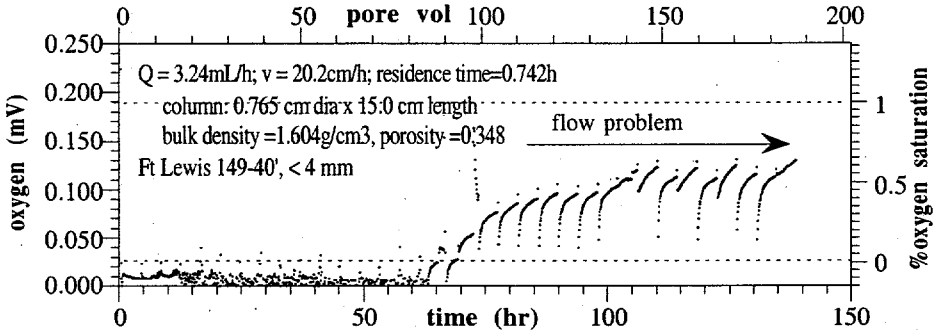

KF4: Disolved Oxygen of Column Effluent (probe #2)

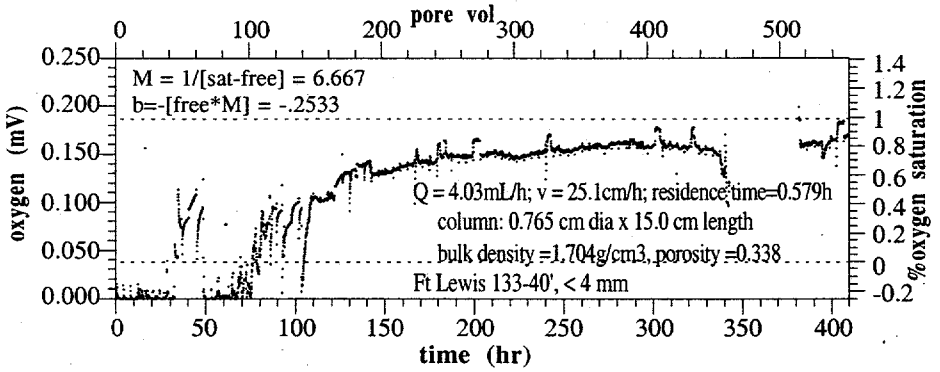

Kf7: Oxygen 2, column effluent

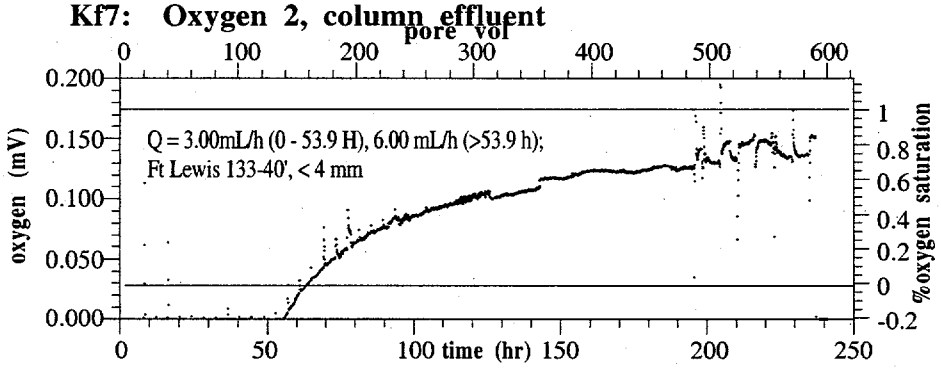

KF10: Column Effluent - Dissolved Oxygen, Probe 1

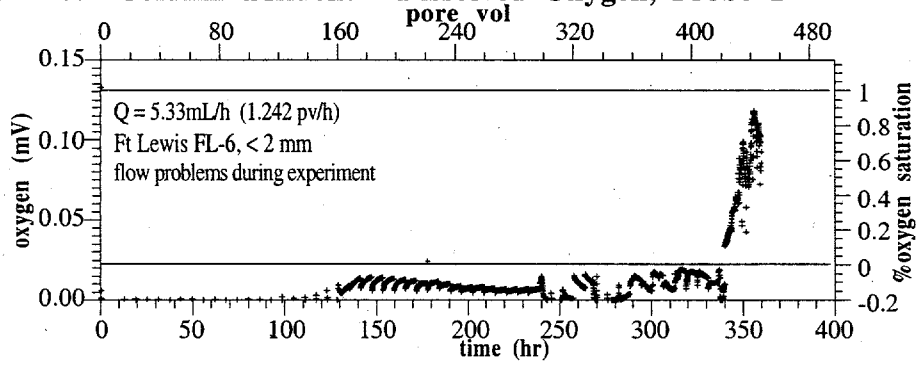

KF11: Column Effluent - Dissolved Oxygen, Probe 2

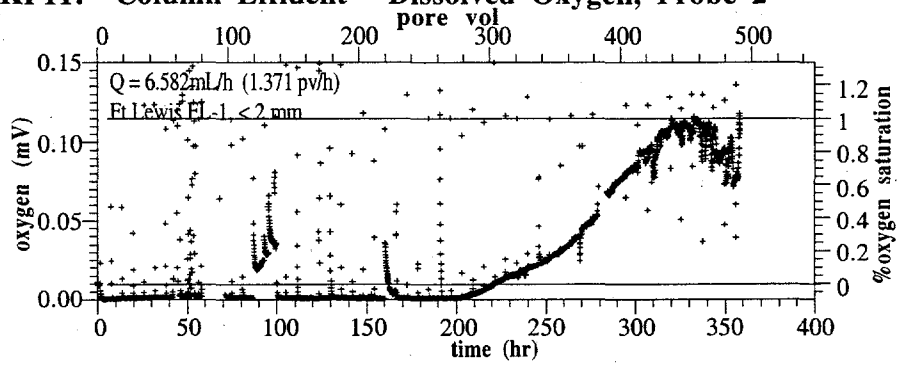

KF16: Dissolved Oxygen in Effluent, Probe 2

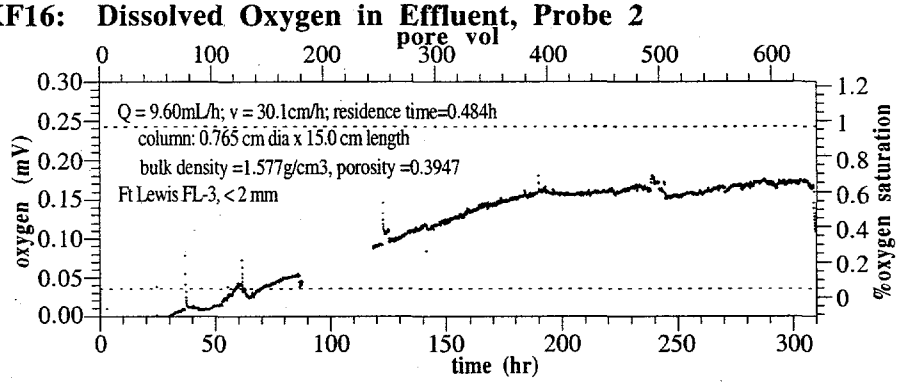

KF16: Dissolved Oxygen Stds, Probe 2

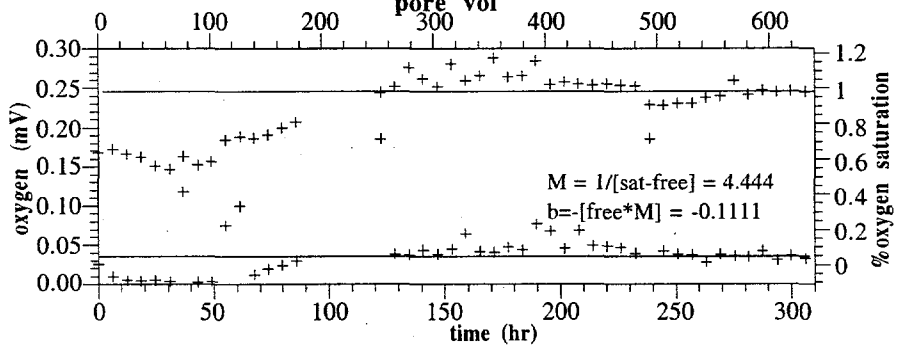

KF43: Dissolved Oxygen from Column, Probe 1

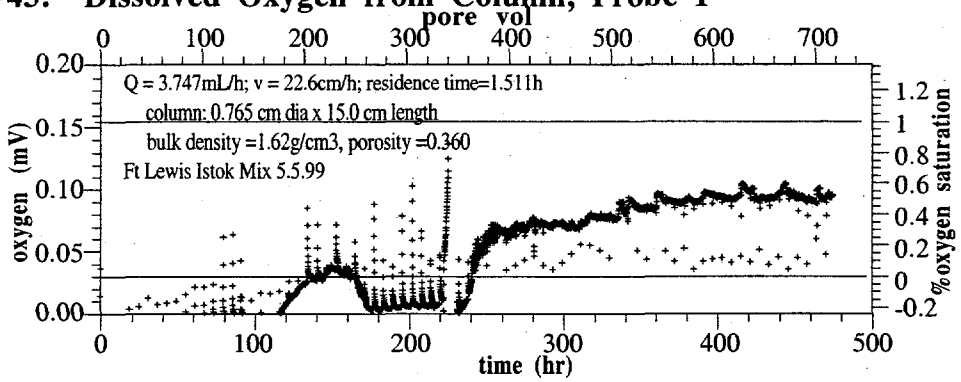

KF45: Dissolved Oxygen Column, Probe 2

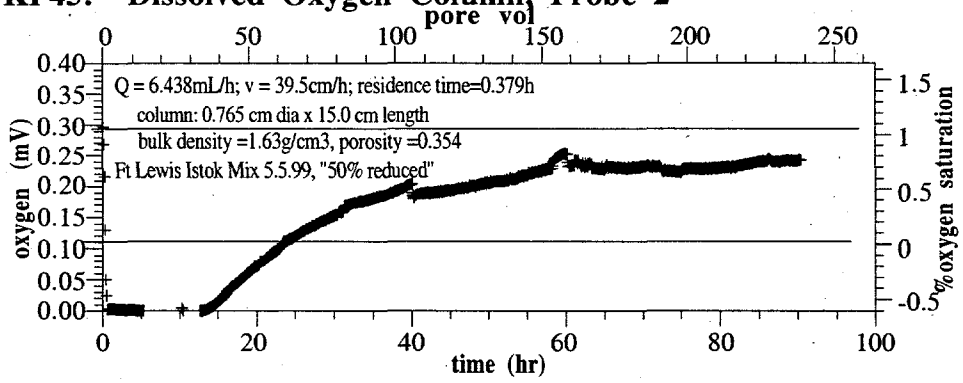

KF47: Dissolved Oxygen in Column, Probe 1

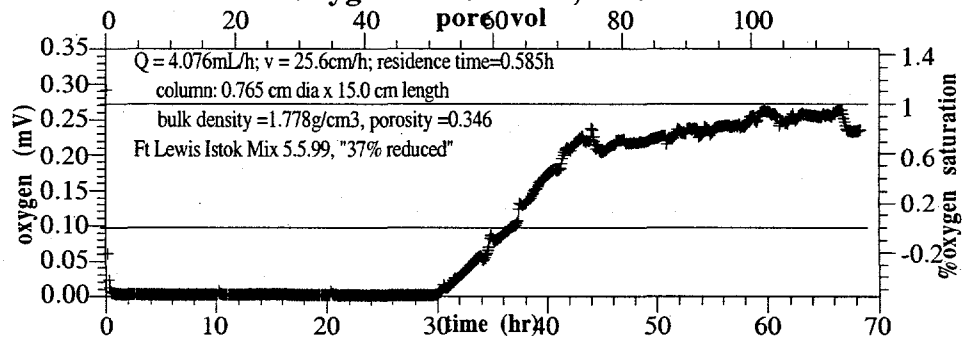

KF48: Dissolved Oxygen Effluent, Probe 1

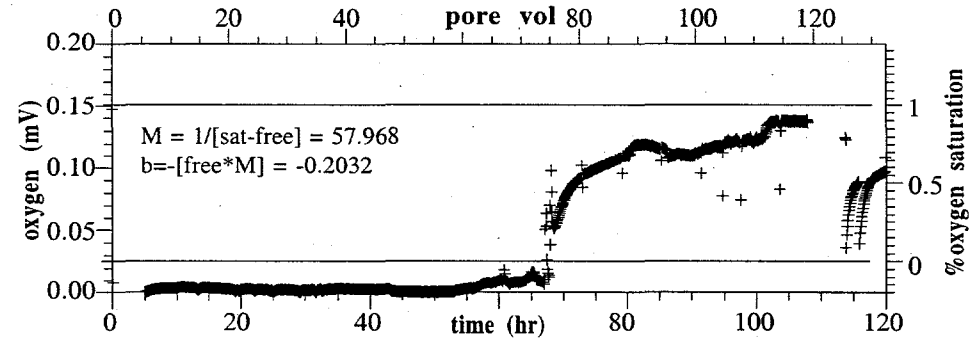

KF51: Dissolved Oxygen Column Effluent, Probe 2

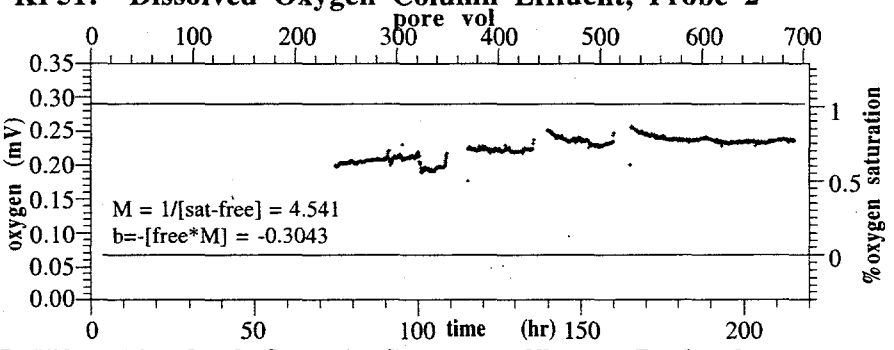

KF52: Dissolved Oxygen Column Effluent, Probe 2

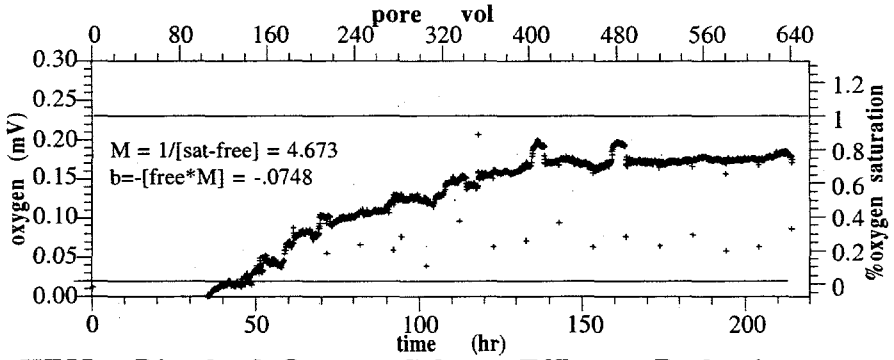

KF55: Dissolved Oxygen Column Effluent, Probe 1

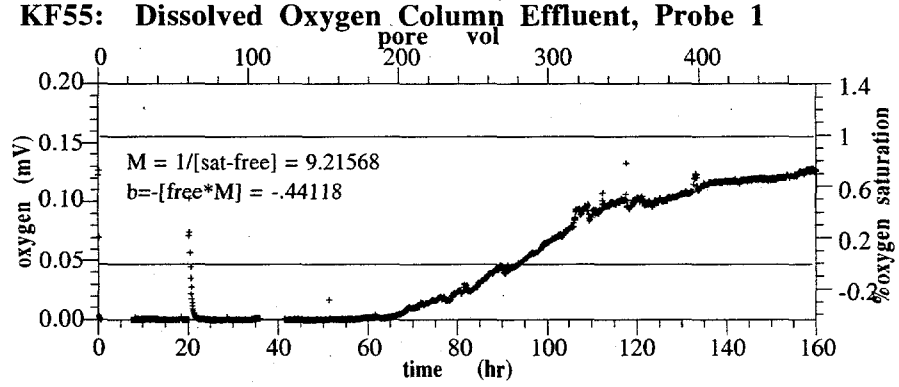

KF56: Dissolved Oxygen Column Effluent, Probe 2

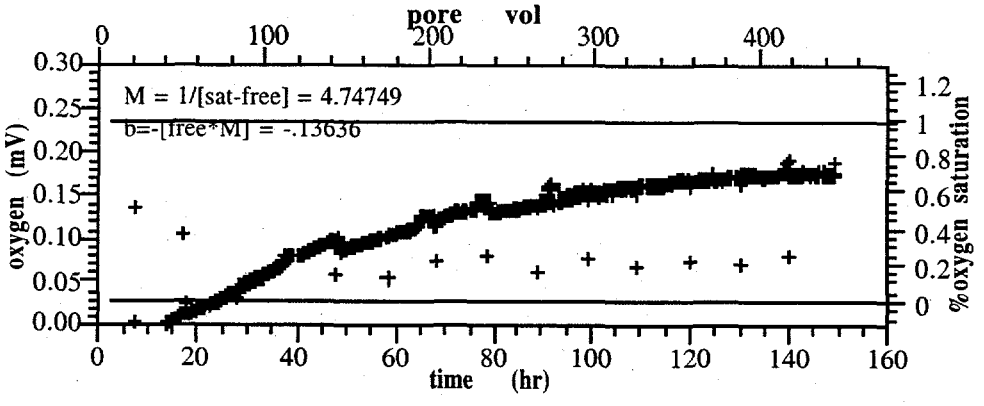

KF60: Dissolved Oxygen Effluent, Probe 1

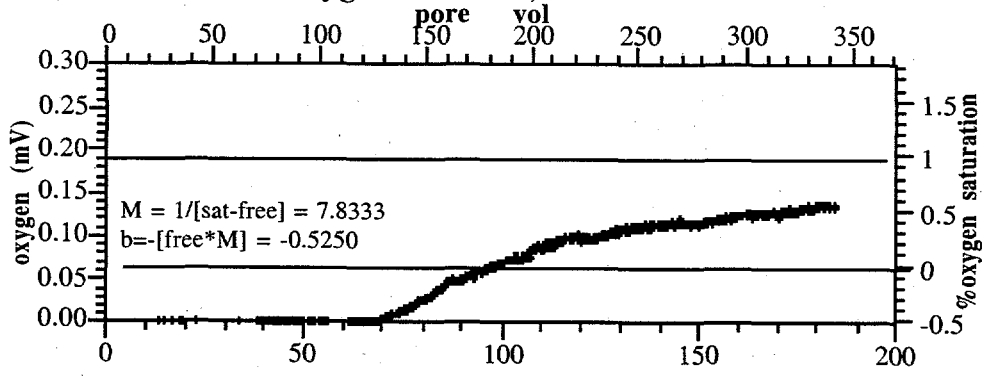

Appendix D

Batch TCE Experiments

KF13: TCE degradation by Dithionite-Reduced Sediment

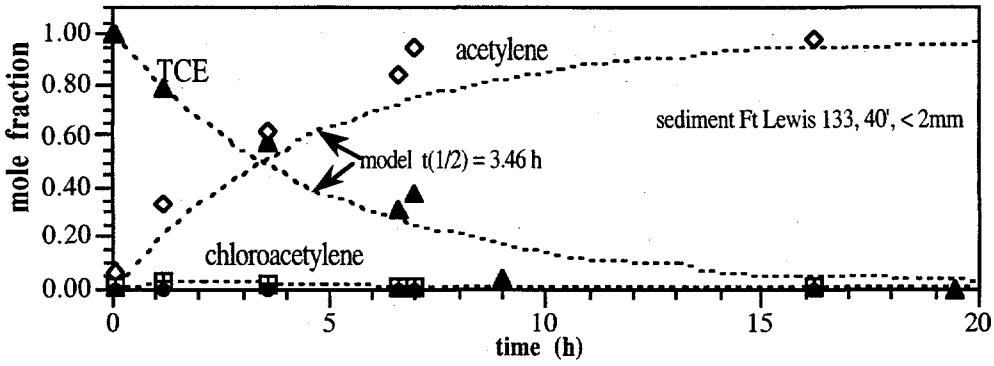

TCE degradation by dithionite-reduced sediment

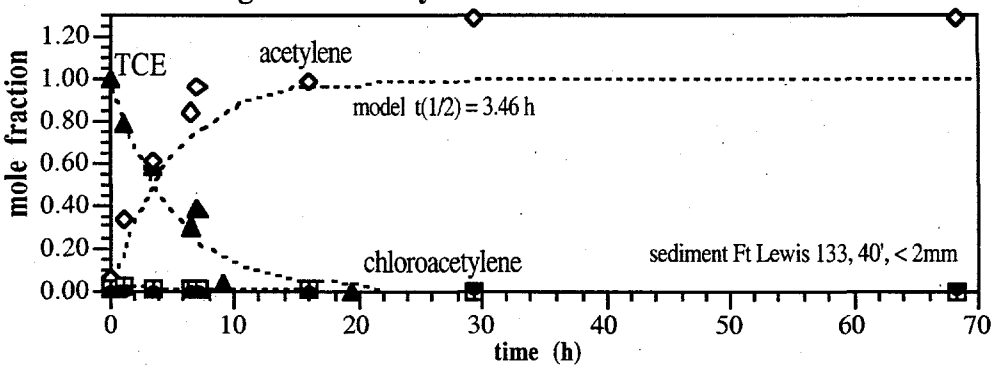

KF13: DCE Nonreactive in Reduced Sediment

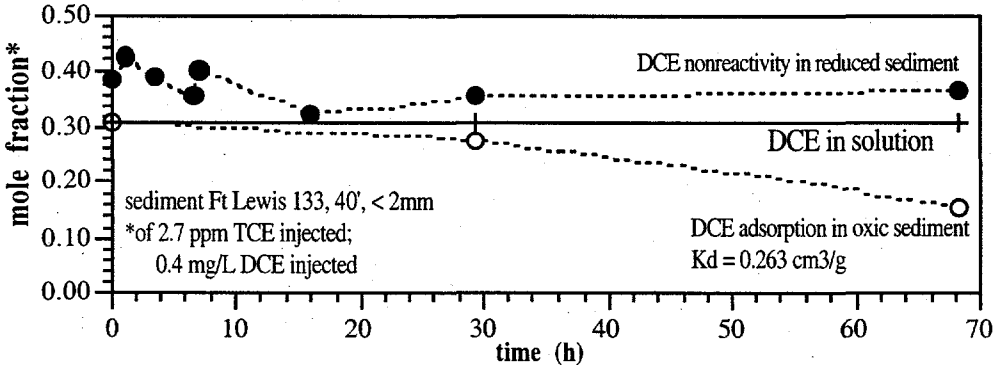

KF13: Vinyl Chloride not Generated, Trace Levels in Groundwater Removed in Reduced Sediment

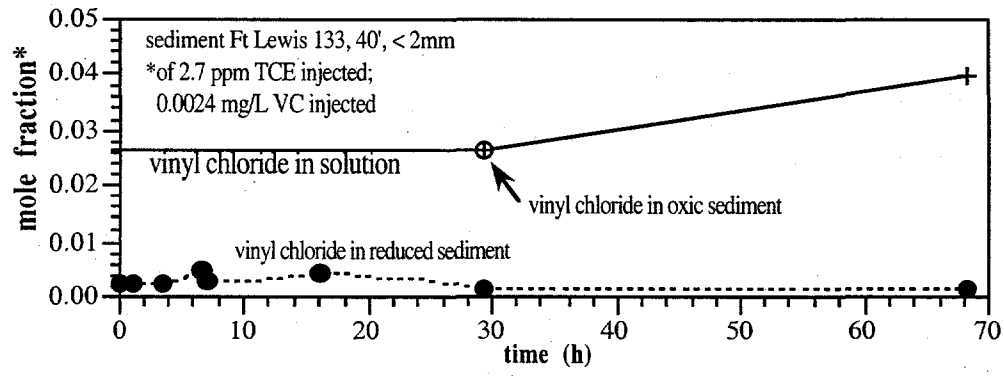

KF24: Batch TCE degradation at 25°C

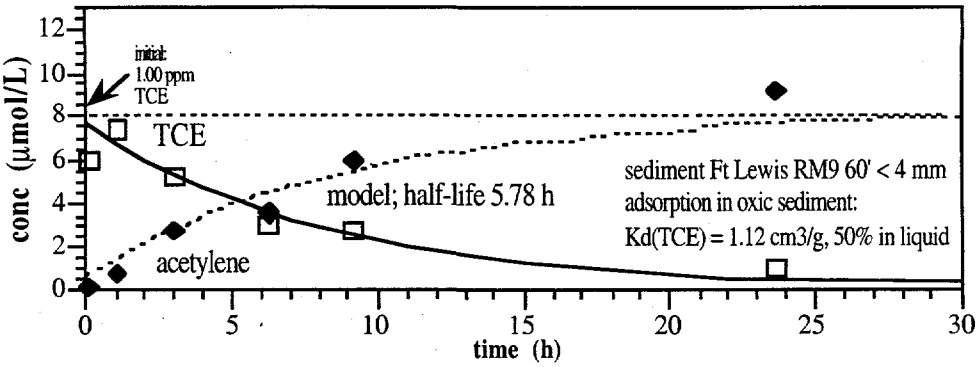

KF25: Batch TCE degradation at 17°C

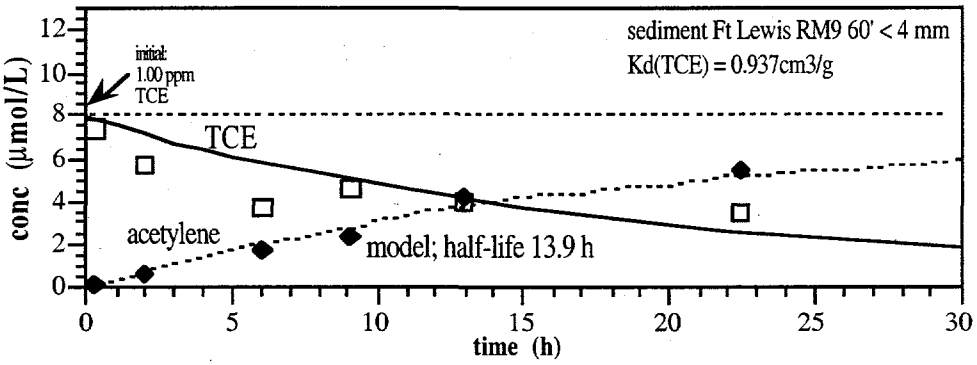

Batch TCE degradation at 10°C

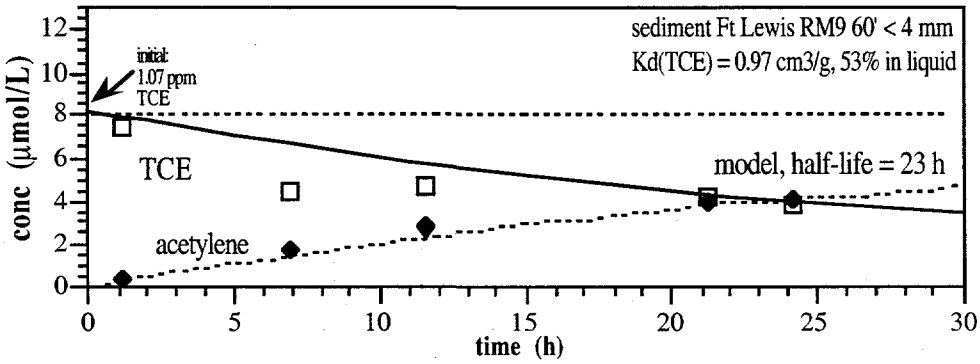

Batch TCE degradation at 10°C

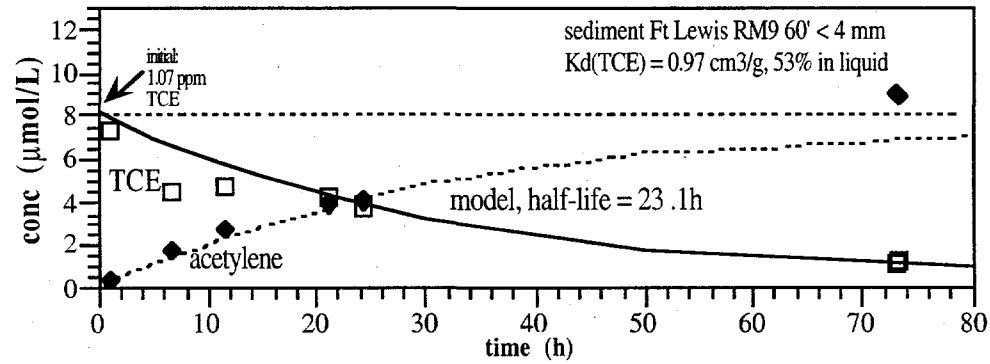

KF33: Batch TCE Degradation at 2°C

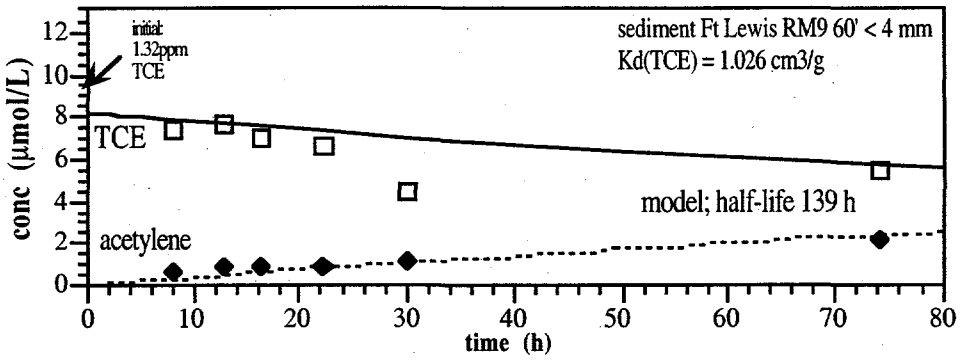

Batch TCE degradation at 42°C

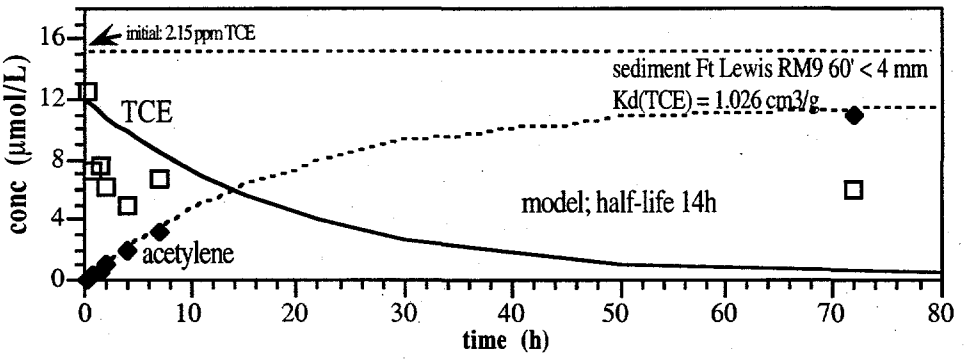

KF40: Sediment Reduction on TCE Degradation Rate

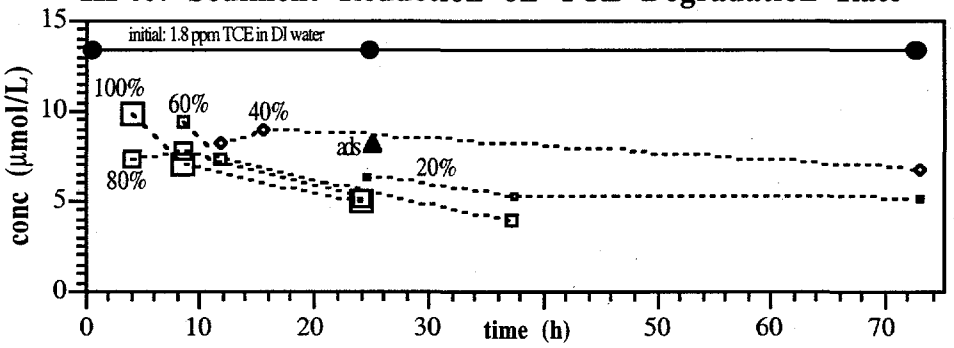

KF40a: 100% Reduced Sediment, Batch TCE Degradation, 25°C

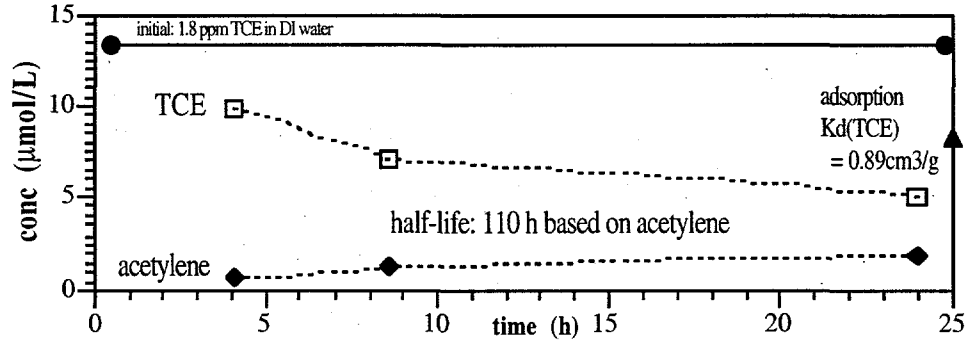

KF40b: 65% Reduced and Batch TCE degradation at 25°C

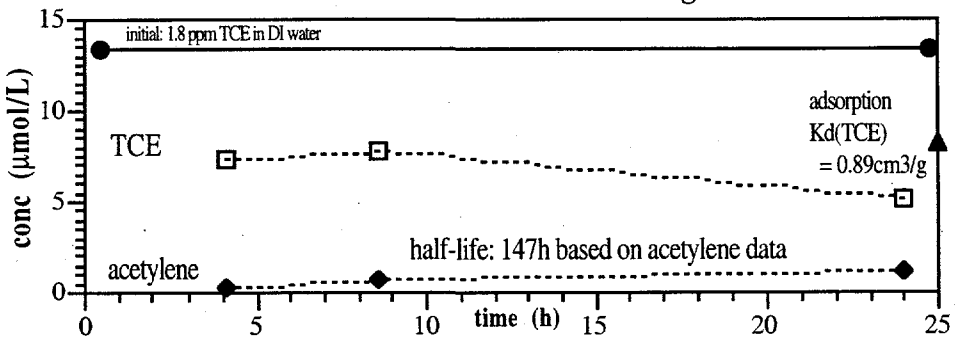

KF40c: 49% Reduced vs Batch TCE degradation, 25°C

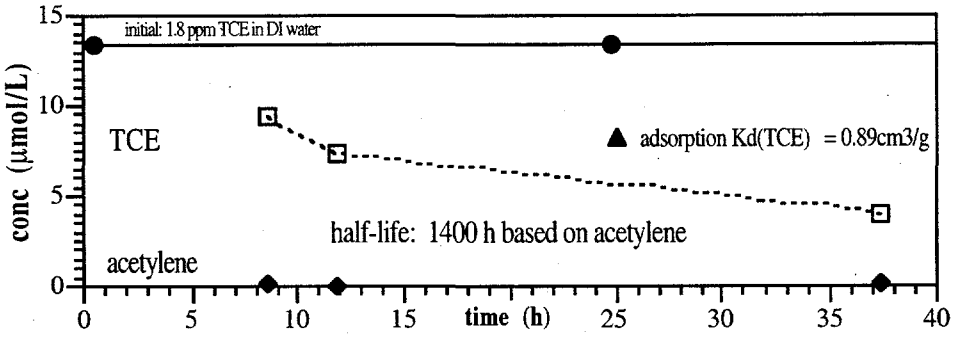

KF40d: 33% Reduced vs Batch TCE degradation, 25°C

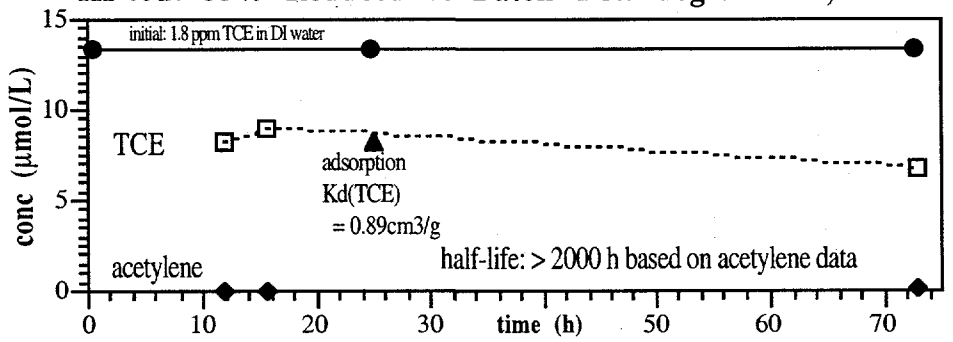

KF40e: 16% Reduced vs Batch TCE degradation, 25°C

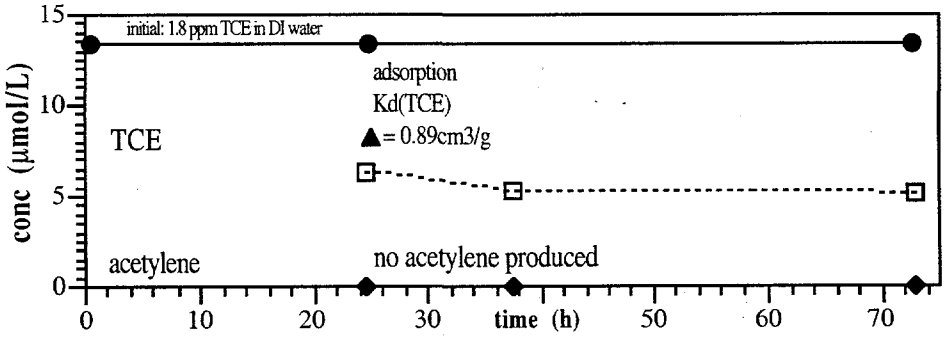

Batch TCE Degradation in Istok Sediment (< 4 mm, 25°C)
4.0% reduced (calculated)

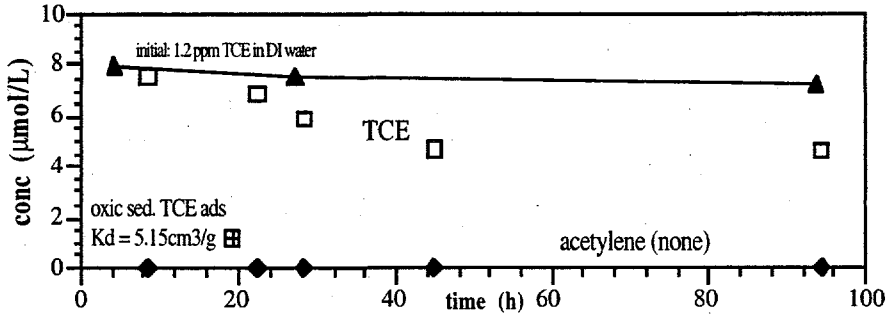

KF42c: Batch TCE Degradation in Istok Sediment (< 4 mm, 25°C)
11.1% reduced (measured, oxygen btc)

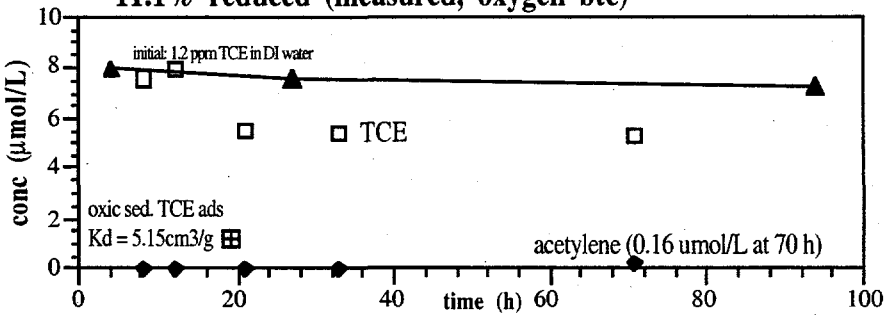

KF42d: Batch TCE Degradation in Istok Sediment (< 4 mm,
27.4% reduced (measured oxygen btc)

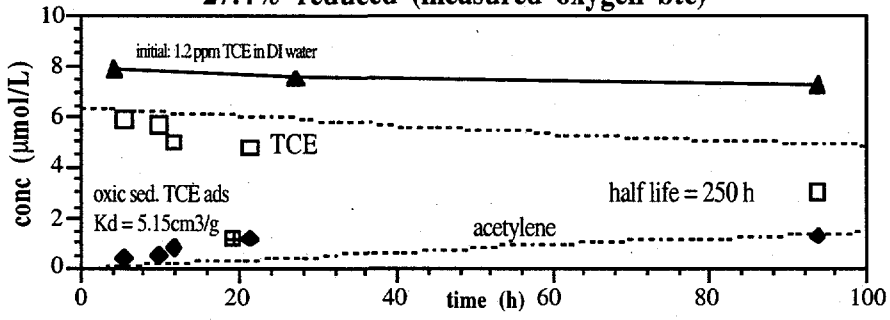

KF42e: Batch TCE Degradation in Istok Sediment (< 4 mm, 25°
27.4% reduced (measured, oxygen btc)

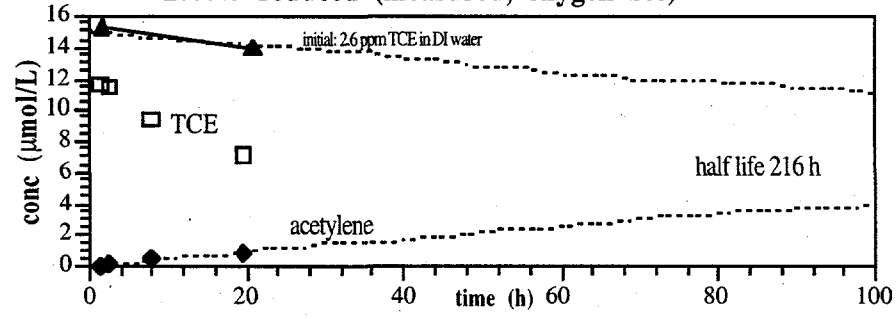

KF42f: Batch TCE Degradation in Istok Sediment (< 4 mm, 25°C)
33.4% reduced (calculated)

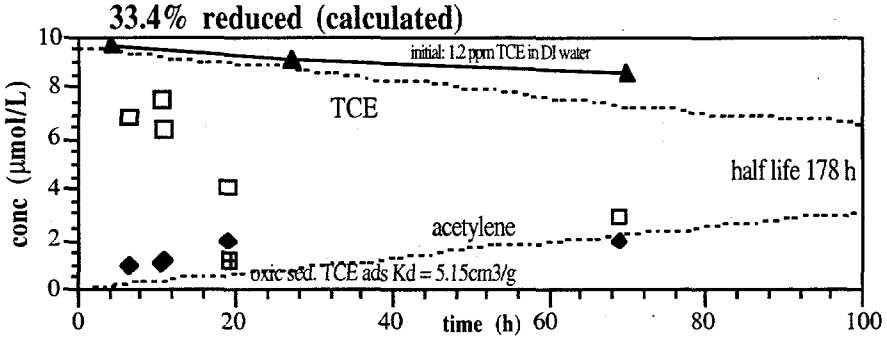

KF42g: Batch TCE Degradation in Istok Sediment (< 4 mm, 25°C)
38.7% reduced (calculated)

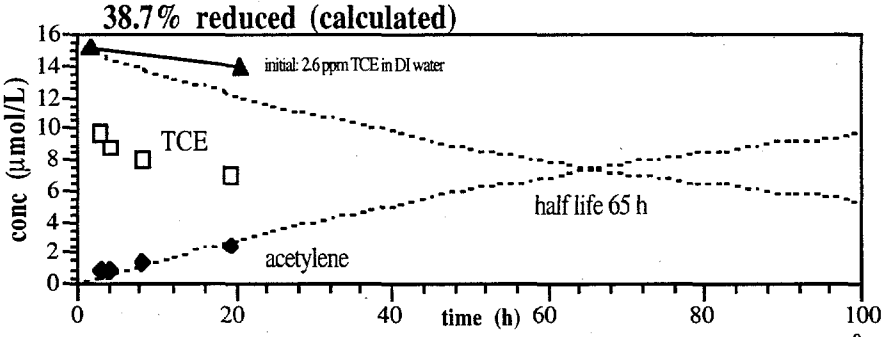

KF42h: Batch TCE Degradation in Istok Sediment (< 4 mm, 25°C)
38.7% reduced (calculated)

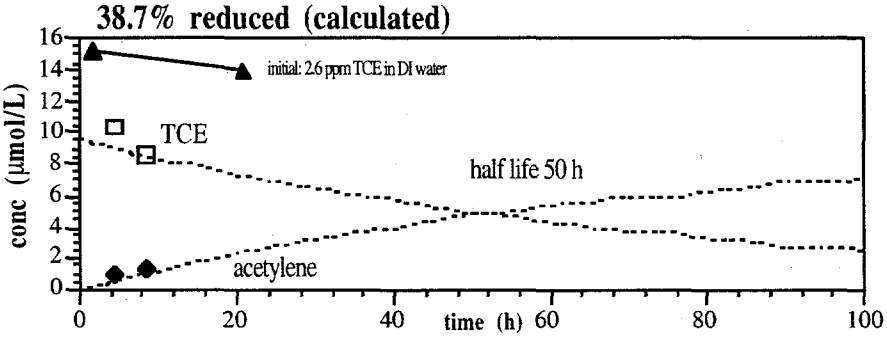

KF42i: Batch TCE Degradation in Istok Sediment (< 4 mm, 25°C)
43.8% reduced (calculated)

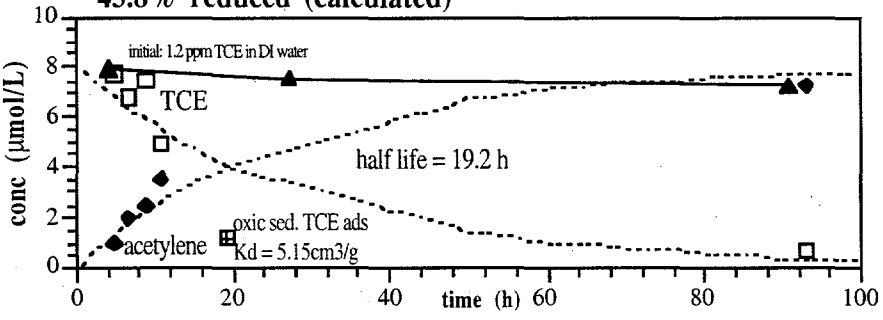

KF42i: Batch TCE Degradation in Istok Sediment (< 4 mm, 25°C)
43.8% reduced (calculated)

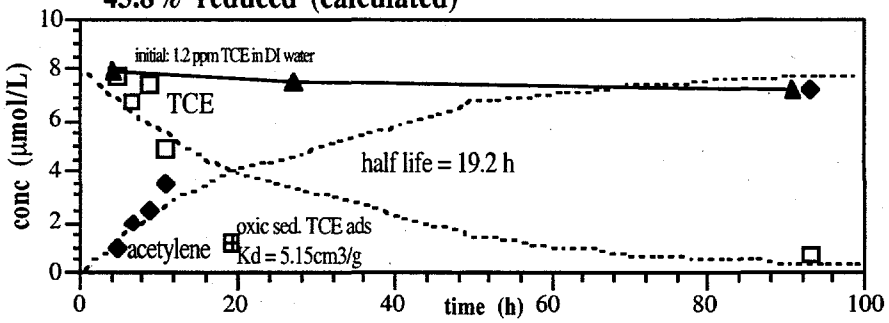

KF42j: Batch TCE Degradation in Istok Sediment (< 4 mm, 25°C)
52.6% reduced (measured oxygen btc)

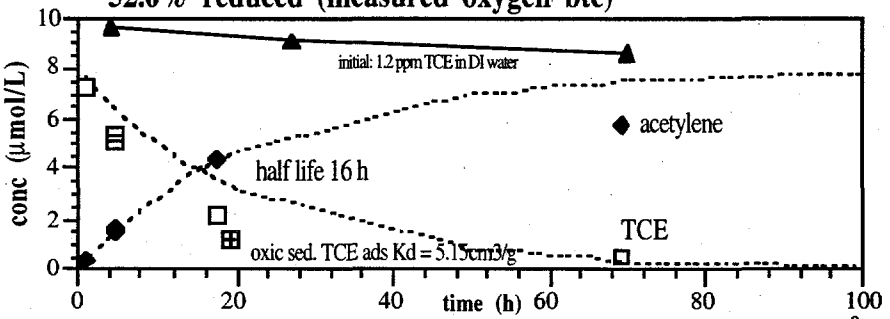

KF42k: Batch TCE Degradation in Istok Sediment (< 4 mm, 25°C)
100% reduced (measured O_2 btc; dithionite/iron = 3.8)

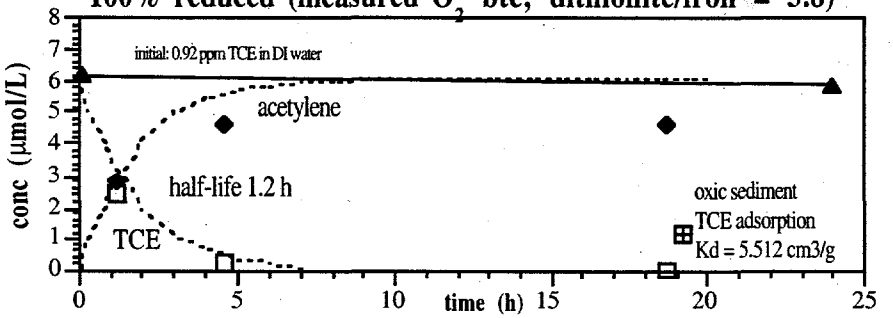

KF42a: Batch TCE degradation at 25°C, RM1 sediment
dith./iron = 4.0, 100% reduced (measured O_2 btc)

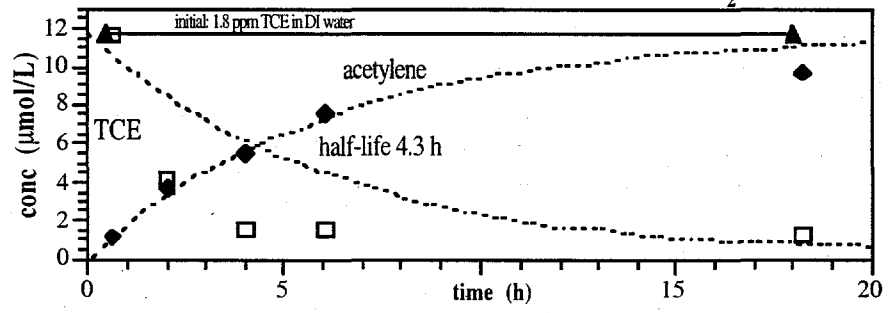

KF62a Batch TCE Degradation:
Reduced by 0.09M dith + 0.09 M K_2CO_3

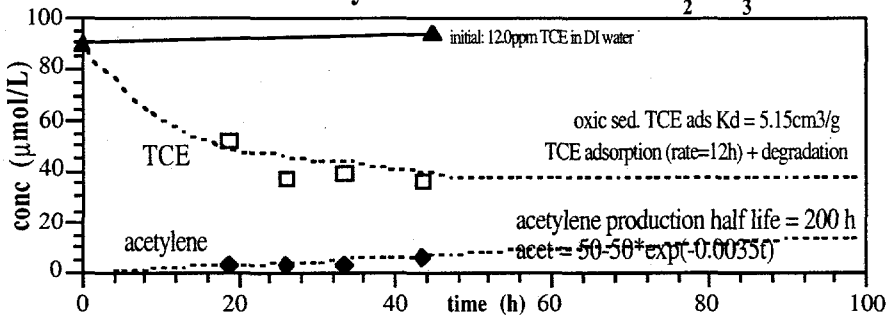

KF62b Batch TCE Degradation:
Reduced by 0.09M dith + 0.045 M K_2CO_3

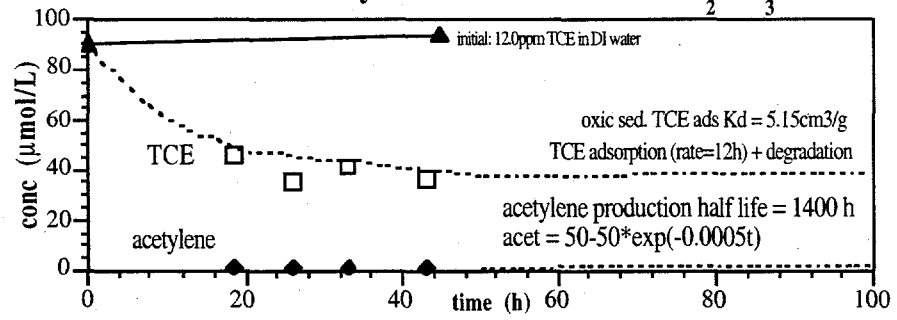

Appendix E

Column TCE Experiments

KF17: TCE Degradation in Ft Lewis Sediment

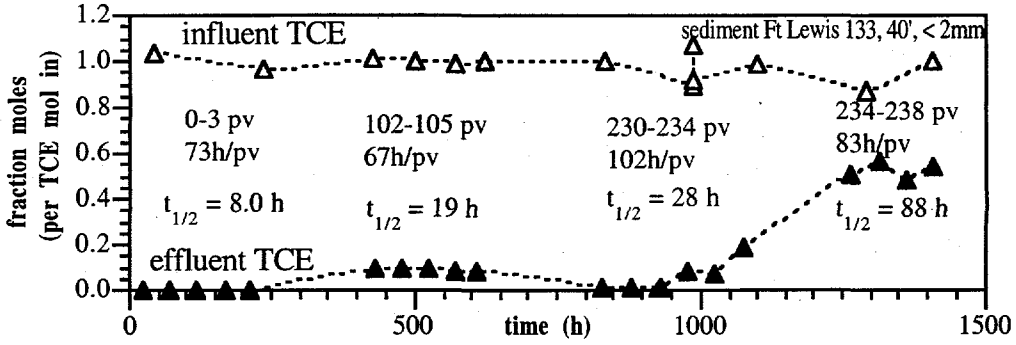

KF17: DCE Reactivity in Ft Lewis Sediment

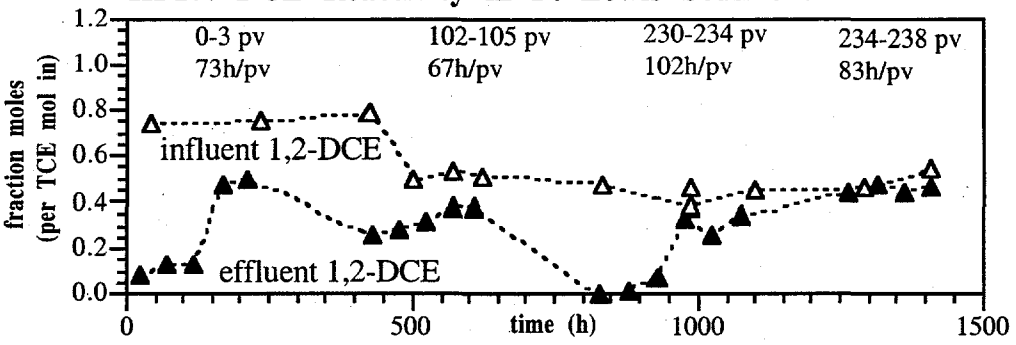

KF17: Acetylene in Reduced Sediment Column

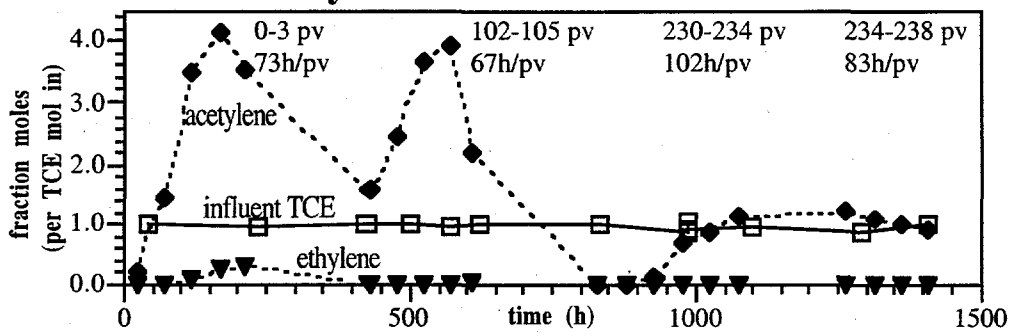

KF17: Chloroacetylene and Vinyl Chloride in Ft Lewis Sediment

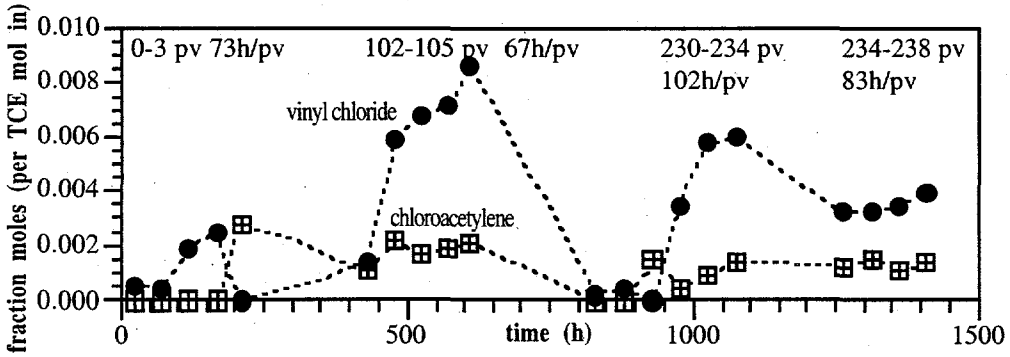

KF23: TCE Degradation in Reduced Sediment Column

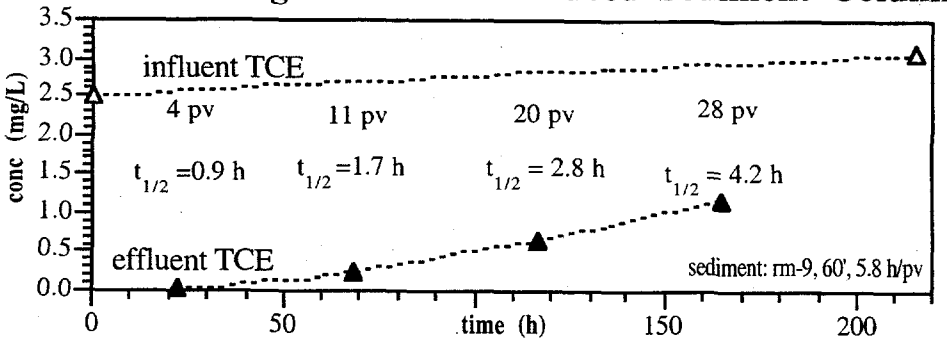

KF23: cis-DCE Mass Loss

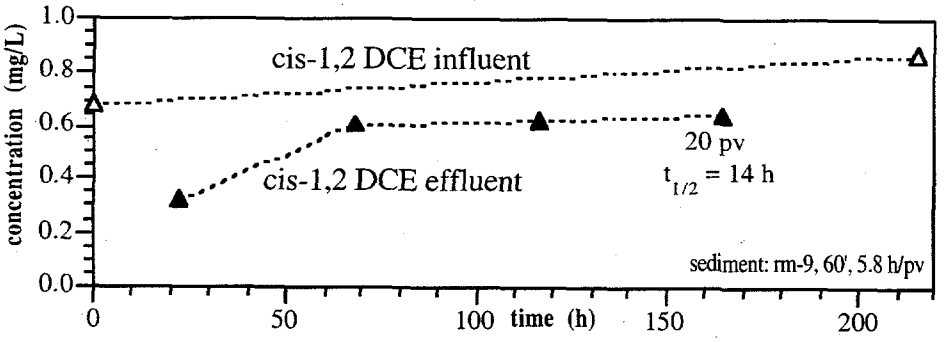

KF23: 1,1-DCE Mass Gain (part of TCE pathway)

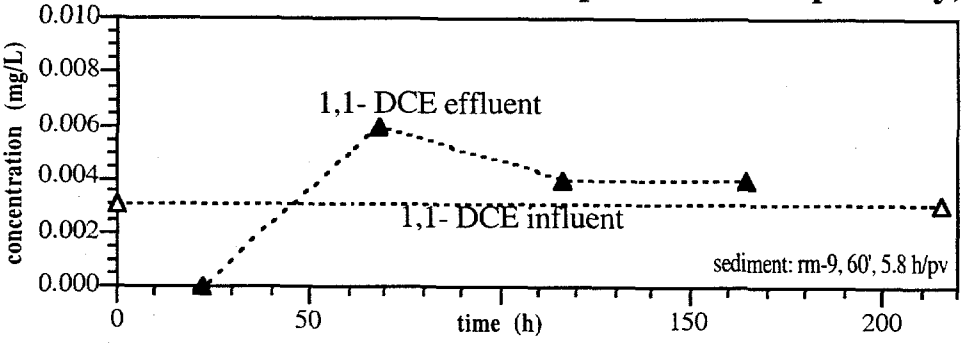

KF23: TCA Degradation by Reduced Sediment Column

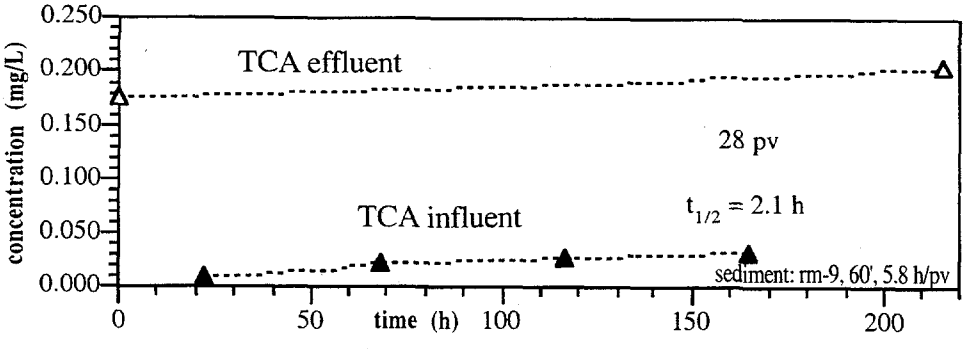

KF38: TCE Degradation with Flow, 10C, 25% Reduced sediment

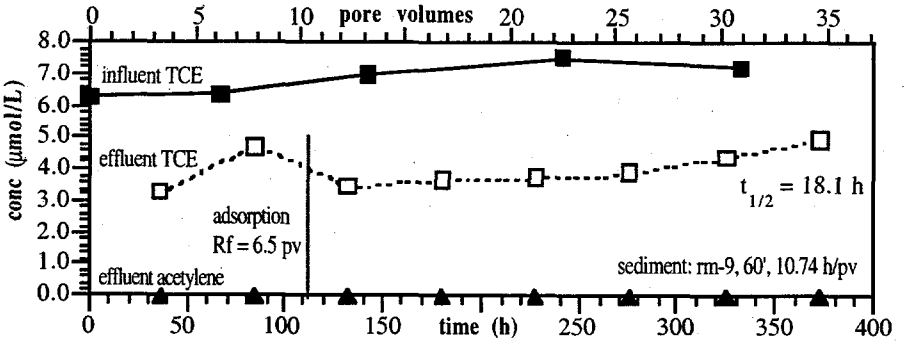

KF39: TCE Degradation with Flow, 10C, 1/4 100% reduced sed

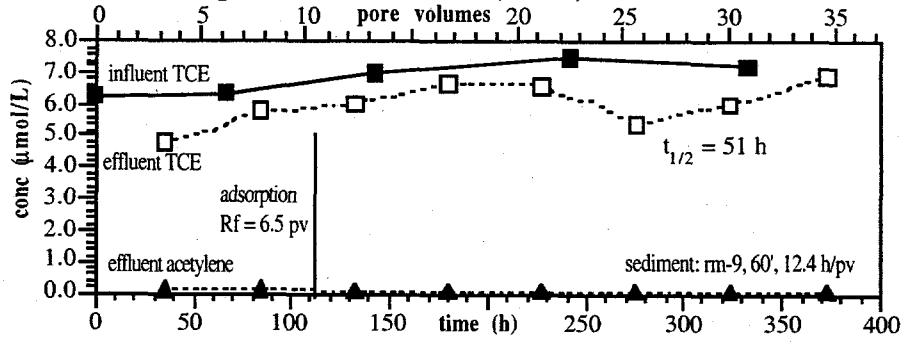

Distribution

No. of Copies

OFFSITE

Steve Cox
U.S. Geological Survey
1201 Pacific Ave., Suite 600
Tacoma, WA 98402

Phil Crawford
Public Works
ATTN: AFZH-PWE, MS-17
Bldg. 2012, Room 323
Fort Lewis, WA 98433-9500

Rick Dinicola
U.S. Geological Survey
1201 Pacific Ave., Suite 600
Tacoma, WA 98402

Sue Kahle
U.S. Geological Survey
1201 Pacific Ave., Suite 600
Tacoma, WA 98402

Bob Kievit
U.S. Environmental Protection Agency
1200 Sixth Avenue 0EA-095
Seattle, WA 98101

Marcia Knadle
U.S. Environmental Protection Agency
1200 Sixth Avenue 0EA-095
Seattle, WA 98101

5 Dennis Korycinski
Public Works
ATTN: AFZH-PWE, MS-17
Bldg. 2012, Room 323
Fort Lewis, WA 98433-9500

No. of Copies

Jeff Randall
CH2M Hill
777 108th Avenue, N.E.
Bellevue, WA 98004-5118

44 **Pacific Northwest National Laboratory**

C. C. Ainsworth	K3-61
J. E. Amonette	K8-96
J. G. Bush	K6-96
K. J. Cantrell	K6-81
J. L. Devary	K6-96
J. C. Evans	K6-96
J. S. Fruchter (10)	K6-96
T. L. Liikala (3)	K6-96
W. J. Martin	K6-81
J. P. McKinley	K3-61
K. B. Olsen	K6-96
C. T. Resch	K3-61
D. S. Sklarew	K6-96
J. E. Szecsody (10)	K3-61
V. R. Vermeul	K6-96
M. D. Williams	K6-36
J. M. Zachara	K8-96
Information Release (7)	K1-06